Microglial activation and clearance of alpha-synuclein in the Parkinson's disease trajectory

Microglial activation and clearance of alpha-synuclein in the Parkinson's disease trajectory

Siri Egenæs

Master Thesis for the title of Master in Pharmacy

45 credits

Department of Pharmacy

The Faculty of Mathematics and Natural Sciences

University of Oslo

May 2022

Sammendrag

Parkinson sykdom (PD) er en progressiv nevrodegenerativ sykdom som rammer 1 % av befolkningen over 60 år. Nevropatologiske funn ved PD er dopaminerg degenerasjon i substantia nigra (SN), samt tilstedeværelse av intracellulære Lewy-legemer. Lewy-legemer består primært av aggregert nevrotoksisk alfa-synuklein (α-syn) og fosforylert α-syn (PS-129). Dannelsen av α-syn rike Lewy-legemer er ifølge Braak hypotesen antatt å begynne i hjernestammen og luktelappen og deretter spres i et forutsigbart mønster til neocortex inkludert anterior cingulate cortex (ACC) ved langt fremskreden sykdom.

Potensielle mekanismer for eliminasjon av α-syn bør undersøkes for å forstå hvorfor proteinet sprer seg fra celle til celle og til slutt akkumulerer intranevronalt og forårsaker nevrodegenerasjon. Tidligere studier har vist at mikrogliaceller selektivt kan fagocytere og degradere α-syn, og med dette ha en nevroprotektiv rolle. Samtidig kan akkumulering av α-syn føre til proinflammatorisk aktivering av mikroglia og med det bidra til nevrodegenerasjon.

Prøver av humant hjernevev fra kontroller med lav og høy PD polygenetisk risiko (PRS), prekliniske individer med Lewy-legemer og pasienter med klinisk og nevropatologisk etablert PD er brukt for å undersøke hvilken rolle og eliminasjonsevne mikroglia har ved ulike stadier av Lewy-legeme sykdom. Immunohistokjemi og konfokalmikroskopi etterfulgt av bildeanalyse i FIJI er gjennomført for å studere mikrogliaaktivering og fagocytose av α-syn og PS-129. Relevante anti- og proinflammatoriske proteiner er kvantifisert ved ELISA og Luminex. Nivåer av α-syn og PS-129 er målt ved semikvantitativ western blotting.

I sykdomsfasen før spredning av Lewy-legemer til ACC ble det her funnet høyere totalnivå av α-syn, mens nivåene av PS-129 i mesencephalon var høyere i sykdomsfasen som inkluderer tilstedeværelse av Lewy-legemer. Mikroglia utviklet en amøboid ved høyere nivåer av α-syn intracellulært. Dette indikerer at mikroglia har en inflammatorisk respons til α-syn akkumulering. I mesencephalon var imidlertid både nivåer av antiinflammatorisk DJ-1 og intracellulært α-syn lavere hos individer med mer uttalt nevropatologisk Lewy-legeme sykdom. Dette kan indikere deaktivering av mikroglia og redusert autofagi av α-syn. Dette kan sammen bidra til å øke α-syn akkumulering som følge av redusert mikrogliaeliminasjon, observert som en økning i post-translasjonell fosforylering av α-syn og utvikling av Lewy legemer.

Abstract

Parkinson's Disease (PD) is a progressive neurodegenerative disease afflicting 1% of the population above the age of 60. PD is pathologically characterized by death of dopaminergic neurons in substantia nigra (SN) and the presence of intracellular Lewy bodies (LB). LBs mainly consist of aggregated neurotoxic alpha-synuclein (α-syn) and phosphorylated α-syn (PS-129). According to the Braak hypothesis, the formation of α-syn-rich LBs begin in clearly defined induction sites in the brainstem and olfactory bulb and advance in a topographically predictable sequence until reaching the neocortex, including anterior cingulate cortex (ACC).

To gain an understanding of why the protein spreads from cell to cell and eventually accumulates in neurons and causes neurodegeneration, potential clearance pathways of α-syn should be investigated. Studies have shown that microglial cells can selectively engulf and degrade α-syn, hence having a neuroprotective role. At the same time, accumulation of α-syn leads to pro-inflammatory activation of microglia, thereby causing neurodegeneration.

To investigate the involvement of microglial activation state and microglial α-syn clearance at different stages of LB disease, samples of human brain tissue from control subjects with low and high PD polygenetic risk, pre-clinical subjects with LBs (incipient PD) and clinically and neuropathologically established PD. To study microglial activation and engulfment of α-syn and PS-129, immunohistochemistry and confocal microscopy followed by analysis in FIJI was performed. Relevant anti- and pro-inflammatory proteins were quantified by ELISA and Luminex. Levels of α-syn and PS-129 were measured by semi quantitative western blotting.

The findings of this study demonstrated higher total α-syn in ACC in the pre-LB phase, and higher PS-129 levels in mesencephalon in the post-LB phase. Microglial cells developed an amoeboid shape associated with increased α-syn levels intracellularly, indicative of an inflammatory response to α-syn accumulation. However, both the anti-inflammatory DJ-1 levels and the amount of microglial α-syn were lower in mesencephalon with more pronounced neuropathological LB disease severity, which might be indicative of microglial deactivation and reduced α-syn autophagy. Together, this might enhance α-syn accumulation through reduced microglial clearance, seen as increased posttranslational phosphorylation of α-syn and LB development.

Acknowledgements

The work presented in this master's thesis was carried out as a part of the Neuroscience research unit at Domus medica, Faculty of Medicine, University of Oslo and Department of Neurology, University Hospital in collaboration with the Neurobiology and Toxicology group at the Department of Pharmacy, Faculty of Mathematics and Natural Sciences at the University of Oslo.

I would like to express my sincere appreciation to my main supervisor, Kaja Nordengen. Your enthusiasm, positivity, passion for neuroscience and way of thinking is inspiring. Thank you for beyond excellent supervision and great discussions throughout the past year and during the writing process. I am so grateful for all the different learning experiences you made possible, and also for all the good laughs along the way. I would also like to thank my co-supervisor, Cecilie Morland, for guidance and inspiring teaching during the master courses, making my attention steer towards the exciting field of preclinical biological studies and neuroscience. Further, it has been a true pleasure to share this time with Gezime Seferi. Thank you for great collaboration, for sharing your knowledge and for filling every day with joy. I also need to thank all the people from other groups at Domus Medica for helping me in the lab.

Of course, I would like to thank my family, boyfriend, and friends for always supporting me in my work and decisions, being patient and for encouraging me. I could not have done this without any of you.

Lastly, I would also like to express my appreciation to my fellow students, Marie, Nora, Sissel, Helena and Lisell. Thank you for filling the past 5 years with so much fun and for creating a great educational environment.

I have enjoyed every single day of working with this project, and I am truly grateful for everyone who has been a part of this past year.

Siri Egenæs,

Oslo, May 2022

Abbreviations

α-syn	Alpha-synuclein
AADC	Amino acid decarboxylase
ANOVA	Analysis of variance
ACC	Anterior cingulate cortex
CNS	Central nervous system
BSA	Bovine serum albumin
DAT	Dopamine transporter
DJ-1	Parkinson's disease protein 7/Parkinsonism associated deglycase
GFAP	Glial fibrillary acidic protein
GWAS	Genome wide association studies
HIER	Heat induced epitope retrieval
HRP	Horseradish peroxidase
Iba1	Ionized calcium-binding adapter molecule 1
IF	Immunofluorescent
IHC	Immunohistochemistry
iPD	Incipient Parkinson's Disease
LB	Lewy body
LBD	Lewy Body Disease
LN	Lewy neurites
NABCA	Normal Aging Brain Collection Amsterdam
NCS	Newborn calf serum
NBB	Netherland's Brain Biobank
PARK7	Parkinsonism Associated Deglycase

PBS	Phosphate-buffered saline
PD	Parkinson’s Disease
PDD	Parkinson’s Disease dementia
PINK1	PTEN-induced kinase 1
PMD	*Postmortem* delay
PD PRS	Parkinson’s disease polygenic risk score
ROS	Reactive oxygen species
PRS	Polygenic risk score
PS-129	Phosphorylated alpha-synuclein (serine 129)
REC	Regional committee for medicinal and health research ethics
ROI	Region of interest
SDS	Sodium dodecyl sulfate
SN	Substantia nigra
SNCA	Synuclein alpha gene
TBST	Tris-buffered saline with 0.1 % tween
TE	Tris-EDTA
TH	Tyrosine hydroxylase
TSD	Services for sensitive data
VMAT2	Vesicular monoamine transporter 2
VTA	Ventral Tegmental Area
WB	Western blot
WT	Wild type

Table of contents

1. Introduction

1.1 Parkinson's Disease

1.1.1 Descriptive epidemiology

Parkinson's disease (PD) is the second most common neurodegenerative disease (1). The estimated prevalence of PD in industrialized countries is 0.3% in the general population (2). The prevalence of PD increases with age and affects 1.0 % of the population above 60 years, and 3.0 % of the population above 80 years (2, 3). Mortality increases after the first decade of disease onset and eventually doubles compared to the normal population (4). Patients with PD have significant morbidity and mortality, in which increase with disease duration (4). PD patients have an estimated mortality ratio of approximately 1.5 compared to control subjects, and approximately 5% decreased survival per year (5). Global Burden of Disease study projects that 12.9 million will be affected by PD by 2040, which is a doubling of cases from 2015, due to increased life expectancy in the general population (6).

1.1.2 Pathophysiology

Neuropathological findings of PD are neurodegeneration of predominantly dopaminergic neurons in substantia nigra (SN) pars compacta and their nerve terminals in striatum, and Lewy bodies (LB) or Lewy neuritis (LN), which are intraneuronal α-synuclein (α-syn)-containing protein aggregates (3, 7). The pathogenesis of PD is assumed to have its onset years prior to clinical debut. The pathology is hypothesized to first manifest in the brainstem and/or olfactory bulb, before progressing to SN and thereafter throughout large parts of the brain (8), see Braak staging below.

SN is a melanin rich dopaminergic nucleus located in mesencephalon, see figure 1, and is often accounted as a part of the basal ganglia (9). The dopaminergic neurons in SN normally project their nerve terminals to the striatal part of basal ganglia, and normal motor function is dependent on this dopaminergic innervation (10). The loss of dopaminergic neurons in PD causes dopamine deficiency in the motor centers of the brain, leading to the cardinal symptoms tremor, rigidity, bradykinesia, and postural instability (10, 11).

A B

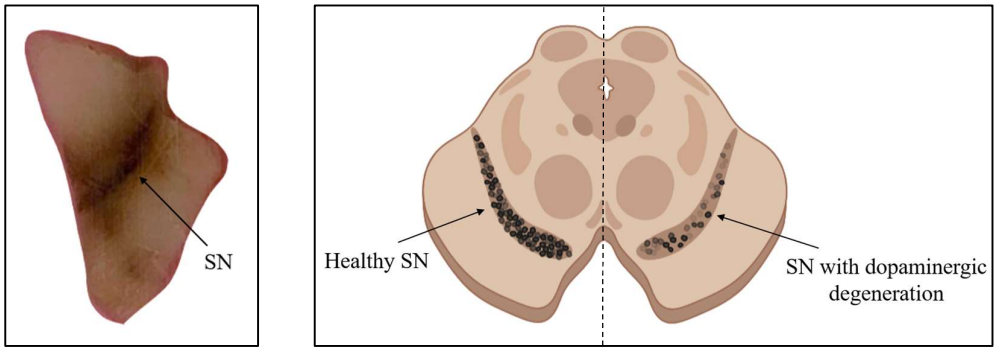

Figure 1. A) *Paraffin embedded mesencephalon received from collaborators illustrating the visible neuromelanin rich area of SN. Image obtained by Siri Egenæs.* ***B)*** *Mesencephalon with SN. Left side represents SN in a healthy individual, showing dark pigmented SN. Right side represents a PD SN, showing remarkably less pigmentation due to degeneration of neuromelanin-containing dopaminergic neurons. Image obtained from BioRender, edited by Siri Egenæs.*

The precise mechanism behind the specific loss of dopaminergic neurons is still unknown, although several pathophysiological mechanisms have been studied. It is believed that the dopaminergic neurons in SN are more susceptible to toxic effects from α-syn and mitochondrial reactive oxygen species (ROS), and therefore are more prone to degenerate (12). This susceptibility could be caused by the total burden of by both mitochondrial ROS, oxidative stress created by monoamine oxidase in dopamine metabolism, as well as ROS and other pro-inflammatory substances released by pro-inflammatory activated microglia (see section 1.2.1) (13, 14). ROS can affect different processes within the neuron, i.e., lysosome function and protein degradation, reduce adenosine triphosphate (ATP) production and increase accumulation of α-syn (12, 15). In addition, several age-related changes are also thought to promote the death of neurons in SN, i.e., mitochondrial defects due to accumulation of mutations in mitochondrial genes and oxidative stress (12).

Further, evidence suggests α-syn affects several key elements in dopamine homeostasis, see figure 2 (13). The synthesis of dopamine occurs in the cytoplasm of presynaptic dopaminergic terminals (13). Tyrosine is the precursor molecule, enzymatically synthesized into dopamine by tyrosine hydroxylase (TH) and amino acid decarboxylase (AADC) (13, 16). Prior to synaptical release, dopamine is sequestered from cytosolic space into synaptic vesicles by the enzyme vesicular monoamine transporter 2 (VMAT2) (17, 18). Dopamine transporter (DAT) is responsible for reuptake of dopamine from the synaptic cleft (18). Decreased vesicle

trafficking when α-syn is overexpressed has been reported, possibly by reducing the activity of VMAT2 (13, 19). *In vivo* imaging of PD brains showed a reduction in VMAT2 (17, 20), in which would be a natural cause of dopaminergic neurodegeneration. However, the reduction of VMAT2 in PD brains was too great to be explained solely by the loss of dopaminergic neurons (17), suggesting VMAT2 as a part of the pathogenesis in PD.

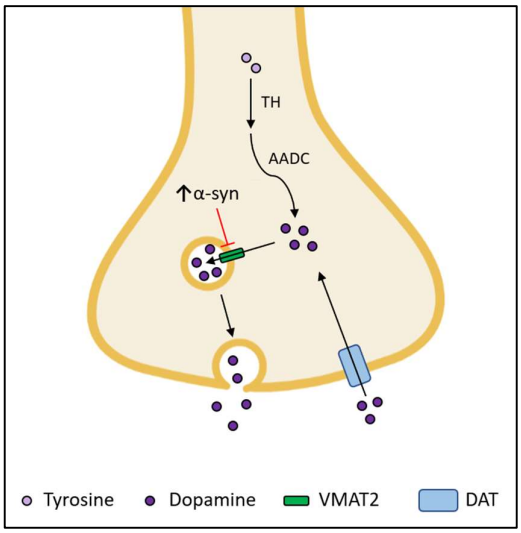

Figure 2. *Simplified illustration of dopamine homeostasis in the presynaptic terminal of dopaminergic neurons. Tyrosine is synthesized to dopamine by TH and AADC (21) . VMAT2 packs dopamine from cytosol into vesicles for release presynaptically. DAT reuptakes dopamine from the synaptic cleft. Overexpression of α-syn may affect VMAT2 by decreasing its sequestering activity, leading to reduced vesicular release (17, 19). Studies have also shown affection of DAT, TH and AADC by α-syn, resulting in less available dopamine (13). Image obtained from BioRender, edited in Microsoft PowerPoint by Siri Egenæs.*

There are also non-motor symptoms in PD, such as depression, pain, sleep disorders, problems with cognition and constipation (22, 23). These non-motor symptoms can manifest at earlier stages during disease progression and are caused by disturbed neurotransmission in different parts of the brain than SN (24, 25).

1.1.2.1 α-syn and post-translational modifications

The protein α-syn is abundantly present in presynaptic neurons, but also in skeletal muscles and the heart (1). Its biological function in health is not completely identified, although α-syn is known to have a role in modulating neuronal membrane stability, presynaptic signaling, vesicular transport, and neuronal plasticity (13, 19, 26). The exact role of α-syn in

neurodegeneration is poorly understood, although its role in PD is genetically proved (26, 27). In PD, it is known that α-syn accumulates intracellularly, mainly in neurons, and there is evidence of α-syn spreading to other neurons by cell-to-cell transfer (28). Further, both the dopamine homeostasis and activation of the immune system seems to be affected by α-syn (13, 29).

Once aggregated, α-syn has a neurotoxic role by impairing subcellular functions and promoting neuronal death (30). Different structures of α-syn can affect mitochondrial dysfunction and vice versa (30). The mechanism of aggregation of α-syn is still unknown (31). One specific region of the α-syn protein is relatively hydrophobic and aggregates in humans, but not in mice α-syn (27).

In PD, several posttranslational modifications, such as phosphorylation and nitration, can occur to α-syn. These posttranslational modifications may be critical in the pathogenesis of PD, namely phosphorylation at $Serine^{129}$ (phosphorylated α-syn, PS-129) (32). The PS-129 isoform enhances the neurotoxicity of α-syn, possibly by increased aggregation of α-syn, although a protective role has also been suggested (32). In PD brains, PS-129 is the most prevalent posttranslational modification form of α-syn, accounting for approximately 90% of the total amount of α-syn (33). On the contrary, only 4% of the total amount of α-syn is PS-129 in healthy individuals (33, 34).

Previous studies have also suggested that α-syn neurotoxicity in PD may result from an imbalance of PS-129 and a neuroprotective isoform of α-syn phosphorylated at tyrosine 125, that inhibit toxic oligomer formation (35).

1.1.3 Braak staging

LBs seem to spread in a topographically predictable pattern throughout the brain, classified by the Braak stages of PD (8, 36). The LB Braak stage is a scale ranging from 0 to 6, where 0 is no LBs, and 6 is LBs abundantly spread throughout the brain, see figure 3. The spreading of LB throughout the PD trajectory is likely caused by prion-like propagation of misfolded α-syn

(27). Misfolded α-syn seems to act like a template, transmitting its structure and aggregation proneness to healthy α-syn, thereby transmitting diseased proteins to new parts of the brain (27, 37, 38). As LBs are associated with PD, Braak staging serves as an appropriate system to describe the neuropathological disease development in PD patients.

Initially, LBs occur in the dorsal motor nucleus of the vagal nerve and the olfactory bulb (Braak PD stage 1) (8, 36). Then, Lewy neurites (LN) and/or LB spread to medulla oblongata (Braak PD stage 2). At Braak stage 1 and 2, patients are asymptomatic. At LB Braak stage 3 and 4, LBs spread to the SN, forebrain and temporal mesocortex (8, 36). By this time, the patients normally start to show symptoms of PD. Thereafter, the pathological process reaches neocortex (Braak PD stage 5), high order sensory association and prefrontal areas (Braak PD stage 6) (8, 36).

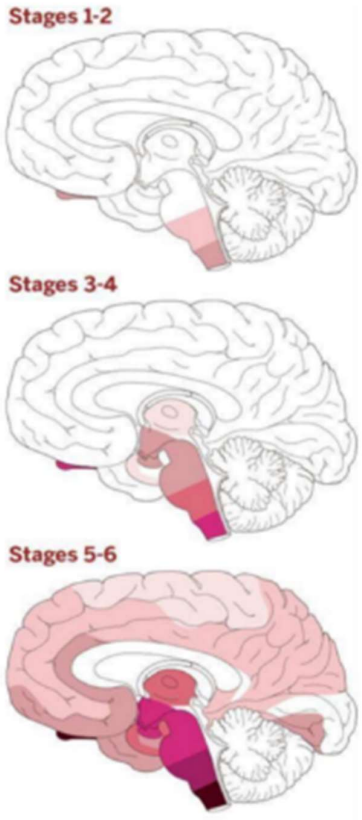

Figure 3. *The spreading pattern of LBs at different Braak stages represented by pink (mild LB affection) to dark red (extensive LB affection). The figure is from Goedert, M (2015).*

1.1.4 Anterior cingulate cortex

Anterior cingulate cortex (ACC) is the anterior part of gyrus cingulate located in neocortex, see figure 4, and is responsible for higher cognitive functions, emotions, and learning (21, 25, 39). Neocortex is a part of the mesocortical pathway, innervated by dopaminergic neurons projecting from ventral tegmental area (VTA) (40). Neocortex is affected by LB pathology in late stages of the PD disease progression (Braak stage 5-6), which is the major cause of PD dementia (PDD) (8, 24). Despite the spread of LBs to neocortex late in the disease progression, studies have suggested that ACC is responsible for cognitive and memory impairment in PD, even in early stages of the disease progression (25). Due to altered dopamine transmission in the mesocortical pathway, ACC is also suggested to be involved in other non-motor symptoms of PD, such as facial apathy, visual hallucinations, as well as a potential underlying cause of depression in PD (25, 40).

Immunohistochemical staining of microglia in ACC tissue from PD patients has demonstrated an association between LBs positive for α-syn and pro-inflammatory activated (41). Hereby,

ACC is characterized by neuroinflammation similarly to SN, but not the same extensive neurodegeneration.

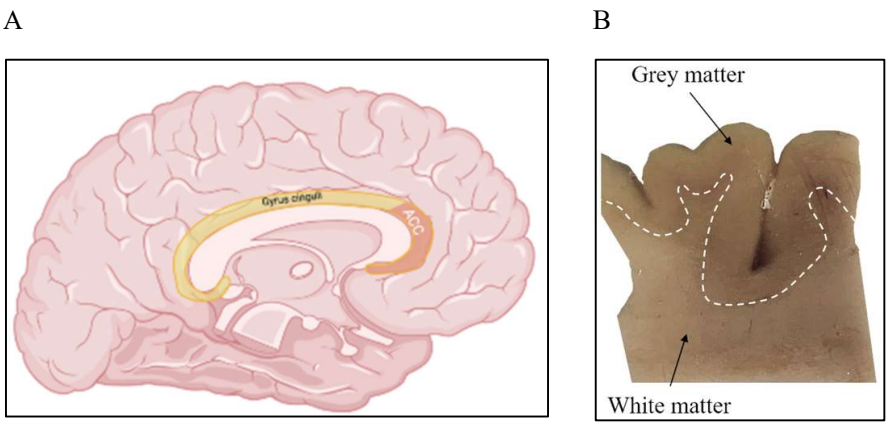

Figure 4 A) *Sagittal view of ACC in (orange) as a part of the gyrus cinguli (yellow). Image is made and edited in BioRender by Gezime Seferi.* ***B)*** *Image of paraffin embedded human ACC tissue showing both grey and white matter. Image captured by Siri Egencæs.*

1.1.5 Non-genetic risk factors

Age is considered to be the biggest risk factor for PD (2, 42). Studies have suggested the reason for this is age-related changes in SN dopaminergic processes that make the neurons susceptible to neurodegeneration (12). Epidemiologic studies have suggested several lifestyle behaviors associated with PD, including smoking, consumption of coffee and alcohol (43). Smoking has shown a 50% decrease in risk of PD (44). However, this association may be biased by reverse causation, as PD patients are more likely than healthy individuals to stop smoking in the prodromal phase of PD due to reduced dopamine and thereby reduced responsiveness to nicotine (45). Caffeine has a well-documented protective effect on PD (44). Other risk factors are exposure to pesticides, drugs, and brain microtrauma (23, 46).

The disease progression and phenotypical expression of PD is probably affected by biological sex (47). Male sex is considered as a moderate risk factor for developing PD (2). Although the risk of developing PD is twice as high in men than women, women have a higher rate of mortality and faster disease progression (47). In addition, symptoms and responsiveness to treatment differ between women and men (47).

1.1.6 Genetics of Parkinson's disease

There are monogenic and polygenic forms of PD, which accounts for 5-10 % and 90-95 % of all PD cases, respectively (44). Monogenic PD is caused by a single gene mutation in one of several genes that have been identified as important in autosomal dominant or autosomal recessive forms of PD (44). Monogenic cases of PD typically have early-onset with more extensive neuropathology (30). Polygenic forms of PD, also referred to as idiopathic or sporadic PD, are caused by single nucleotide polymorphisms in multiple genes associated with PD where the risk contribution of each polymorphism varies (48, 49).

In 2019, the fifth meta-analysis of genome wide association studies (GWAS) in PD was conducted. 90 risk loci for developing PD have so far been identified from more than 37.000 PD subjects, 1.4 million control subjects, as well as 17.000 individuals with a parent with PD (48). Studies have found that genes in monogenic and polygenic PD genes overlap, suggesting that both forms of PD have some common pathological mechanisms (50). By compiling the significant gene variants from the GWAS, it is possible to generate PD polygenic risk scores (PD PRS) (51). PD PRS can then be used as a prognostic tool to predict an individual's cumulative effect of genetic risk, and hereby identify patients with a high genetic risk of developing PD (51).

1.1.6.1 SNCA

The *SNCA* gene encodes for α-syn. As a presynaptic nerve terminal protein, α-syn was originally identified as a non-amyloid beta component of Alzheimer's disease (52). Mutations and polymorphisms in the gene coding for α-syn, SNCA, is strongly associated to PD pathogenesis for both familial and idiopathic forms of the disease (32). Multiplication of SNCA alleles results in familial PD due to excessive α-syn levels, and through SNCA mutations the important role of α-syn in PD was revealed (53, 54). There are several known pathogenic mutations in the α-syn protein, in which amino acid substitution can or will lead to changes in α-syn's tertiary structure depending on the mutation site (55). This misfolding exposes the hydrophobic parts of the molecule that are more prone to aggregation, thereby promoting the formation of LBs and disease progression (56).

1.1.6.2 PARK7

The *PARK7* gene encodes for the Parkinson's disease protein 7 (DJ-1) protein. DJ-1 is present in many cells and tissues, including neurons and glial cells in the brain (57). DJ-1 has multiple anti-oxidative stress effects protecting dopaminergic neurons against degeneration, i.e., by regulation of transcription, chaperone function, and ROS scavenger (58-60).

Mutations in DJ-1 were first associated with monogenic forms of PD, resulting in early onset of PD (60, 61). Later, DJ-1 has also been associated with idiopathic PD (61, 62). WT DJ-1 forms soluble dimers, while mutant forms of DJ-1 misfolds causing impaired dimerization, thereby losing the ability to exert its biological functions (60, 63, 64). Further, the DJ-1 protein contains three cysteine residues important for antioxidant function, with C^{106} being the most essential for biological function (60). A mutation in C^{106} prevents self-oxidation and translocation to mitochondria, resulting in loss of neuroprotective effect of DJ-1 (63, 65).

The DJ-1 protein has been associated with several pathological mechanisms in PD. The chaperone actions of DJ-1 assure correct folding of proteins (57, 60). This protective effect is lost with DJ-1 mutations, thereby losing the effect of DJ-1 on inhibiting α-syn aggregation (60, 66). DJ-1 is also found to colocalize with toxic neurofibrillary tangles consisting of hyperphosphorylated tau in PD, which could be due to the chaperone activity of misfolded tau protein in PD (61, 67, 68). Mutations in DJ-1 are also shown to increase phosphorylation of tau, making tau more prone to aggregate (67).

1.1.6.3 PINK1/Parkin

PINK1 and Parkin are two proteins important for maintaining mitochondrial homeostasis by the same biochemical pathway (69, 70). The PTEN-induced kinase 1 (PINK1) is encoded by the *PARK6* gene, while *PARK2* encodes for Parkin (69). PINK1 is a kinase localized on mitochondria having a role in the removal of damaged mitochondria organelles by activation of Parkin (69, 71). Parkin is a E3 ubiquitin ligase which regulates the degradation of proteins by ubiquitinating, marking proteins with ubiquitin for degradation by proteasomes and lysosomes (7, 70, 71). Mutations in the PINK1 and Parkin proteins seem to make dopaminergic neurons susceptible for degeneration and cause early and juvenile onset of PD, respectively (70, 72).

1.1.7 Treatment for Parkinson's disease

All drugs for treating PD are based on the principle of restoring the dopamine balance, either with levodopa along with a decarboxylase inhibitor, in which inhibits the degeneration of levodopa enabling a larger amount the levodopa molecules to pass the blood-brain-barrier; dopamine receptor-2 agonists; Catechol-O-Methyltransferase (COMT-) inhibitors in which increases the effect on levodopa-decarboxylase treatment; Monoamine oxidase (MAO-B)-inhibitors (21). Treatment using these drugs will improve the motor symptoms of PD but have not been proved to slow the disease progression. Hence, new approaches are needed. In order to develop neuroprotective therapies more insight about what molecular events causing neurodegeneration, e.g., microglia's role in neuroinflammation and α-syn clearance, is needed.

PD patients lacking adequate control using levodopa therapy with significant motor symptoms can be treated by deep brain stimulation (DBS) (73). DBS is a surgical procedure where electrodes inhibiting overactive areas are implanted in the subthalamic nucleus and/or globus pallidus interna depending on the patient's symptoms (73, 74). However, DBS can worsen depression and psychiatric disorders (73).

1.2 Neuroinflammation in Parkinson's Disease

Neuroinflammation and activation of the immune system are key factors in the pathophysiology of neurodegeneration, which is a common pathological feature of several neurological diseases, such as Alzheimer's disease and PD (75). Both animal and human PD studies have indicated that neuroinflammation occurs early in the PD trajectory (76, 77), but it remains unclear whether neuroinflammation is a cause or result of neurodegeneration.

Microglia are central nervous system (CNS)-resident innate immune cells vital in maintaining CNS homeostasis by phagocytosis and releasing mediators of immune response (29, 78-80). Although the immune response of microglia during inflammation is a beneficial process for neural health, excessive pro-inflammatory activation may contribute to neurodegeneration (80).

1.2.1 Microglial phenotypes and their role in neuroinflammation

During disease progression and microglial activation, the microglial cells change morphology and receptor expression (81). Different phenotypes of microglia have been identified on the

basis of these changes, in which include ramified (resting) microglia, primed/reactive microglia and amoeboid microglia (81).

In healthy brains, microglia are in a resting state scanning the environment for potential neuronal threats by continuously extending and retracting their processes, hereby contributing to neuronal health and survival in the central nervous system (78, 82, 83). Ramified microglia are characterized by a small cell body with many thin ramifications (80, 81).

Several pathologic events or change in brain homeostasis can change the microglial activation state (83). Reactive microglia can exhibit either a neurotoxic or neuroprotective phenotype, see figure 5 (80). Anti-inflammatory activation supports anti-inflammatory responses by phagocytosis and secretion of anti-inflammatory cytokines, such as interleukin-(IL) 4, IL-10 and IL-13 among others (28, 84). Anti-inflammatory IL-4 and IL-13 suppress the production of pro-inflammatory cytokines, hereby protecting neurons from injury (85).

Anti-inflammatory microglia (and reactive astrocytes) also release glial-derived neurotrophic factor (GDNF) and brain-derived neurotrophic factor (BDNF), in which seem to be the most potent factors in supporting SN dopaminergic neurons (41, 86). GDNF's neurotrophic mechanism of action is complex, involving at least four different pathways, one of which induce kinase activity in pathways promoting cell survival, differentiation, growth and synaptic plasticity (87). In animal models, GDNF is shown to protect and promote regeneration of dopaminergic neurons in mesencephalon, hereby being a potential neuroprotective therapy for PD (87-89). Despite the neurotrophic effects seen in animal models, clinical trials of administration of GDNF into SN in PD patients have not met the primary endpoints, although demonstrating a beneficial effect in some patients (90).

Fractalkine is a chemokine that can modulate neuroinflammation caused by microglia (77). Previous studies have demonstrated a high level of fractalkine in early PD stages, and lower levels with disease progression (91). Herby, fractalkine is indirectly connected to the loss of dopaminergic neurons in PD via modulation of microglial activation (77).

Injury, stress or disease can lead to microglial pro-inflammatory activation, in which changes microglial morphology and function (92). When pro-inflammatory activated, microglia transform towards an amoeboid shape with a less round cell body and fewer, thicker and shorter ramifications (81). The pro-inflammatory activated microglia are shown to contribute to neuroinflammation in PD by secreting factors such as pro-inflammatory substances that lead to neurotoxicity and attenuate microglial phagocytosis, as well as ROS (81, 85). IL-6 is a

pro-inflammatory mediator released by microglia, seemingly in the early stages of PD (76). Polymorphisms in the pro-inflammatory chemokine monocyte chemoattractant protein-1 (MCP-1) are associated with PD (93). MCP-1 induce chemotaxis of other pro-inflammatory factors and cells, enhancing their expression, further contributing to the neuroinflammation in PD (94).

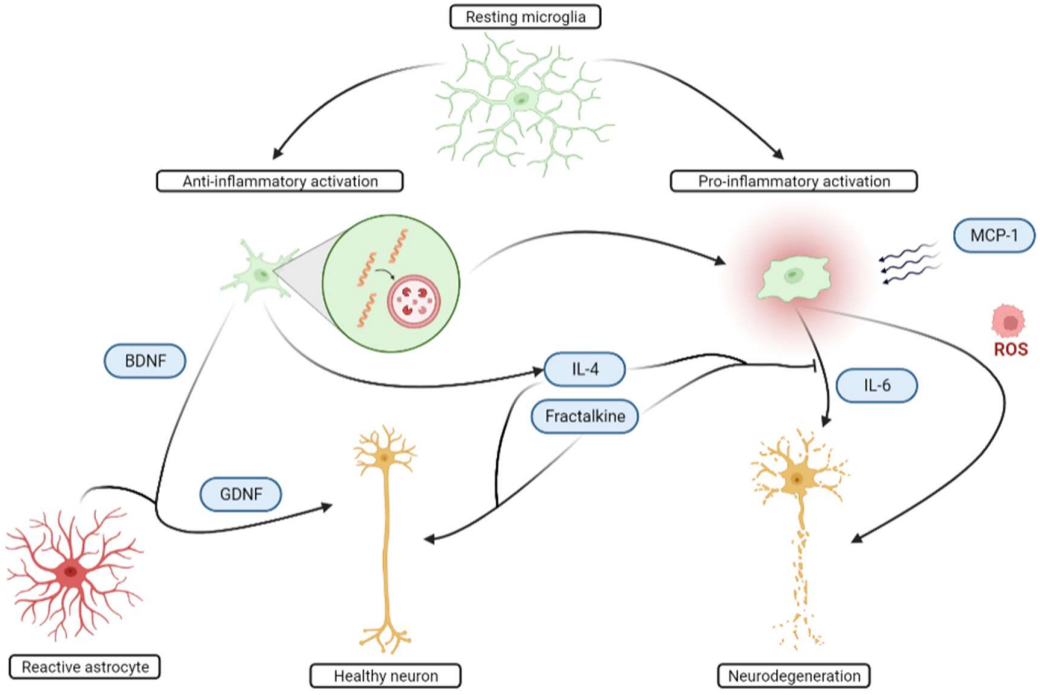

Figure 5 *Microglial activation states and involvement in neuronal health and -degeneration. Ramified microglia become reactive when triggered by the microenvironment, leading to an anti-inflammatory or pro-inflammatory activation (80). Anti-inflammatory microglia secrete anti-inflammatory cytokines, such as IL-4, and the neurotrophic factors BDNF and GDNF (84, 89). GDNF is also secreted by reactive astrocytes (76). Neurotrophic factors promote neuronal health, while IL-4 and fractalkine modulate neuroinflammation by inhibiting the release of pro-inflammatory cytokines (41, 85). When pro-inflammatory activated, microglia gain an amoeboid shape and release pro-inflammatory factors and generate ROS, in which promote neurodegeneration (85). MCP-1 enhances the pro-inflammatory response by chemokine activity (94). Synucleinphagy is shown as a clearance pathway of α-syn. Excessive accumulation of α-syn leads to a pro-inflammatory activation (29). The figure is made by Siri Egenæs in BioRender.*

1.2.2 Microglial clearance of α-syn

Microglia contributes to regulation of deposition and spreading of α-syn, thereby having an essential role in the disease progression of PD as LBs and LNs consist mainly of aggregated α-syn (29, 36). Previous studies have provided evidence for the cell-to-cell transfer of aggregation prone α-syn (95). For this to happen α-syn must be released extracellularly and be

engulfed by other cells (95). Neurons can release internalized α-syn extracellularly as a response to stress, injury, or stimulation (29). When α-syn is present in extracellular space, microglia can engulf α-syn by selective autophagy, called synucleinphagy, via the TLR-4-NF-kB-p62 pathway demonstrated by *in vitro* and *in vivo* in animal models (29). The downstream effect of this pathway is ubiquitination of α-syn, leading to degradation by lysosomes (29). Increased α-syn accumulation and dopaminergic degeneration was seen in the same study when synucleinphagy was interrupted in mice expressing human α-syn (29). Synucleinphagy leads to pro-inflammatory activation of microglia, in which have been shown to have less efficient clearance of α-syn (29).

2. Aims of the study

This study aims to investigate the involvement of microglial activation and α-syn clearance in the PD trajectory represented by human tissue from control subjects with low and high PD PRS, pre-clinical subjects with LBs (incipient PD) and established PD. Even though microglia are thought to have a key role in PD through favorable α-syn clearance, but potentially also neuroinflammation. It remains unknown whether neuroinflammation is a primary factor initiating cell death, or a secondary factor due to cell death. If neuroinflammation is a primary and significant cause of neurodegeneration, neuroprotective therapies must be initiated prior to pronounced neurodegeneration. Therefore, the onset of neuroinflammation is crucial to establish.

The total α-syn and PS-129 load, microglial autophagy of α-syn and PS-129 and microglial activation states will be investigated by Luminex, enzyme-linked immunosorbent assay (ELISA), western blot and immunohistochemistry staining and confocal imaging. Neurotrophic or neurodegenerative markers will be measured as possible measures of neuronal health related to microglial activation and clearance efficiency.

- The degree of immune activation and how early immune activation occurs in the PD trajectory.
- Whether immune activation is a result of neurodegeneration, or if immune activation occurs without neurodegeneration.
- How total α-syn and PS-129 load are related to disease stage and microglial activation and microglial α-syn and PS-129 clearance efficiency.

3. Materials and methods

Table 1. *List of chemicals, reagents and kits used in the study.*

Chemicals	**Manufacturer**
2-Mercaptoethanol	Sigma-Aldrich, USA
Bovine Serum albumin	Sigma Aldrich, USA
Ethanol	Antibac, Norway
Formic acid	Sigma Aldrich
Neo-Clear^{TM}	Merck, USA
Newborn Calf Serum	Merck, USA
PBS Tablets	Thermo Fisher Scientific, USA
Skim Milk Powder	Sigma-Aldrich, Switzerland
Sodium citrate dihydrat	Sigma Aldrich, USA
TBS-Tween ^{TM} tablets	Medicago, Sweden
Tris-EDTA buffer solution	Sigma Aldrich, USA
Tris/SDS/Glycine buffer	Bio Rad, USA
Triton X-100	Sigma Aldrich, USA
Reagents	**Manufacturer**
4,6-diamidino-2-phenylindole (DAPI), D9542-5MG	Sigma-Aldrich, USA
Anti-alpha-synuclein (mouse)	BD BioSciences, USA
Anti-GAPDH	Sigma Aldrich, USA
Anti-GFAP chicken	Merck, USA
Anti-GFAP mouse	Cell signaling technology, USA
Anti-Iba1 goat	Abcam, UK
Anti-Iba1 rabbit	Wako, Japan
Anti-Alpha-synuclein (phosphor S129)	Abcam, UK
Alexa Fluor^{TM} 405 Donkey anti-Mouse	Thermo Fischer Scientific, USA
Alexa Fluor^{TM} 488 Donkey anti-Chicken	Thermo Fischer Scientific, USA
Alexa Fluor^{TM} 488 Donkey anti-Goat	Thermo Fischer Scientific, USA
Alexa Fluor^{TM} 594 Donkey anti-Mouse	Thermo Fischer Scientific, USA
Alexa Fluor^{TM} 647 Donkey anti-Rabbit	Thermo Fischer Scientific, USA
ECL^{TM} Prime Luminol Enhancer Solution A	Cytiva, Italy
ECL^{TM} Prime Peroxide Solution B	Cytiva, Italy
Donkey anti-goat IgG (H+L), Secondary antibody, HRP	Thermo Fisher Scientific, USA

Goat anti-Mouse IgG (H+L), Secondary antibody, HPR	Thermo Fisher Scientific, USA
Goat anti-Rabbit IgG (H+L), Secondary antibody, HPR	Thermo Fisher Scientific, USA
Laemmli Sample Buffer, #1610747	BioRad, USA
Prolong Gold Antifade Mountant	Thermo Fisher Scientific, USA
SIGMAFAST ™ Protease inhibitor tablets	Sigma Aldrich, USA
Restore™ PLUS Western Blot Stripping Buffer	Thermo Fischer Scientific, USA
Super Pap Pen Large	Electron Microscopy Sciences, USA

Kits	**Manufacturer**
Human magnetic Luminex Treg Cytokine Array Kit-12 Plex (CAR-K-LX-128)	Creative Biolabs, England
Human NFL ELISA kit	MyBioSource.com, USA
Human VMAT2 ELISA kit	MyBioSource.com, USA
Pierce™ BCA Protein Assay Kit	ThermoFisher Scientific, USA
Trans-Blot Turbo Mini 0.2 µm PVDF Transfer Pack	Bio-Rad, USA

3.1 Study design

To answer the research questions, a cross sectional design representing the disease development from healthy, pre-clinical/incipient LBD and established PD. All patients were selected based on their clinical characterization, neuropathological characterization and PD PRS, in addition to age, sex and *post mortem* delay (PMD) when tissue availability allowed. The PD group was significantly younger than both iPD ($p < 0.05$, ANOVA with Bonferroni correction) and controls ($p < 0.05$, ANOVA with Bonferroni correction).

Information about every study subject was received which included available data about autopsy, anamnesis, and lifestyle. Human brain tissue from the included subjects was obtained from to Dutch brain banks – The Netherland's Brain Bank Netherlands (NBB) and Normal Aging Brain Collection Amsterdam (NABCA) through collaborators. The received brain tissue came in different forms, both freshly frozen and paraffin embedded fixed tissue. Characteristics of the subject groups based on these tissue subgroups are presented in table 2 and 3.

Table 2 *Between-group comparisons of subject and tissue quality characteristics of cohort with paraffin embedded postmortem brain tissue*

	Groups based in genetic, neuropathological, and clinical staging (n=36)				**Statistical tests**				
	Controls (n)		**iPD (14)**	**PD (10)**	***F* / χ^2 / η^2 / *(p)***	**Low- *vs* high-risk**	**Ctr *vs* iPD**	**Ctr *vs* PD**	**iPD *vs* PD**
	Low-risk (6)	**High-risk (6)**							
Age Mean (SD)	90.5 (7.8)	81.2 (8.2)	85.1 (7.0)	76.7 (7.6)	*F*=4.8 η^2=.31 (**<.05**)	‡n.s.	‡n.s.	‡**<.05**	‡**<.05**
Sex Female n (%)	4 (66.7)	6 (100.0)	10 (71.4)	5 (50.0)	χ^2=0.1, (n.s.)	*	*	*	*
Brain weight Mean (SD)	1050.4 (85.0) n=5	1096.3 (50.2) n=3	1162.8 (93.4) n=10	1264.6 (124.8) n=10	*F*=5.6, η^2=.41 (**<.01**)	‡n.s.	‡n.s.	‡**<.01**	‡n.s.
PD PRS Mean (SD)	-0.0214281 (0.001262) n=6	-0.0121206 (0.001755) n=6	-0.0187196 (0.002940) n=13	-0.0166984 (0.004416) n=3	*F*=13.8 η^2=.6 (**<.001**)	‡**<.001**	‡n.s.	‡n.s.	‡n.s.
LB Braak Mean (SD)	0 (0)	0 (0)	3.5 (0.9)	5 (0.8)	*F*=91.0, η^2=.9 (**<.001**)	‡n.s.	‡**<.001**	‡**<.001**	‡**<.01**
PMD Mean (SD)	432.5 (182.3)	445 (70.9)	397.5 (112.6)	436 (149)	*F*=0.3, η^2=.03 (n.s.)	*	*	*	*
Tissue pH Mean (SD)	6.69 (0.14) n=5	6.64 (0.13) n=2	6.54 (0.26) n=10	6.58 (0.27) n=10	*F*=0.4, η^2=.05 (n.s.)	*	*	*	*

*Abbreviations: PD, Parkinson's disease; iPD, incipient PD; ctr, control; SD, standard deviation; n, number of cases; %, percentage; PD PRS, PD polygen risk score; LB Braak, Lewy body Braak staging; PMD, post mortem delay; n.s., non-significant; F, F statistic; χ^2, chi square statistic; η^2, eta-squared; vs, versus; *, no post-hoc comparisons performed; †, no value; ‡ ANOVA post-hoc. All p values are Bonferroni corrected.*

Table 3. *Between-group comparisons of subject and tissue quality characteristics of cohort with fresh frozen brain tissue.*

	Groups based in genetic, neuropathological, and clinical staging (n=22)					**Statistical tests**	
	Controls (9)		**LBD (13)**		***F* / χ^2 / η^2 / *(p)***	**Low- *vs* high-risk**	**Ctr *vs* LBD**
	Low-risk (5)	**High-risk (4)**	**iPD (12)**	**PD (1)**			
Age Mean (SD)	91.0 (8.6)	77.0 (6.5)	84.3 (6.7)		F=4.3, η^2=.31 (**<.05**)	‡**<.01**	‡n.s.
Sex Female n (%)	4 (80.0)	4 (100.0)	9 (69.2)		χ^2=0.2, (n.s.)	*	*
Brain weight Mean (SD)	1033 (87.2) n=4	1041 (†) n=1	1141.33 (94.5) n=9		F=2.1, η^2=.28 (n.s.)	*	*
PD PRS Mean (SD)	-0.0214514 (0.001409) n=5	-0.0121103 (0.001413) n=4	-0.0190130 (0.003109) n=11		F=16.0, η^2=.65 (**<.001**)	‡**<.001**	‡n.s.
LB Braak Mean (SD)	0 (0)	0 (0)	3.6 (1.0)		F=59.6, η^2=.86 (**<.001**)	‡n.s.	‡**<.001**
PMD Mean (SD)	451 (197.5)	476.3 (66.0)	401.5 (106.7)		F=0.7, η^2=.06 (n.s.)	*	*
Tissue pH Mean (SD)	6.7 (0.2) n=3	† (†) n=0	6.5 (0.3) n=9		F=1.5, η^2=.13 (n.s.)	*	*

*Abbreviations: PD, Parkinson's disease; iPD, incipient PD; ctr, control; SD, standard deviation; n, number of cases; %, percentage; PD PRS, PD polygen risk score; LB Braak, Lewy body Braak staging; PMD, post mortem delay; n.s., non-significant; F, F statistic; χ^2, chi square statistic; η^2, eta-squared; vs, versus; *, no post-hoc comparisons performed; †, no value; ‡ ANOVA post-hoc. All p values are Bonferroni corrected.*

The study population can be divided into two main groups based on neuropathological findings postmortem: control subjects and subjects with LBD. The control group consists of patients without LBs (Braak stage 0). The control group can be further divided into the subgroups of low-risk controls and high-risk controls. The LBD group are patients with neuropathological findings of LBs. The LBD group can also be divided into two subgroups: patients with clinically established PD and patients with incipient PD (iPD). The iPD group had neuropathological findings consistent with LBD (Braak stage 2-5) but did not have a clinical diagnosis of PD while alive. See figure 6 below for an overview of the study design.

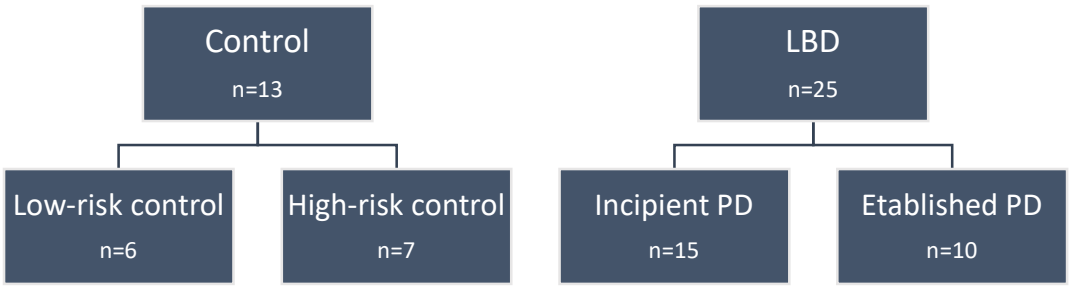

Figure 6 *Schematic overview of the study design representing a cross sectional version of the PD trajectory.*

The division of low-risk and high-risk controls are based on the mean polygenic risk score (PD PRS) of a cohort of control subjects (n = 302) analyzed by MD PhD Lasse Pihlstrøm and Prof. Mathias Toft. Low risk controls have a PD PRS lower than PD PRS_{mean} - 1 SD, while high risk controls have a PD PRS higher than PD PRS_{mean} + 1 SD, see figure 7.

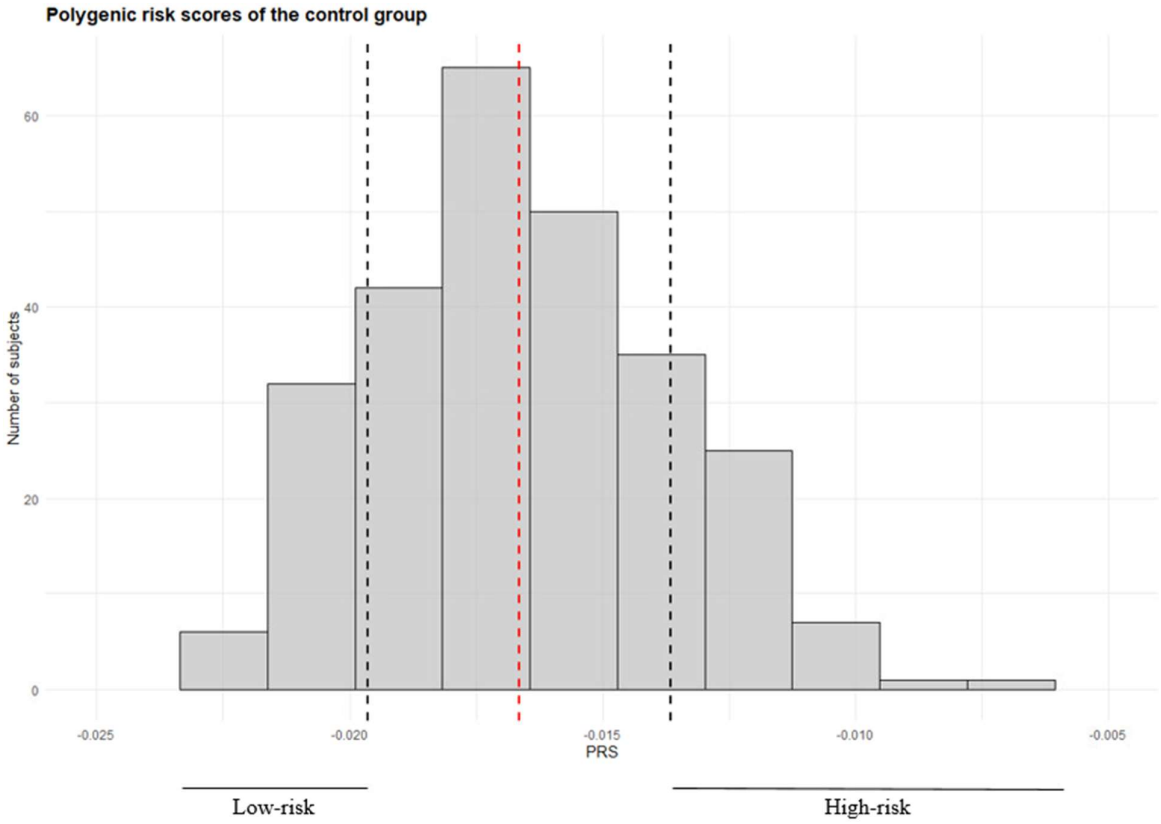

Figure 7. *Polygenic risk scores of the control group (n=302) with red dashed line indicating the mean PD PRS (-0.016643716). The black dashed lines indicate PD PRS$_{mean}$± 1 SD. Subjects with more extreme PD PRS than the black dashed lines represent low-risk controls (PD PRS < -0.0196352344) and high-risk controls (PD PRS > -0.0136521976).*

3.1.1 Tissue treatment

At NABCA and NBB, the left hemisphere and left brainstem were dissected and snap-frozen and stored at -80 °C (96, 97). The right hemisphere and right brainstem were formalin fixed for 3-4 week at NABCA and 4 weeks at NBB prior to dissection (96, 97).

Freshly frozen tissue of mesencephalon and ACC was received from the patients in which it was available. All freshly frozen tissue from NABCA was small and anatomically unrecognizable. while the freshly frozen tissues from NBB were larger. The freshly frozen tissue from NBB was dissected by Kaja Nordengen to ensure that all mesencephalon tissue samples included a part of SN. After dissection, some tissue samples were put in fixation for 24 hours prior to paraffin embedding at the Department of Pathology, Oslo University Hospital RadiumHospitalet.

3.2 Animals

Four female wild type (WT) mice (16 weeks of age) were obtained from collaborators at the Department of Comparative Medicine (KMP). The mice were euthanized in a carbon dioxide chamber and decapitated. The brains were removed, and the midbrain and ACC were dissected out on ice. Peripheral organs were removed, put in tubes, and immersed in liquid nitrogen.

3.3 Homogenization and sonication

The tissue of both humans and mice was homogenized and sonicated to be used for Luminex, Enzyme-linked Immunosorbent Assay (ELISA) and western blotting. All tissues were weighed and transferred to new 1.5 ml Eppendorf tubes (Eppendorf, Germany), which were kept on ice. Tris-EDTA (TE)-buffer containing protease inhibitor (Sigma Aldrich, USA) was added in an amount equal to 10% of the tissue weight. A plastic pestle was used to homogenize brain tissue for approximately 30 seconds. Non-brain tissue required more than 30 seconds of homogenization and were treated sequentially with the pestle and placed back on ice until sufficiently homogenized.

Subsequently, the samples were diluted 1:1 with a TE-buffer containing 4% sodium dodecyl sulfate (SDS). The samples were then run at least ten times through a 21G cannula and syringe. Using a water bath, the homogenates were heated for 5 minutes at 95°C.

Because several proteins of interest, such as GDNF and DJ-1 (98, 99), are localized in the nucleoplasm, sonication was performed to solubilize the nuclear membranes. Sonicators produce ultrasonic sound waves, causing tissue to disrupt due to mechanical stress. 100-400 µl of the homogenate depending on the remaining volume of the samples was transferred to 1.5 ml Bioruptor® Microtubes (Diagenode, USA) with Caps for Bioruptor® Pico. The tubes were sonicated in Bioruptor Rico (Diagenode, USA) for four cycles, with each cycle having 30 seconds on-time, 30 seconds off-time.

The water bath was kept at 4°C by the Minichiller 300 (Diagenode, USA). Because ultrasonic waves produce heat, there was a pause for at least ten minutes between each round of sonication. While not being sonicated, all samples were kept on ice. After sonication, all samples were transferred back to their tubes and mixed with a syringe, before making aliquots

of 450 µl in 0.5 ml PCR tubes (Eppendorf, Germany). Some samples were kept at -20°C until they were sonicated, while others were sonicated directly after homogenization. All samples were stored at -80°C subsequent to sonication.

The largest pieces of brain tissue, as well as peripheral mouse organs, were difficult to get completely homogenized using the plastic pistil and syringe. Before pooling the sonicated homogenate and aliquoting, these samples were sonicated multiple times until the solution was equally homogenized as the other samples.

3.4 Protein measurement

The protein concentration in the homogenates had to be determined prior to quantitative techniques to ensure a comparable level of protein between samples. Both BCA-assay and NanoDrop were used to measure the protein concentration in homogenates.

3.4.1 NanoDrop

Human tissue samples for western blotting were protein measured using the Protein A280 program on NanoDrop 2000C Spectrophotometer (Thermo Fisher Scientific, USA). NanoDrop measures absorbance and hereby protein concentration by Beer's law.

TE-buffer was added as a blank sample in order to adjust for absorbance caused by the diluent in the homogenates. Then, 1,5 µl of each sample was pipetted onto the measurement pedestal. Each sample was analyzed at least three times due to variations in measurements. The measurement pedestal was wiped off in between each application. The final protein concentration of a sample was set to the mean of the measurements. All samples were kept on ice during the protein measuring.

Protein concentration of the tissue homogenate prior to ELISA and Luminex was measured using the same procedure as described above using NanoDrop One (Thermo Fisher Scientific, USA).

3.4.2 BCA-assay

The 96-well plate (Thermo Fisher Scientific, USA) and Pierce^{TM} BCA Protein Assay Kit (Thermo Fisher Scientific, USA) was used to detect and measure the protein concentrations in

the mice tissue. This technique is based on the color change due to the reduction reaction of Cu^{2+} to Cu^{1+} caused by added amino acid residues, enabling colorimetric detection (100).

10 µl of the standards and 5 µl of 1:20 diluted samples were added to the wells according to the pre-determined plate-setup. A total of 200 µl BCA Protein Reagent A (Thermo Scientific, USA) and BCA Protein Reagent B (Thermo Fisher Scientific, USA) were mixed in a 50:1 ratio and added to the wells. The plate was then incubated in 37°C for 60 minutes with a lid. The CLARIOstar microplate reader (BMG Labtech, Germany) was used to measure the absorbance at 562 nm. The linear standard curve generated by the absorbance and protein concentration of the bovine serum albumin (BSA) standards was used to calculate the protein concentration in the samples.

3.5 Western blotting

Western blotting is a technique using antibodies to identify, test antibody specificity and estimate quantities of expressed proteins extracted from tissues or cells (101). In western blotting, proteins in homogenate are separated by molecular weight using gel electrophoresis. The proteins are transferred from the gel to a membrane and can then be identified by primary and horseradish peroxidase (HRP)-conjugated secondary antibodies diluted in blocking solution (102).

Samples were prepared for western blotting by diluting the homogenates with TE-buffer to a final protein concentration of 2 µg/µl for the use of anti-α-syn and anti-PS-129, and 1 µg/µl for the use other all other antibodies. Samples were prepared using Laemmli Sample Buffer (Bio-Rad, USA) and 2-Mercaptoethanol (Sigma Aldrich, USA).

Different approaches were made in order to optimize the conditions for antibody specificity, i.e., different blocking solutions, concentration of primary antibodies and amount of protein loaded to the gels were tested.

One sample from each patient was loaded to wells in gels. After gel electrophoresis, the gel was blotted to a membrane using the Trans-Blot Turbo Transfer System (Bio-Rad, USA) at 2.5 A and 25 V for 30 minutes.

After gel electrophoresis and blotting, the final membranes presented in this study were blocked in dry milk for 1 hour and incubated with primary antibody diluted in dry milk overnight at 4°C to prevent nonspecific protein-interactions. The membranes were then

incubated with primary antibody overnight in 4°C. The following day, the membranes were washed with Tris-buffered saline with 0.1% tween (TBST) (Medicago, Sweden) prior to and after 1 hour incubation with secondary HRP-conjugated antibody diluted in dry milk. Chemiluminescent reagents ECL™ Prime Luminol Enhancer Soulation A (Cytiva, Italy) and ECL™ Prime Peroxide Solution B (Cytiva, Italy) were added to the membranes before image acquisition using the ChemiDoc Touch Imaging System (Bio-Rad, USA).

3.5.1 Antibody validation

Antibody quality depends on the antibody and can differ between batches (103). To ensure reproducibility and specificity, antibody validation should be performed to validate new antibodies or new batches of antibodies (103). Antibodies that might be used at the IHC staining, were validated using western blotting. This included antibodies directed against Ionized calcium binding adaptor molecule-1 (Iba1) (produced in goat and guinea pig), α-syn, PS-129 and glyceraldehyde-3-phosphate dehydrogenase (GAPDH). To decide which tissues that were most likely to illustrate antibody specificity for the different antibodies, homogenates from mice tissues were selected based on The Human Protein Atlas (proteinatlas.org). All antibodies were tested with mice brain tissue, as well as the most promising tissue to not contain the protein in question according to protein atlas.

The final antibodies used for IHC were in addition tested with human brain homogenate. Final concentrations of antibodies and protein concentration per well used for antibody validation is summarized in table 4 below.

Table 4. *Concentration of primary antibodies, secondary antibodies and protein used for antibody validation.*

Antigen	Species	Primary AB concentration	Secondary AB concentration	Protein (µg/well)	Source, catalog number
α-syn	Mouse	1:500	1:80,000	20	BD Biosciences, #610787
PS-129	Rabbit	1:400	1:10,000	20	Abcam, ab51253
Iba1	Goat	1:1000	1:10,000	10	Abcam, ab5076
GAPDH	Rabbit	1:100,000	1:10.000	20	Sigma Aldrich, G9545

3.5.2 Semi quantitative Western blotting

20 µg protein was added to each well in a 10% Criterion™ TGX™ Precast Gel (Bio-Rad, USA). The samples were primarily sorted after increasing Braak stage. If multiple subjects had the same Braak stage, the study subjects were sorted after from lowest to highest age. PS-129 and α-syn were to be quantified using a monoclonal antibody against GAPDH as loading control. GAPDH is a so-called housekeeping protein involved in the glycolysis and is present in large amounts in almost all types of tissue (104).

During antibody validation, the signal from GAPDH was a lot stronger than the signal from α-syn and PS-129, causing GAPDH to override the signals from α-syn and PS-129. Therefore, the membrane was cut in half horizontally right above 25 kDa. The membrane with molecular weights higher than 25 was then used for GAPDH, and the lower part of the membrane with molecular weights below 25 was used for PS-129 and α-syn. The four membrane parts were treated identically at the same time. The image acquisition of GAPDH was performed prior to α-syn and PS-129 as the acquisition time for GAPDH was less than 5 minutes, leading to a minimal difference in treatment of the membranes.

Quantification of both α-syn and PS-129 was performed sequentially on the same membranes as the bands of the two target proteins would overlap if run simultaneously. The membranes were therefore stripped with Restore™ PLUS Western Blot stripping Buffer (Thermo Scientific, USA) for 7 minutes after each round and washed with TBST. The stripping procedure causes some protein loss from the membrane, which could cause problems with estimating quantities. Because PS-129 gave the weakest signal, PS-129 was quantified in the first run. Meanwhile, the GAPDH loading control was used to correct for the loss of protein during stripping.

The quantitative analysis was performed by measuring chemiluminescence signals of protein bands at 19 kDa for α-syn and 18 kDa for PS-129, as well as background above the bands. A region of interest equal to the largest band was used to measure all regions of interest. The background signal was subtracted from the band signal to correct for background. These measurements were normalized against the chemiluminescent signals for the loading control GAPDH-band at 36 kDa, in which was obtained in the same way.

3.6 Preparation of homogenate samples for ELISA and LUMINEX

Human brain tissue homogenate aliquots of 450 µl were transferred into 1,5 ml Eppendorf tubes. After protein measurement, all samples were spinned down at 16000xg for 4 minutes at 4°C using Centrifuge 5415 R (Eppendorf, Germany). Subsequently, all samples were diluted to 2,663 mg/ml with TE-buffer to a total volume of at least 450 µl, without including the pellet.

3.7 Enzyme-linked Immunosorbent Assay (ELISA)

ELISA was used for *in vitro* quantitative measurement of human vesicular monoamine transporter 2 (VMAT2) at Department of Medicinal Biochemistry, Oslo University Hospital Ullevål, and ran by specialist bioengineer Anne-Marie Siebke Trøseid.

The ELISA sandwich enzyme immunoassay kit for VMAT2 (MyBiosource.com, USA) is highly sensitive and specific for detection of VMAT2 in human tissue. The microtiter plate from the kit is pre-coated with a VMAT2 specific antibody. When samples are added with a biotin-conjugated antibody preparation specific to VMAT2. Avidin conjugated with HRP was added to each well before incubation for 15-25 minutes at 37°C. Biotin-conjugated antibody and enzyme-conjugated avidin cause the color to change only in the wells containing VMAT2. Addition of sulphuric acid terminates the enzyme-substrate reaction, and the color change is measured spectrophotometrically at a wavelength of 450 nm $\pm$ 10 with a VERSAmax tunable microplate reader (Molecular Devices, USA). The VMAT2-concentration can then be determined by comparing the optical density of the samples compared to the standard curve.

An ELISA sandwich enzyme immunoassay kit for neurofilament light chain (NFL) (MyBiosource.com, USA) was also performed following the same protocol as VMAT2.

3.8 Luminex

Luminex is a multiplex method for quantification of multiple analytes in one sample. A human prefixed 12-analyte kit (Creative Biolabs, England) was used to detect and quantify biomarkers of interest at Department of Medicinal Biochemistry Oslo University Hospital Ullevål, run by PhD Hans Christian Dalsbotten Aass. The markers Luminex kit was chosen to cover both anti-inflammatory (DJ-1, fractalkine IL-4, IL-10 and IL-13) and pro-inflammatory (MCP-1, IL-6, YKL-40 and eotaxin), as well as markers indicating neurodegeneration (tau)

and neurotrophic factors (BDNF and GDNF) to investigate immune and degenerative characteristics of the study subjects.

The assay is based on color-coded beads covalently bound to capture antibodies directed against different targeted biomarkers (105). When the homogenate is added to a well with a mixture of beads, the biomarkers of interest are bound to the antibodies (105). Biotinylated antibodies are used for detection and makes a sandwich with the target analyte and capture antibody (105). Then, streptavidin conjugated with phycoerythrin (PE) is added, and binds to the detection antibody (105). The principle of the Luminex assay is illustrated in figure 8.

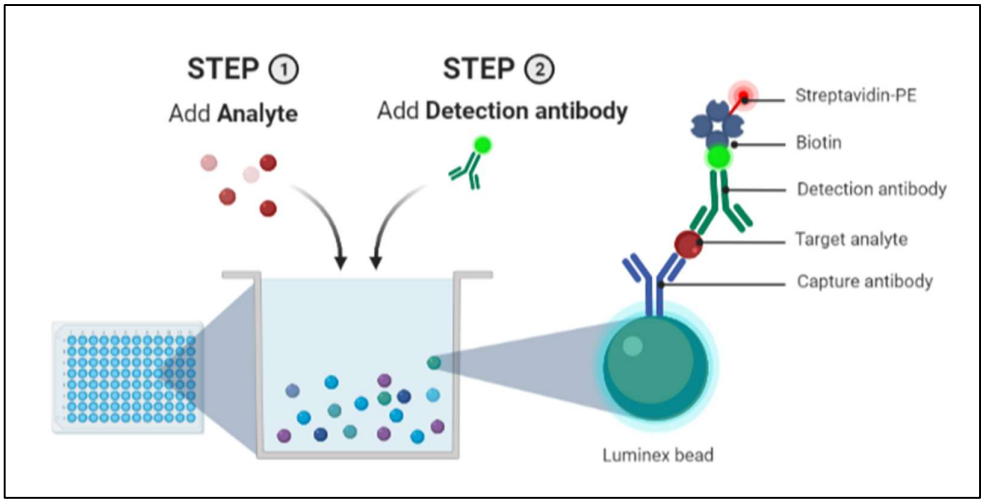

Figure 8. *Luminex assay principle. Image obtained from BioRender. The surface of the microsphere beads is covered with capture antibodies that bind specifically to the target analyte (105). A biotinylated detection antibody conjugated with streptavidin-PE binds to the target analyte, making a sandwich (105). Image obtained in BioRender.*

The Luminex assay analyzer Bio-Plex-200 system (Bio-Rad, USA) is a flow cytometer that uses two lasers to individually scan the beads flowing through. One of the lasers identifies the bead region and the analyte by excitation. The other laser identifies the fluorescence of the PE-signal of the detection antibody.

A pilot test was performed prior to the main testing on Luminex using samples of human tissue homogenate from one control subject and one subject with LBD. Different dilutions were tested to decide a protein concentration in range for most analytes.

3.9 Microtome Sectioning

Microtome sectioning was performed using Microtome HM355S (Thermo Fisher Scientific, USA), connected to a cooling unit (Cool-Cut, Thermo Fisher Scientific, USA), see figure 9. The water bath was filled with MQ-water and heated to 42.8°C by Section Transfer System (Thermo Fisher Scientific, USA). A knife was mounted to the microtome in a 10-degree angle. The paraffin blocks were put on ice for at least 20 minutes before trimming. The ACC-blocks were trimmed until at least a part of both white and grey matter was sectioned. Mesencephalon-blocks were trimmed until the whole tissue was included in the sections to ensure SN presence. 50 sections of 5 µm thickness were obtained from each block. Sections were separated and placed on positively charged glass slides using wooden toothpicks. The sections were then dried in a heating cabinet at 60°C for 60 minutes to melt off some of the paraffin. Sections were then stored in boxes at room temperature.

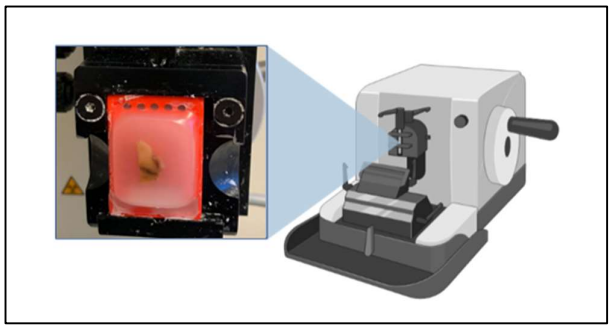

Figure 9. *A microtome was used for sectioning of the human brain tissue. The brain tissue was paraffin embedded onto plastic holders, which were mounted on the microtome Cool-Cut. Image obtained from BioRender. Picture captured by Siri Egencæs.*

3.10 Antibody verification IHC

In order to minimize recognition of undesirable antigens, antibody specificity testing was performed. One section from human ACC PD was stained with anti-Iba1 goat and anti-GFAP chicken, and one section from human SN control was stained with Iba1 goat, Iba1 rabbit, GFAP chicken and GFAP mouse. In total, images of 50 anti-Iba1 positive cells were obtained. The microglial specificity was determined by manually counting the number of cells that were positive for anti-Iba1 goat and/or rabbit and not overlapping with anti-GFAP chicken and/or anti-GFAP mouse. Images were obtained using a confocal microscope (LSM 710, Carl Zeiss) with laser wavelengths 405 nm, 488 nm, 594 nm and 647 nm.

3.11 Immunohistochemistry

Indirect immunofluorescence enables visualization and distinguishing of cell structures by specific staining with antibodies (106). This technique is carried out by using an unmarked, primary antibody directed to a specific epitope, along with a secondary antibody that binds specifically to the constant region of the primary antibody, covalently bound to a fluorophore (106).

Antigen retrieval must be optimized for the different antigens; hence several methods are in use (107). Heat-induced epitope retrieval (HIER) in a water bath with citrate buffer pH 6 and Tris-EDTA pH 9 was performed with all relevant antibodies, as well as immersion in undiluted formic acid for 10 minutes followed by 10 minutes in MQ-water. After several IF-experiments using test sections from the human brain tissue, citrate buffer pH 6 in addition to protecting the sections by the coverslip-paperclip method, see figure 10, were decided as the best choice for optimal epitope availability for the relevant proteins in this study. All antibodies were also tested in a concentration gradient of the recommended concentration based on information received from NBB and the producer in the different antigen retrieval solutions.

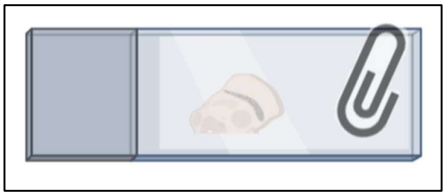

Figure 10 *Illustration of the paperclip-coverslip method. Image obtained from BioRender. A coverslip is carefully placed on top of the section prior to antigen retrieval and secured with a loosened paperclip. The coverslip protects the section allowing HIER with higher temperature and better preservation of cell morphology (108). Paperclip image obtained from MS PowerPoint, edited by Siri Egenæs.*

The sections were deparaffinized by immersing in NeoClear® (Merck, Germany) (3x10 min) and dehydrated by immersing in EtOH 100% (Antibac, Norway) from a freshly opened bottle (5 min). The sections were then rehydrated in a gradient of EtOH, starting with 100% EtOH for 5 minutes; 96% EtOH for 5 minutes; 80% EtOH for 5 minutes; 70% EtOH for 5 minutes. The sections were then immersed in distilled water for 5 minutes.

Sections were washed in 10 mM citrate buffer pH 6.0. All the slides were then incubated in a water bath for 20 minutes at 90°C in a preheated 10 mM citrate buffer with pH 6.0. The sections were then cooled down in room temperature for 20 minutes and rinsed briefly in phosphate buffered saline (PBS).

After antigen retrieval, the slides were encircled with a Super PAP pen (Electron Microscopy Sciences, USA) and incubated in blocking solution (3% newborn calf serum (NCS), 1% BSA, 0.05% Triton X-100 in PBS) for 1 hour and 30 minutes in a moisture chamber at room temperature. Primary antibodies were diluted in blocking solution, hereby the microglial marker Iba1 (goat anti-Iba1, 1:64) was combined with α-syn (mouse anti-α-syn, 1:500) and PS-129 (rabbit anti-PS-129, 1:500). Primary antibody incubation was performed overnight in a moisture chamber at room temperature.

The following day, slides were rinsed 3 x 10 minutes in PBS and then incubated with secondary antibodies donkey anti-goat Alexa Fluor 488 (1:1000), donkey anti-mouse Alexa Fluor 594 (1:1000) and donkey anti-rabbit Alexa Fluor 647 (1:1000) for 2 hours in moisture chamber at room temperature covered by aluminum foil to protect from light. The slides were then rinsed in PBS (3 x 10 min), incubated with DAPI (1:5000) for 15 minutes, and then rerinsed in PBS (3 x 10 min). Sections were mounted with ProLong Gold Antifade Mountant (ThermoFisher, USA) and coverslips were added. Slides were stored at 4°C.

3.12 Confocal microscopy

A confocal laser scanning microscope (LSM710, Carl Zeiss) was used to acquire the images. For detection of the fluorescence signals, four laser beams were focused onto the tissue. Laser wavelengths were 405nm, 488 nm, 594 nm and 647 nm. The lasers excite the fluorophore attached to the secondary antibodies. When excited, fluorophores emit signals for detection at their expected wavelength (109).

Areas with neuromelanin were used to ensure SN localization in mesencephalon, see figure 11. In ACC, the localization of the cortex was ensured by visual control of the objective after insertion of the section.

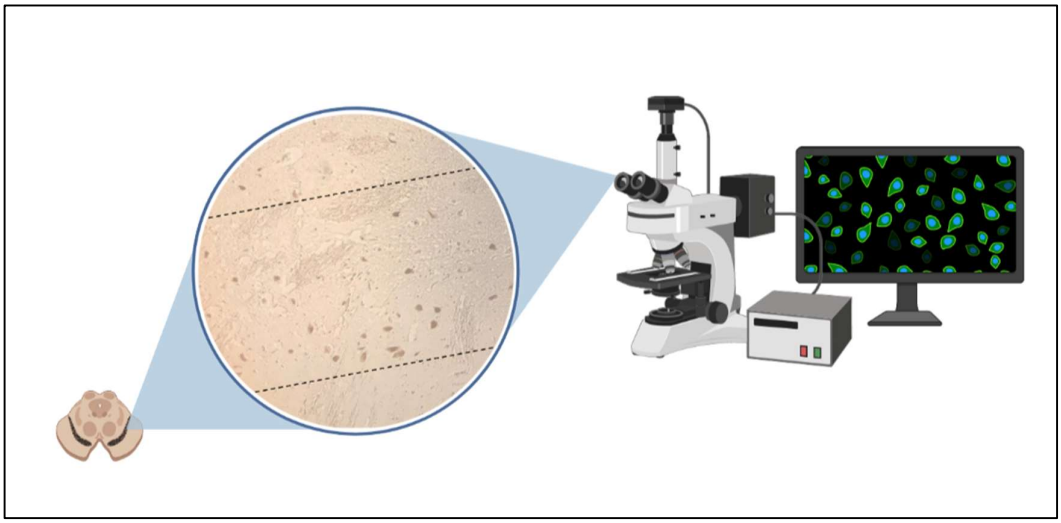

Figure 11. *Image of localization of SN in mesencephalon from an LBD patient using a confocal microscope. Distinct areas with neuromelanin can be visually detected despite dopaminergic degeneration in order to ensure SN localization and direction of movement in the section. The picture is taken with a 10x objective. Figures obtained from BioRender and modified by Siri Egenæs; Image obtained by Siri Egenæs.*

Prior to image acquirement, all sections were blinded using a coding list kept on TSD. Z-stacks were taken to analyze microglial activation and microglial α-syn and PS-129. Stacks were obtained using Zen 2011 by setting an interval where the lowest and highest slice were determined based on the first and last slice without signal of Iba1. Stacks were taken with 0.75 interval. Range of stacks depended on this interval. Settings for the different channels were optimized using the "Range indicatior" function in Zen 2011. The settings were saved to be used for all images. These settings remained untouched for the channels of DAPI, α-syn and PS-129, but the channel for Iba1 had to be adjusted to a higher laser strength for many images due to weak staining.

3.13 Analysis of confocal images – microglial activation

The confocal images were analyzed in FIJI (version 1.53c, ImageJ, USA). As the brain tissue had been differently treated before paraffin embedding, they required different settings during both image acquisition and analysis in order to represent the actual cell morphology. This, in addition to artefacts from secondary antibodies and proteaceous areas, made automated analysis impossible. Therefore, images were analyzed manually.

All images were first set to the same settings, and then slightly adjusted for the Iba-1 channel in order to enable particle analysis in FIJI. If possible, as little contrast as possible was added to distinct the cells from the background. Then, if the processes were connected without adjusted contrast, but were disconnected with increased contrast, lines to connect the processes to the soma were outlined manually, with a maximum of 3 pixels. Increasing contrast sometimes also disconnected the soma, making the cell count as two if not connected. Therefore, unconnected somas were also outlined. If adjusting the contrast did not work, cells were outlined manually prior to setting the threshold. If these cells were completely defined by the manual outlined mask, they were excluded from the analysis. Artefacts near Iba1 positive cells were removed manually to avoid overestimation of these cells. As this type of analysis takes a significant amount of time to do this precisely, only a subgroup of subjects was analyzed.

The images were processed with maximum intensity projection to optimize microglial processes for phenotype analysis. The channels for Iba1, staining the soma, and DAPI, staining the nuclei, were merged to identify microglia. Iba1 positive cells with positive DAPI nuclei were identified as microglia.

Then, the Iba1 channel was analyzed separately to create masks (including holes) of regions of interest (ROI). Perimeter and circularity of masks were measured to be used as parameters of microglial activation, see figure 12. Perimeter is the circumference of the cell, measured as the number of pixels in microns (110). A small perimeter indicates few processes. Circularity and perimeter are inversely proportional, in which also indirectly describes the cell area when the two parameters are compared, see formula in figure 12B below. Microglia are known to gain a smaller and rounder shape with few processes when pro-inflammatory activated compared to ramified microglia (29). The pro-inflammatory phenotype would therefore have a smaller perimeter and a higher value of circularity than ramified microglia (110).

A B

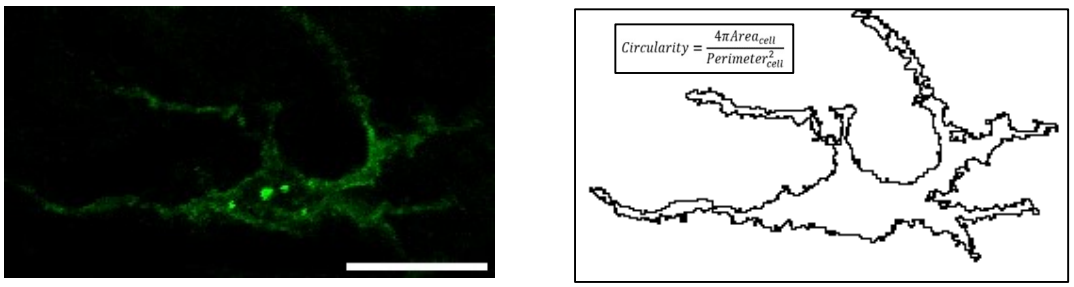

Figure 12 *Image of analyzed microglial cell* ***(A)*** *and the corresponding outline of the mask equal to the cell perimeter* ***(B)****. The circularity is calculated from the perimeter as follows from the formula in B. The scale bar represents 15 µm.*

The masks of microglia were then skeletonized whereof number of branches, end-point voxels and junctions were measured. The pro-inflammatory microglial phenotype has fewer branches, end-point voxels and junctions compared to ramified microglia (110, 111).

The total count of microglia analyzed was 474, with the basis of 10 cells per brain area per subject. Confocal images from SN and ACC were obtained from each subject, except from one low risk control, where only SN sections were received.

3.14 Analysis of confocal images – microglial clearance of α-syn and PS-129

The ROIs from the Iba1 channels were applied to maximum intensity projections of the channel of α-syn and PS-129 separately, see figure 13. Both mean gray value and fraction of area (%area) was measured to represent intracellular α-syn and PS-129. To correct for nonspecific signals from secondary antibodies, the mean gray value and fraction of area with signal from the respective channels were measured in negative controls. 3 squares of the same size, as well as the total frame was analyzed. The mean gray value was used as a control of intensity by using the difference between mean gray value in the negative controls and the mean gray value in the images for analysis. If the intensity of the images for analysis were weaker than the intensity from the negative control, the fraction area was set to 0. If the image for analysis were more intense than the negative control, the net area fraction was calculated by subtracting the fraction of area in the negative control section from the area in the section of interest. If the value was negative, the fraction of area was set to 0.

As α-syn have a more widespread, less patchy, staining pattern, the mean gray value was used as a measurement of the amount of α-syn intracellularly in addition to percentage of stained area (which had a roof of effect for α-syn and not PS-129).

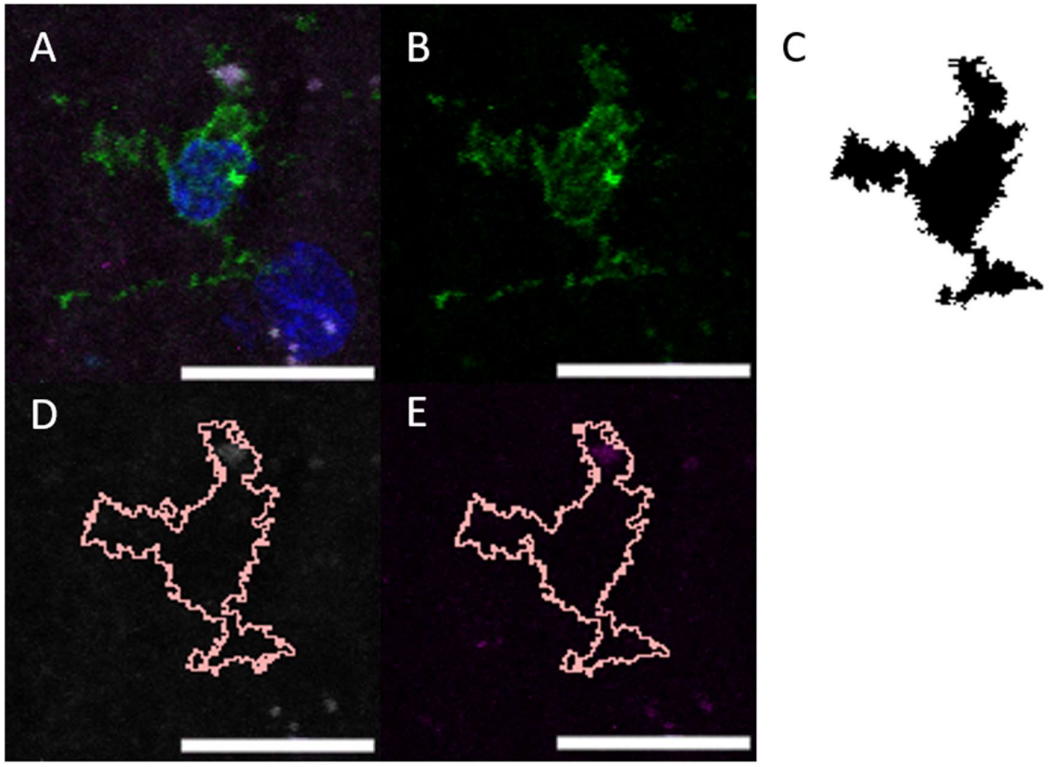

Figure 13 *Workflow of analysis of intracellular α-syn and PS-129.* ***A)*** *Merged channels of DAPI (blue), anti-Iba1 (green), anti-α-syn (white) and anti-PS-129 (magenta).* ***B)*** *Channel of Iba1.* ***C)*** *Mask/ROI of anti-Iba1 positive microglia in B.* ***D)*** *Channel of anti α-syn with microglial ROI* ***D)*** *Channel of anti-PS-129 with microglial ROI. Intensity by mean gray value and fraction (%) of anti- α-syn and anti-PS-129 was measured within the ROI. The scale bar represents 15 µm.*

3.15 Intensity measurements

As mentioned, the tissues of the sections have been stored and fixated differently. Most of the sections originate from tissues that were immersion fixed for 4 weeks at NBB and NABCA immediately after dissection. From a subgroup of patients, we received fresh frozen mesencephalon tissue, and a part of these including SN were kept frozen, while the other half was fixated for 1 day prior to paraffin embedding. For some cases we also had the other half of the brain stem that was fixated for 4 weeks before embedding. As fixation masks epitopes and H_2O present in the tissue at the time of freezing can lead to crystallization and cause holes in the tissue, we expected the tissue in which was fixated directly after dissection to have

better preserved morphology and lower antigenicity than sections that was fixated subsequent to freezing.

The selection of differently treated tissue from both hemispheres of the same patient, enabled the possibility to calculate a correction factor to be used in the image analysis. In order to adjust for differences in antigenicity the storage and treatment could cause, mean gray value was measured to quantify intensity. 6 Z-stacks from the differently treated hemispheres in 4 patients were analyzed using the channel for α-syn. The 11 middle images from each stack were merged using Z-project with average intensity. Equal sized squared was used for every image to measure the mean gray value, SD, minimum and maximum, see table 5. The intensity measured by mean gray value varied between 0.01 and 3.96, and the mean intensity was 0.17 (freshly frozen) and 1.20 (fixed). A Wilcoxon signed-rank test showed that there was a significant difference in mean gray value between the sections fixated for 1 day and the sections fixated for 4 weeks (Z=-3.285, p = 0.001). The effect size was then calculated by dividing the z value by the square root of the total amount of images ($n_{\text{freshly frozen}} + n_{\text{fixated}}$). This gave an effect size of -0.49, indicating a moderate to large effect size (69). Since the freshly frozen pictures were in minority, they were the ones adjusted in intensity by multiplying with 2.04 (1/0.49).

Table 5. *Statistics of differences in mean gray value of the sections treated differently using Wilcoxon Signed Rank test (SPSS.). Mean gray value is significantly different between the sections that were freshly frozen prior to 1 day of fixation (n=21) and fixated for 4 weeks (n=24).*

	Mean Gray value (N=45)					**Statistical test**	
	Mean	**SD**	**95% CI**	**Min**	**Max**	**Z**	***p***
Freshly frozen	.17	.2	[.09, .26]	.01	.81		
Fixated	1.20	1.1	[.74, 1.65]	.05	3.96	-3.285	.001**

3.15 Ethical considerations

3.15.1 Human tissue

The use and storage of human brain tissue have been approved by the Regional Committee for Medical and Health Research Ethics (REC) South East (REC-number REC255638). As the time of storage exceeds 2 months, a project specific biobank has been established at the

Neuroscience research unit at Oslo University Hospital (OUS). The project is also approved by the Data protection official at OUS (approval number 21/10382). This approval includes the use of patient-sensitive data associated with the tissue samples, i.e., sex, age and anamnesis. All such data has been kept and analyzed in Services for sensitive data (TSD).

Further on, the project is approved by scientific committees locally at NBB and NABCA and is in addition attached/rooted to Amsterdam UMC (Academic Medical Center and VU University Medical Center) where it has its own biobank number (METc-number 2021.0554). All patients have given consent *ante mortem* to donation, storage, and delivery of autopsy material to collaborators abroad for analysis. A broad consent has been given to neurological research.

3.15.2 Animal tissue

For this master thesis, mice tissue was used in *in vitro* experiments. This follows from Norwegian regulation of the use of animals in experiments ("Forskrift om bruk av dyr i forskning"), in which states that an *in vitro* animal experiment cannot use genetically modified animals, animals with harmful or an inadequate phenotype, and that organ harvesting must occur after death, defined as neck dislocation in this study. Such *in vitro* experiments are exempt from FOTS approval by the Norwegian Food Safety Authority. The experiments were however approved by the Institute of Comparative Medicine at the University of Oslo.

For ethical use of animals in research "the three Rs" (replace, reduce, and refine) by Russell and Birch applies (112, 113). In this lies that if one can, one should use non-animal objects if possible and appropriate, reduce the number of animals used and refine the animal models to minimize the discomfort of the animals. The animals used in this study were animals in excess. Only *in vitro* experiments were performed.

3.16 Statistics

Statistical analyses were performed with RStudio version 1.4.1717 (Boston, MA, USA), version 26 of SPSS (Chicago, IL, USA) and Microsoft Excel in the Services for sensitive data (TSD) server at the University of Oslo. Graphs were made using the ggplot2 package in RStudio and SPSS.

Outliers were defined as observations outside the inter quartile range (IQR) and were in general excluded if not otherwise stated. ELISA and Luminex results were measured as duplicates. Duplicates with coefficient of variation (CV) > 25% were excluded. *P* values < 0.05 were considered significant.

3.16.1 Comparisons of means and medians

Comparisons of means and medians were analyzed between controls vs LBDs, and low-risk vs high-risk vs LBD if satisfactory sample size in each group. As LB pathology spreads to mesencephalon at Braak stage 3, subgroups of Braak stage 0-2 vs. 3-5 were chosen for comparisons of the mesencephalon data.

When assumptions of normality and homogeniety was met, ANOVA was performed to examine whether there were group difference. To assess the assumptions of ANOVA, preliminary tests of normality and homogeniety of variance (Levene's test) was performed in SPSS. Some variables were transformed in order to achieve normality. For the comparisons where these assumptions were not met, non-parametric tests were performed. If two groups were compared, a Wilcoxon rank sum test was performed (RStudio). If three groups or more were compared, Kruskal-Wallis was performed (SPSS).

For groupwise comparison of means, covariates were tested to see whether they contributed to the analysis, but the covariates did not lead to a better model fit. Therefore, parsemonious models using only the measurements against different subgroups were chosen.

Group differences in age at death, *post mortem* brain weight, pH in *post mortem* brain tissue, *post mortem delay* (PMD), PD polygenic risk score (PD PRS) and LB Braak stage were analyzed using one-way ANOVA with contrasts to compare low-risk, high-risk, iPD and PD groups. Group differences in sex were measured with chi-square test (SPSS). Post-hoc analysis was Bonferroni corrected.

The measurability of different biomarkers was analyzed using Fisher's exact test (SPSS), due to unmet assumptions of the chi-square test.

3.16.2 Linear regression models

Linear regression models were used to investigate interactions of measurements from ELISA, Luminex, WB and confocal imaging by relevant variables. The Bayesian Information

Criterion (BIC) was used to choose the best fit of the different regression models, testing three models with values as raw data, log-transformed and squared root transformed for every model. In addition, evaluation of normal distribution of the model residuals by Shapiro-Wilk testing and visual inspection of the residual plots was done. All models were first tested with either Braak stage, main group (control vs. LBD), group (low-risk, high-risk and LBD) and PD PRS, as well as the independent variables age of death, PMD and sex. Then, the models were optimized by excluding the most insignificant ($p>0.2$) independent variables stepwise. The final models are presented in the chapters below.

Not all subjects had assigned a PD PRS. Therefore, the models including PD PRS as an independent variable have a lower sample size compared to the other models.

In order to increase statistical power, duplicate measurements and/or measurements from both mesencephalon and ACC were used in linear mixed regression models (RStudio, lme4 package) with patient ID and location (mesencephalon/ACC) as random intercepts. The same assesments were done for deciding model fit and choice of independent variables in the linear mixed regression models as described above.

4. Results

4.1.1 WB antibody specificity of α-syn, PS-129 and Iba1

Specificity testing of antibodies directed against α-syn, PS-129 and Iba1 was performed using western blotting. For antibodies against α-syn and PS-129, 20 µg of mouse whole brain, 20 µg of human brain from ACC from a non-demented control and 20 µg of human brain from ACC from a PD patient was loaded to each lane, in addition to 20 µg of mouse heart tissue as a negative control. Empty lanes were included between the mice and human tissue membrane for α-syn due to bleed through of bands in preliminary testing. Membranes are presented in figure 14.

Anti-α-syn produced bands in the lanes loaded with human brain tissue at the expected molecular weight at approximately 19 kDa. The anti-α-syn produced no specific band at 19 kDa in mouse heart tissue, used as a negative control, but several unspecific bands at variable molecular weights. In mouse brain tissue, the anti-α-syn produced one main band slightly higher than the band seen from human brain tissue, in addition to weaker unspecific bands.

One specific α-syn band in human brain tissue, not present in tissue described to be absent of α-syn, demonstrates antibody specificity.

Anti-PS-129 produced bands at approximately 18 kDa in the lanes loaded with both human and mouse brain tissue. The predicted molecular weight for PS-129 is 14 kDa, although the observed band size is 17-18 kDa according to the manufacturer in western blot settings similar to those used in this thesis. A band was not visible in the lane loaded with mouse heart, which indicates antibody specificity.

For anti-Iba1, mouse whole brain, mouse midbrain, mouse ACC and human ACC from a non-demented control was used. Mouse kidney was included as a negative control. Iba1 produced bands at its expected molecular weight of 16 kDa in human ACC, as well as weak bands in all brain tissue samples from mice. No band was produced in the lane loaded with mouse kidney, hence indicating antibody specificity. There were also weak bands produced at approximately 30 kDa, in which could be dimeric Iba1.

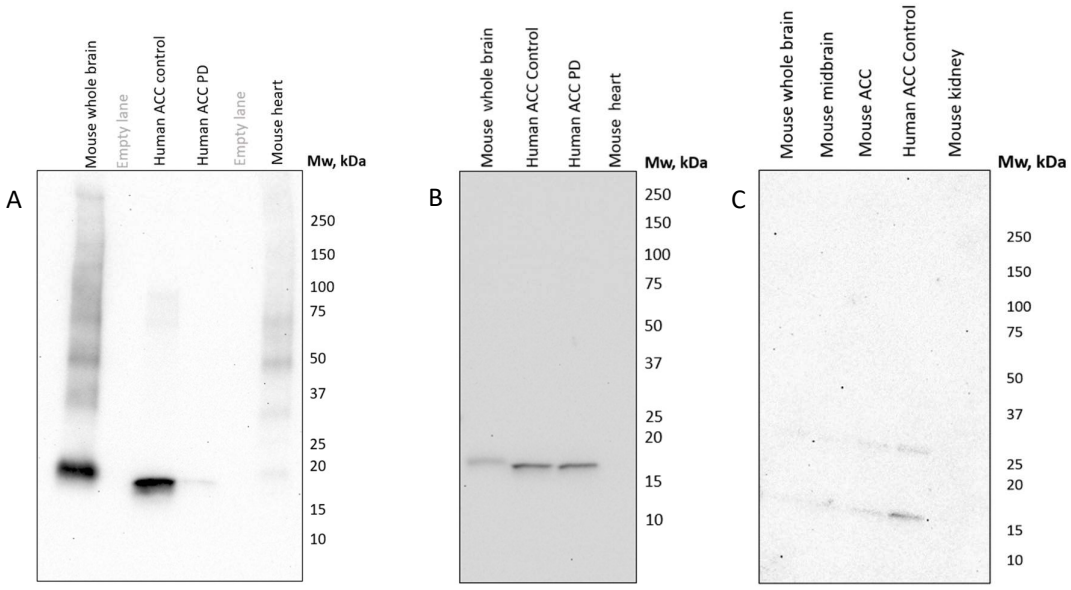

Figure 14 *Membranes illustrating antibody specificity on membranes loaded with 20 µg/lane.* ***A)*** *Membrane incubated with α-syn antibody (1:500). The α-syn antibody gave a specific band at approximately 19 kDa in the lane of human control ACC and a weak band at human ACC PD. Mouse heart homogenate served as a negative control, demonstrating antibody specificity.* ***B)*** *Membrane incubated with antibody against PS-129 (1:500) gave bands at approximately 17 kDa in homogenates from mouse whole brain, human control ACC, and human ACC from PD patient. Heart homogenate did not produce any band, demonstrating PS-129 specificity.* ***C)*** *Anti-Iba1 produced bands at approximately 16 kDa in brain human ACC tissue and mouse brain tissue. There was no band in the lane of the mouse kidney, illustrating antibody specificity.*

4.1.2 IHC antibody specificity of Iba1 goat

Specificity testing of anti-Iba1 produced in goat was also performed by IHC. To confirm that anti-Iba1 from goat specifically stain microglia in fixed human brain tissue, images of 50 Iba1

positive cells were obtained after IF-staining of two sections: 26 goat Iba1-positive cells from a section double-stained with anti-Iba1 from goat (488) and anti-GFAP from chicken (594) and finally 24 goat Iba1-positive cells from a section quadruple-stained with anti-GFAP from mouse (405), anti-Iba1 from goat (488), anti-GFAP from chicken (594) and anti-Iba1 from rabbit (647).

The number of cells overlapping with anti-GFAP from mouse, anti-GFAP from chicken and anti-Iba1 from rabbit was quantified. All Iba1 goat positive cells were also Iba1 rabbit positive, while none of the Iba1 goat positive cells were positive for any of the GFAP antibodies, see figure 15. Hence, Iba1 goat has good microglial specificity and could be used without an astrocyte marker. This allowed the usage of nuclei staining with DAPI, further improving the selection of Iba1 positive cells for quantification.

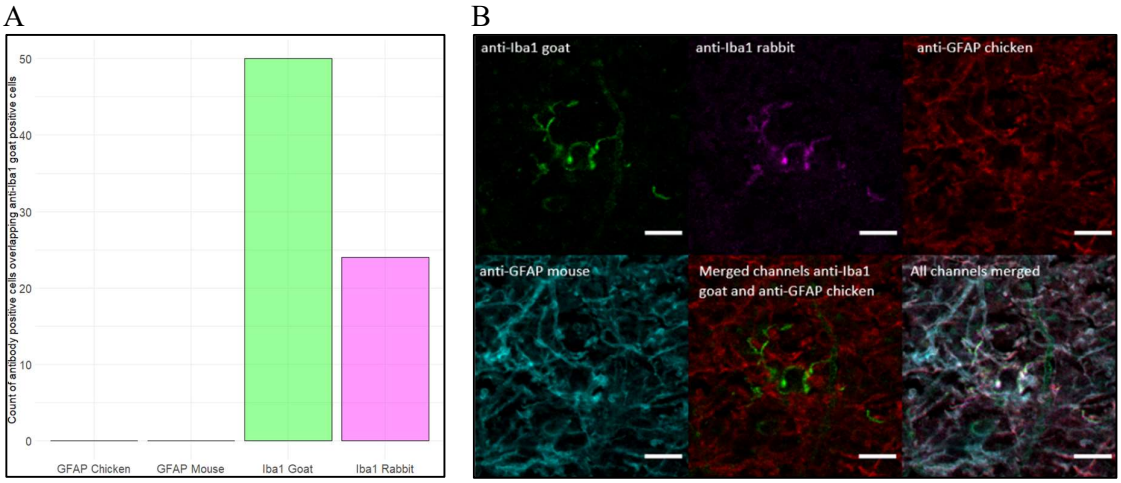

Figure 15 *Specificity testing of anti-Iba1 from goat on fixed human brain tissue.* ***A)*** *Count of GFAP Chicken (0%, n=24), GFAP Mouse (0%, n=50) and Iba1 Rabbit (100%, n=24) positive cells overlapping with Iba1 goat positive cells (n=50).* ***B)*** *Confocal images from the quantification with channels for anti-Iba1 from goat (green), anti-Iba1 from rabbit (magenta), anti-GFAP from mouse (teal) and merged channels. The scale bar represents 10 µm.*

4.1.3 Specificity controls on Luminex and ELISA

Specificity testing was performed using blank controls and tissue dilution gradients.

4.2 Luminex and ELISA quantification of neuroinflammation and -degeneration markers in mesencephalon and ACC

The concentration of proteins relevant for neuroinflammation and neurodegeneration was measured in homogenates from mesencephalon (including SN) and ACC, see table 7. A test run with a sample concentration gradient was performed before the final set-up to ensure a sample dilution that fitted as many of the analytes in the multiplex as possible. All samples were run in duplicates and adjusted to the same protein concentration in the final set-up.

Some biomarkers were not measurable in these assays, see table 6. All biomarkers with a reasonable number of detectable samples were included in the following sections.

Table 6. *Overview of detectable and undetectable biomarkers measured with the Luminex and ELISA assay.*

	Anti-inflammatory markers	**Pro-inflammatory markers**	**Neurodegenerative markers**	**Neuroprotective markers**
Detectable	IL-4 PARK7/DJ-1 Fractalkine	MCP-1 IL-6	VMAT2	GDNF
Not detectable	IL-10 IL-13	YKL-40 Eotaxin	Tau NFL	BDNF

Table 7. *Protein concentration (ng/ml) in brain tissue homogenates standardized to protein concentration 2.63 ng/ml, without covariate correction.*

	Groups based in genetic, neuropathological, and clinical staging (n=22)					
	Mesencephalon incl. SN			**Anterior cingulate cortex (ACC)**		
	Controls (9)		**LBD (13)**	**Controls (5)**		**LBD (4)**
	Low-risk (5)	**High-risk (4)**	**iPD (12), PD (1)**	**Low-risk (2)**	**High-risk (3)**	**iPD (4), PD (0)**
VMAT2 Mean (SD)	0.675 (0.0) n=2	0.461 (0.1) n=3	0.589 (0.2) n=7	† (†) n=0	† (†) n=0	0.345 (†) n=1
Fractalkine Mean (SD)	166.4 (100.5) n=2	750.3 (†) n=1	112.0 (80.3) n=2	428.7 (†) n=1	55.3 (†) n=1	329.0 (226.6) n=2
IL-4 Mean (SD)	14.12 (†) n=1	10.2 (5.54) n=2	13.66 (10.8) n=9	27.5 (†) n=1	4.6 (2.9) n=3	27.5 (†) n=1
DJ-1 Mean (SD)	86662.1 (10258.3) n=5	78266.9 (8057.2) n=4	79095.2 (11359.5) n=13	59245.7 (†) n=1	65671.97 (10972.7) n=3	56043.2 (6674.9) n=4
GDNF Mean (SD)	0.96 (0.38) n=4	1.17 (0.62) n=3	1.27 (1.0) n=13	2.14 (†) n=1	0.285 (0.25) n=2	0.11 (†) n=1
MCP-1 Mean (SD)	† (†) n=0	9.3 (9.7) n=2	15.5 (11.9) n=3	† (†) n=0	2.4 (†) n=1	16.13 (†) n=1
IL-6 Mean (SD)	2,3 (1,0) n=2	† (†) n=0	1.53 (1.5) n=4	0.2 (†) n=1	† (†) n=0	† (†) n=0

Abbreviations: SN, substantia nigra; LBD, Lewy Body disease; PD, Parkinson's disease; iPD, incipient PD; ctr, control; VMAT2, vesicular monoamine transporter 2; SD, standard deviation; n, number of cases; IL, interleukin; GDNF, glial cell-derived neurotrophic factor; MCP-1, monocyte chemoattractant protein-1; †, no value. The superscript in each group for each marker, indicates subject number with levels within the detection range.

4.2.1 DJ-1 significantly decreased with increasing LBD severity

DJ-1 concentrations in brain homogenate were compared in subgroups for mesencephalon and ACC separately by one-way ANOVA (SPSS). One observation was outside the IQR and therefore defined as an outlier. This observation had to be excluded in order to get the model residuals normally distributed. The outlier origined from an ACC sample of a low-risk control and was approximately twice the size of the other observations of ACC.

None of the subgroups had significantly different means, see figure 16. However, there seemed to be a declining trend of DJ-1 concentration with LBD. The further division into low-risk and high-risk controls, shows that the low-risk controls tend to have higher DJ-1 concentrations than both high-risk control and LBD subjects, although not significantly.

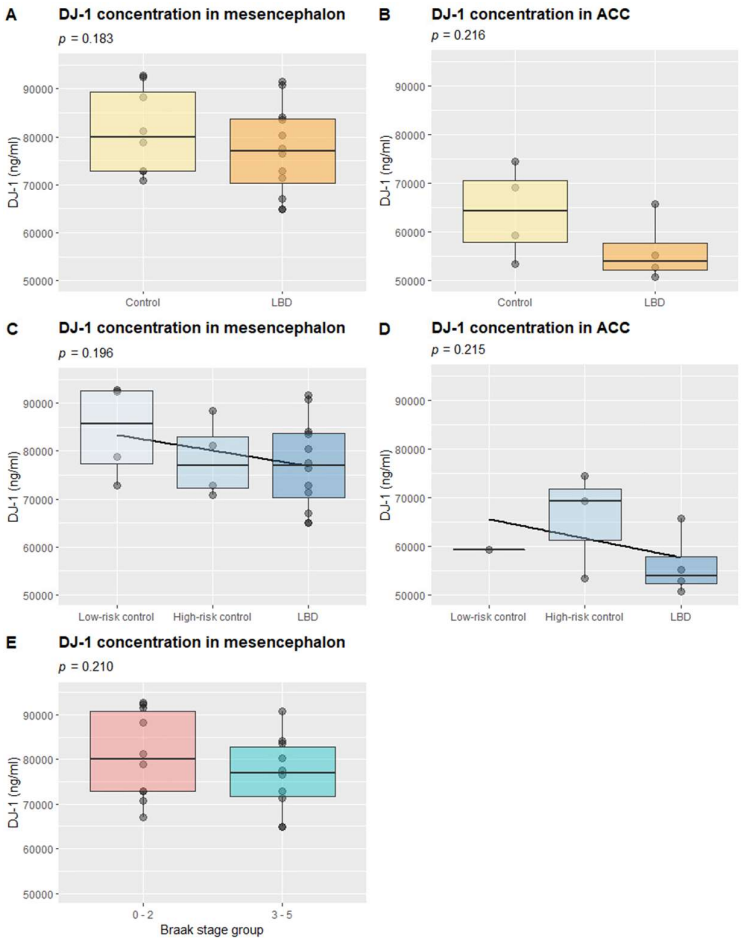

Figure 16. *Boxplot of DJ-1 concentration in mesencephalon and ACC.* ***A)*** *Control vs LBD, mesencephalon: F(1,19) = 1.911, p = 0.183, One-way ANOVA, SPSS.* ***B)*** *Control vs. LBD, ACC: F(1,6) = 1.909, p = 0.216, One-way ANOVA, SPSS.* ***C)*** *Low-risk controls vs high-risk controls vs LBD mesencephalon: F(2,18) = 1.786, p = 0.196, One-way ANOVA, SPSS.* ***D)*** *High-risk controls vs LBD, ACC: F(1,5) = 2.016, p = 0.215, One-way*

ANOVA, SPSS. The low-risk control was excluded from the analysis. ***E)*** *Braak 0-2 vs 3-5, mesencephalon: F(1,19) = 1.682, p = 0.210, One-way ANOVA, SPSS.*

Semi-logarithmically (loglin) transformation was performed, as this was the best fit for all regression models including DJ-1. All models of DJ-1 by LBD severity are presented in table 8.

The linear mixed model of DJ-1 against the main group (merged low-risk and high-risk controls vs. LBD) had a significant interaction between DJ-1 concentration and all independent variables. The model estimates a coefficient of 9% decrease in absolute DJ-1 concentration by going from control to LBD, with a 95% CI of -1 to -17% decrease in absolute DJ-1 concentration. When dividing the control group into low-risk and high-risk vs. LBD (parameter "Group"), the interaction was not significant for neither the group parameter (p = 0.056) nor age (p = 0.051), but it did show a significant interaction between DJ-1 and PMD (p = 0.046). Although not statistically significant, the models show a clear trend of decreasing DJ-1 with LBD.

The linear mixed model including DJ-1 against Braak stage, both parameters Braak stage (p = 0.040) and age (p = 0.009) were significant, suggesting a 2% decrease in absolute DJ-1 concentration with increasing Braak stage, see figure 17, and 0.7% increase in absolute DJ-1 concentration with increasing age. PMD was not significant in this model (p = 0.060).

According to the models, it seems like DJ-1 concentration decreases with increasing LBD severity, and that age and PMD as parameteres should be included to describe this interaction. Linear mixed models including only age or PMD are both significant (p = 0.002 and p = 0.034, respectively).

Table 8. *In the linear mixed models, a significant effect on protein concentration was found for the main group (control vs. LBD) and Braak stage, both decreasing the protein concentration.*

Parameter	Coefficient	SE	95% CI	t (53)	P
(Intercept)	10.75	0.28	[10.18, 11.32]	37.90	< .001 **
Maingroup	-0.09	0.04	[-0.17, -0.01]	-2.36	0.022 .
Age	$6.81e^{-03}$	$2.62e^{-03}$	[0.00, 0.01]	2.60	0.012 .
PMD	$-3.55e^{-04}$	$1.68e^{-04}$	[0.00, 0.00]	-2.11	0.039 .
(Intercept)	10.97	0.33	[10.32, 11.62]	33.71	< .001 **
Group	-0.05	0.03	[-0.10, 0.00]	-1.94	0.058
Age	$5.68e^{-03}$	$2.85e^{-03}$	[0.00, 0.01]	1.99	0.051
PMD	$-3.64e^{-04}$	$1.78e^{-04}$	[0.00, 0.00]	-2.04	0.046
(Intercept)	10.75	0.28	[10.18, 11.32]	37.90	< .001 **
Braak	-0.02	0.01	[-0.04, 0.00]	-2.11	0.040 .
Age	$7.28e^{-03}$	$2.68e^{-03}$	[0.00, 0.01]	2.72	0.009 *
PMD	$-3.28e^{-04}$	$1.71e^{-04}$	[0.00, 0.00]	-1.92	0.060

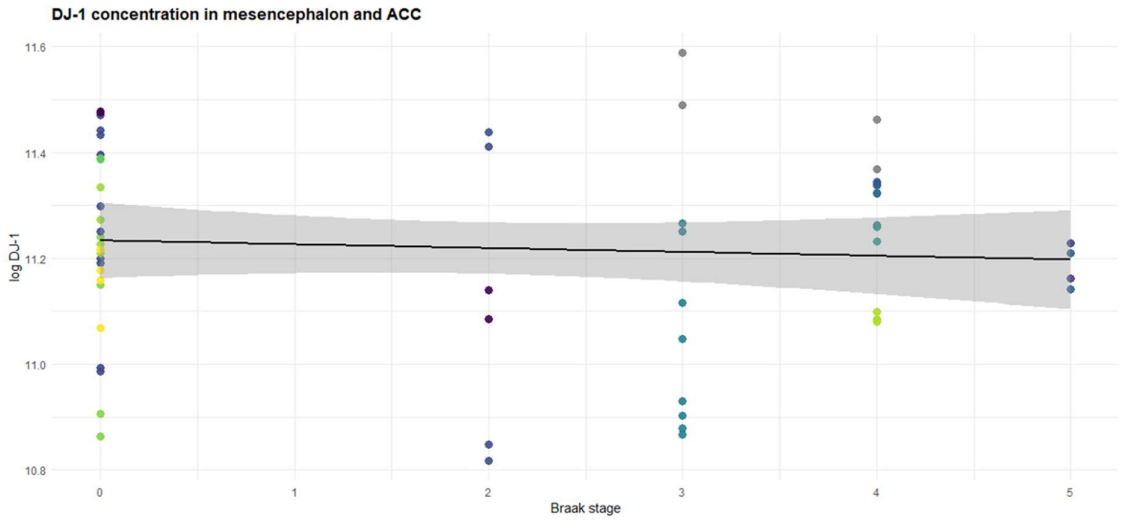

Figure 17. *Linear regression model of DJ-1 vs Braak stage including duplicate values from both mesencephalon and ACC. The model had significant declining protein concentration by increasing Braak stage (n=29). Colors represent PD PRS.*

Moreover, the means of the DJ-1 data was logarithmically transformed and used in linear models to investigate whether the interactions were specific to brain area. In mesencephalon,

the interaction between Braak stage, age and PMD by DJ-1 concentration showed a significant 2% decline in absolute DJ-1 concentration with increasing Braak stage (p = 0.041), consistent with the findings in the linear mixed model. The same interaction with Braak stage and DJ-1 was insignificant in ACC (p = 0.453). Linear regression models of DJ-1 vs. Braak stage in mesencephalon and ACC are presented in table 9 and figure 18.

Table 9. *The linear models of DJ-1 vs. Braak stage in mesencephalon was significant. Braak in ACC did not show a significant interaction.*

	Parameter	Coefficient	SE	95% CI	t (17)	P
Mesencephalon	**(Intercept)**	10.94	0.27	[10.37, 11.50]	41.18	< .001**
	Braak	-0.02	0.01	[-0.05, 0.00]	-2.21	0.041 .
	Age	$6.63e^{-03}$	$2.69e^{-03}$	[0.00, 0.01]	2.47	0.025 .
	PMD	$-3.84e^{-04}$	$1.76\ e^{-04}$	[0.00, 0.00]	-2.19	0.043 .
ACC	**(Intercept)**	11.03	0.07	[10.86, 11.21]	155.45	< .001**
	Braak	-0.03	0.03	[-0.11, 0.05]	-0.80	0.453

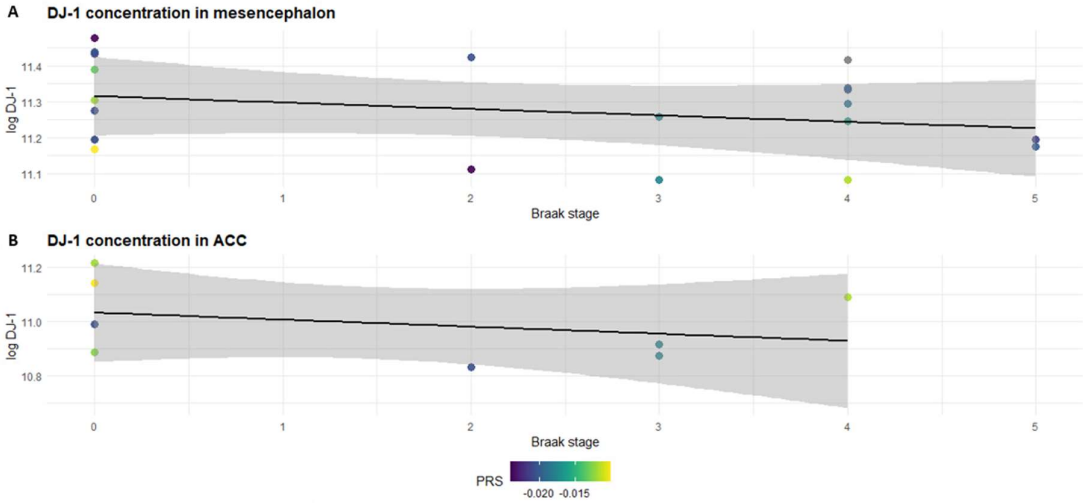

Figure 18. *Linear regression models of DJ-1 concentration by Braak stage.* ***A)*** *In mesencephalon, the Braak stage coefficient was negative, but not significant (n=21).* ***B)*** *In ACC, the declining trend was the same, but not significant (n=8).*

4.2.2 DJ-1 demonstrated a non-significant trend of increasing with PD PRS in ACC

The linear mixed model of DJ-1 against PD PRS resulted in PMD as the only significant variable (p = 0.040), suggesting PD PRS does not affect the concentration of DJ-1 overall, see table 10. In the linear models considering the effect of PD PRS on DJ-1 in mesencephalon and ACC seperately, there was a conflicting trend. In mesencephalon, DJ-1 was not correlated to

PD PRS (p = 0.763), while in ACC DJ-1 concentrations show a tendency of increase with PD PRS at borderline significance (p = 0.056) see table 11. Although neither of these interactions were significant, ACC gives the interaction with the lowest p-value (p = 0.056) of the three models despite including the lowest sample size (n = 8). Although being ambiguous, the 95% CI for ACC is weighted more towards an increase of DJ-1 with increasing PD PRS. This tendency can also be observed in figure 16 D. The linear models for mesencephalon and ACC are presented in figure 19.

Table 10. *DJ-1 concentration did not show a significant relationship with PD PRS in the linear mixed model.*

Parameter	Coefficient	SE	95% CI	t (50)	p
(Intercept)	10.54	0.26	[10.02, 11.07]	40.26	< .001 **
PD PRS	5.41	6.20	[-7.04, 17.86]	0.87	0.387
Age	$8.53e^{-03}$	$3.23e^{-03}$	[0.00, 0.02]	2.64	0.011 .

Table 11. *The linear models of DJ-1 by PD PRS did not show a significant interaction in mesencephalon. A tendency of increasing DJ-1 concentration with increasing PD PRS was shown in ACC.*

	Parameter	Coefficient	SE	95% CI	t (17)	P
Mesencephalon	**(Intercept)**	10.59	0.25	[10.05, 11.13]	41.63	< .001**
	PD PRS	-2.10	6.85	[-16.56, 12.36]	-0.31	0.763
	Age	$7.67e^{-03}$	$3.46e^{-03}$	[0.00, 0.01]	2.22	0.040 .
	Parameter	**Coefficient**	**SE**	**95% CI**	**t (6)**	**P**
ACC	**(Intercept)**	11.35	0.16	[10.97, 11.74]	72.51	<.001**
	PD PRS	23.16	9.79	[-0.80, 47.11]	2.37	0.056

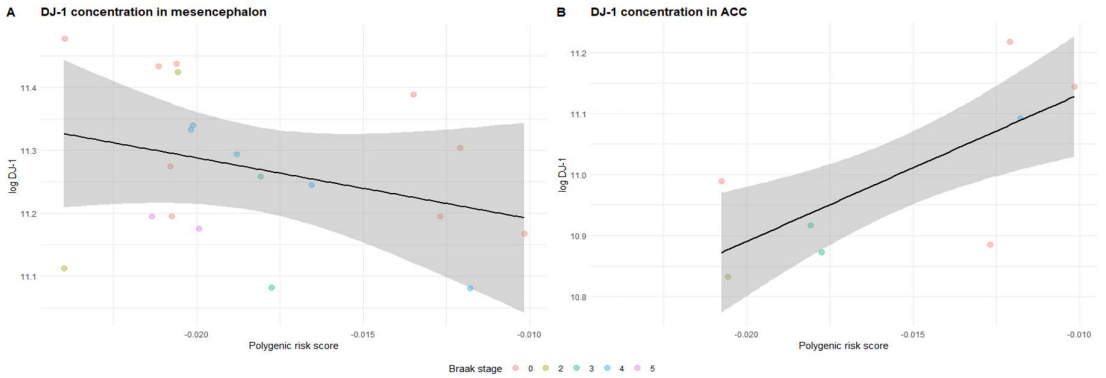

Figure 19. *Linear regression models of DJ-1 by PD PRS.* ***A)*** *In mesencephalon, PRS did not have a significant effect on DJ-1. The coefficient is negative with increasing PD PRS.* ***B)*** *In ACC, PD PRS did not show a statistically significant effect on DJ-1. The trend is increasing DJ-1 in ACC with increasing PD PRS.*

4.2.3 GDNF had no significant interactions with LBD severity

Means of GDNF concentration were compared both as subgroups for mesencephalon. The majority of homogenates from ACC did not have a measurable GDNF concentration, see section 4.2.6. Subgroup differences of GDNF concentrations for ACC were therefore not analyzed separately.

To compare means of GDNF concentration between subgroups, one-way ANOVA (SPSS) was used. Neither control vs LBD (p = 0.922) nor low-risk vs high-risk vs LBD (p = 0.829) had significantly different means, suggesting disease progression is not relevant for GDNF presence in mesencephalon, see figure 20.

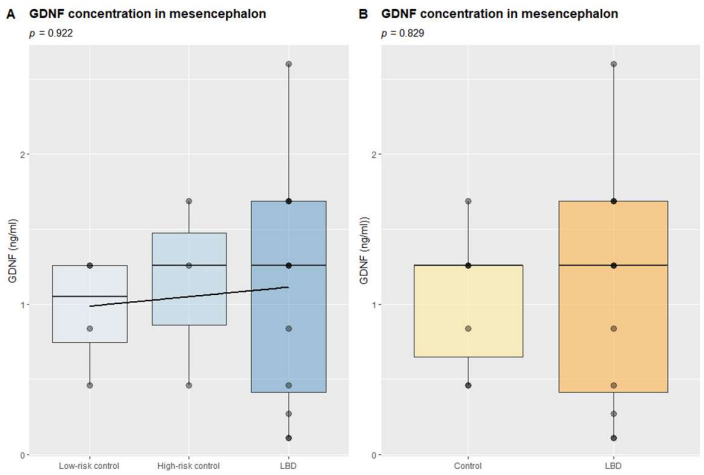

Figure 20. *Boxplot of GNDF concentration in mesencephalon* ***A)*** *Low-risk controls vs high-risk controls vs LBD: F(2, 16)=0.081, p = 0.922 (One-way ANOVA SPSS) and* ***B)*** *Control vs LBD: F(1, 17)=0.829, p = 0.829 (One-way ANOVA, SPSS).*

The interactions of LBD severity and GDNF were further analyzed using linear mixed regression models. GDNF data were transformed to square root values for the best regression model fit. The linear mixed model included ACC (n=4) and mesencephalon (n=15). Neither parameter of LBD severity turned out significant, consistently suggesting that GDNF is not affected by disease progression or clinical group. Age was the only independent variable significant for GDNF concentration, showing association between higher GDNF levels with increasing age. The linear mixed models of GDNF by disease progression and clinical groups are listed in table 12.

Table 12. *In the linear mixed models of GDNF by disease progression, age was the only significant or nearly significant independent variable. Neither intercept nor independent variables representing disease progression were significant.*

Parameter	Coefficient	SE	95% CI	t (53)	P
(Intercept)	0.01	0.51	[-1.03, 1.05]	0.02	0.981
MainGroup	$-8.66e^{-03}$	0.10	[-0.21, 0.19]	-0.09	0.930
Age	0.01	$5.90e^{-03}$	[0.00, 0.02]	2.07	0.045 .
(Intercept)	0.06	0.57	[-1.09, 1.21]	0.11	0.913
Group	-0.01	0.06	[-0.14, 0.11]	-0.21	0.836
Age	0.01	$6.10e^{-03}$	[0.01, 0.02]	1.93	0.061
(Intercept)	0.01	0.50	[-1.01, 1.03]	0.02	0.980
Braak	-0.01	0.03	[-0.06, 0.04]	-0.43	0.672
Age	1.21	$5.94e^{-03}$	[0.00, 0.02]	2.06	0.046 .

4.2.4 GDNF significantly decreases with increasing PD PRS

Square root transformed GDNF data was then used in a mixed linear regression model, analyzing the effect of PD PRS in mesencephalon and ACC. PD PRS significantly decreased with increasing PD PRS (p = 0.019). Neither age, PMD nor sex described this relation. The 95% CI indicates a decrease in GDNF of -52.35 to -4.99 in GDNF concentration. See table 13 and figure 21 for the model of GDNF by PD PRS. As most measurements of GDNF originate from mesencephalon, this interaction should be interpreted with caution for ACC.

Table 13. *GDNF concentration was significantly affected by PD PRS in the linear mixed model.*

Parameter	Coefficient	SE	95% CI	t (35)	p
Intercept	0.55	0.21	[0.12, 0.98]	2.60	0.014 .
PD PRS	-28.67	11.66	[-52.35, -4.99]	-2.46	0.019 .

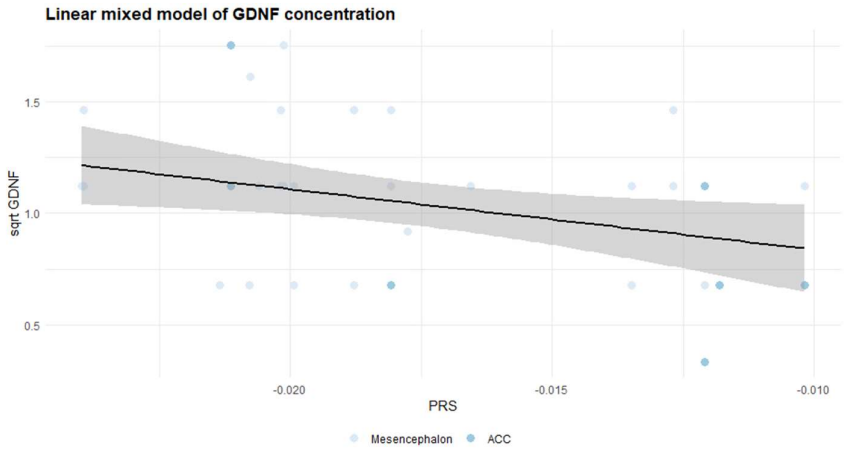

Figure 21. *Linear model of sqrt GDNF concentration by PD PRS in mesencephalon and ACC shows a significant declining trend (n=15). Colors represent the brain area of the measurement. The graph includes duplicate values of GDNF.*

4.2.5 VMAT2 did not show any significant interactions or differences

The results of VMAT2 quantification 7 homogenates could not be trusted to be precise measurements and are to be reported as not measurable as they were below the lowest point of the standard curve (<0.312 ng/ml). Means of the VMAT2 concentration with CV <25% and above 0.312 ng/ml were compared using one-way ANOVA (SPSS). There was no significant difference in the means between control and LBD, nor Braak stage 0-2 and 3-5, see figure 22.

Square root duplicate values from the ELISA assay of VMAT2 with CV<25% and values above the lower limit of certain detection according to the standard curve (0.312 ng/ml) were used in linear mixed models. There were no significant interactions with neither Braak stage (p = 0.511), Braak groups (p = 0.304), subject groups (p = 0.454) nor PD PRS (p = 0.257).

Further, in the ELISA assay both homogenates from this study and cerebrospinal fluid (CSF) samples from a different study were quantified simultaneously. VMAT2 was not detectable in any of the CSF-samples showing that levels of VMAT2 in CSF is much lower (if present) than in brain tissue.

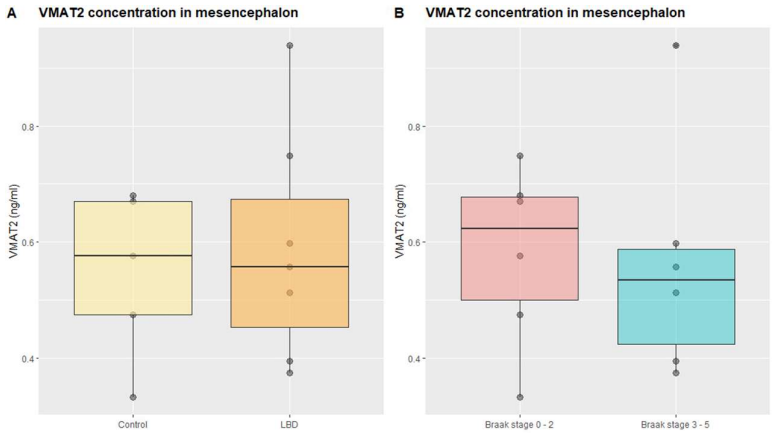

Figure 22. GDNF comparisons in mesencephalon. **A)** Control vs LBD: F(1,10)=0.164, p = 0.694 (one-way ANOVA, SPSS). **B)** Braak stage 0-2 vs 3-5: F(1,9) = 1.344, p = 0.276 (one-way ANOVA, SPSS). The outlier in Braak stage group 3-5 was excluded in the ANOVA comparison presented in B.

4.2.6 Measurability of biomarkers by brain area and subject group

The measurability of the different biomarkers by subject group and brain area was performed using the chi square function in SPSS, see table 14. The assumptions of the chi square test were not met in any cases. Therefore, all p-values provided are generated by Fisher's Exact Test (SPSS). For VMAT2, some proteins were detectable in the ELISA assay but were measured to below the certain lower limit of detection (<0.312 ng/ml) that followed by the standard curve. These are in this analysis considered as not measurable.

The only protein showing significant difference in measurability was GDNF. There was a significant difference in which brain area GDNF could be measured, $p < 0.001$ (Fisher's Exact test, SPSS). 20 of 22 (90.9%) mesencephalon homogenates had a measurable GDNF concentration, compared to 4 of 9 (44.4%) of the ACC homogenates. Some of the GDNF measurements were excluded in the one-way ANOVA presented earlier due to being outliers but were indeed measurable, hence included in the analysis of measurability. VMAT2 was borderline significantly more measurable in mesencephalon compared to ACC (p=0.077, Fisher's exact test, SPSS).

Table 14. *Measurability of proteins in brain tissue homogenate standardized to protein concentration 2.63 ng/ml. All values are given as % measurable of the total.*

	Subject group		**Brain area**		**Statistical tests**	
	Control (14)	**LBD (17)**	**Mesencephalon (22)**	**ACC (9)**	**Control vs. LBD**	**Mesencephalon vs. ACC**
GDNF	71.4% n=10	82.4% n=14	90.9% n=20	44.4% n=4	$p = 0.632$	p< .001 **, eta=0.841
VMAT2	71.4% n=10	70.6% n=12	54.5% n=18	11.1% n=4	$p = 1.000$	$p = 0.077$
Fractalkine	42.9% n=6	44.4% n=4	22.7% n=5	55.6% n=5	$p = 0.688$	$p = 0.158$
IL-4	50% n=7	58.8% n=10	54.5% n=12	55.6% n=5	$p = 0.716$	$p = 0.665$
MCP-1	28.6% n=4	23.5% n=4	27.3% n=6	22.2% n=2	$p = 1.000$	$p = 1.000$
IL-6	28.6% n=4	23.5% n=4	31.8% n=7	11.1% n=1	$p = 1.000$	$p = 646$

4.2 Semi quantitative western blotting

Band intensity of α-syn, PS-129 and GAPDH were measured by FIJI (version 1.53c, ImageJ, USA) as described previously. One sample did not give any signal from neither GAPDH, α-syn nor PS-129. This subject was excluded from the analysis.

The data did not achieve a normal distribution despite several transformation attempts. Therefore, Wilcoxon rank sum tests were performed to examine whether the distribution of α-syn n, PS-129 and the ratio between PS-129 and α-syn was different across the control group and the LBD group. For mesencephalon, subjects with Braak stage 0-2 and 3-5 were also compared. Kruskal-Wallis tests were used to analyze differences in distribution between low-risk, high-risk and LBD.

4.2.1 Quantification of α-syn

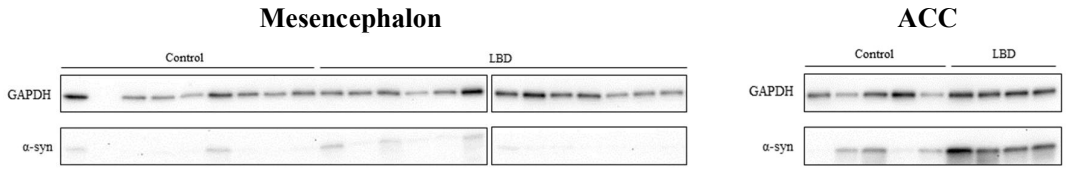

Figure 23. *Western blot membranes of a -syn and GAPDH with mesencephalon and ACC homogenate.*

Signals of GAPDH and α-syn were measured in FIJI, see membranes in figure 23. There were no significant differences in α-syn signal between either comparison for mesencephalon, see figure 24. In ACC, there was a significant difference in α-syn signal between the control group and LBD group (p = 0.032), confirming a higher ACC level of α-syn in LBD subjects. The difference between low-risk, high-risk and LBD was not significant in ACC (p = 0.079), although there is a trend to be seen of increasing α-syn in high-risks compared to low-risks, and LBD compared to both other groups, see figure 24 D.

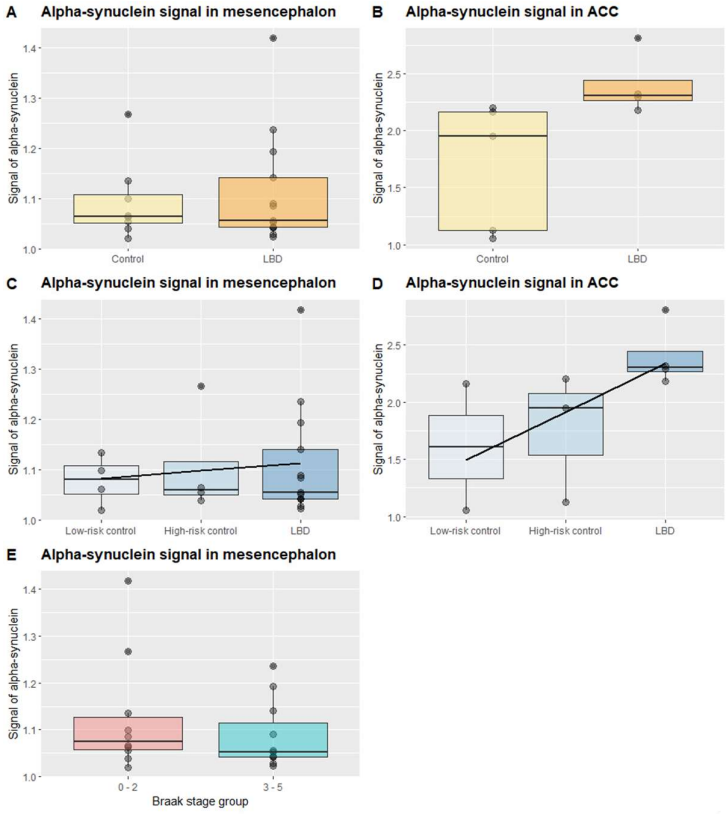

Figure 24. *Boxplots of α-syn signal* ***A)*** *Controls vs LBD in mesencephalon: W=52, p = 1.000 (Wilcoxon rank sum with continuity correction, RStudio).* ***B)*** *Controls vs LBD in ACC: W=1, p = 0.03175 (Wilcoxon rank sum*

with continuity correction, RStudio). ***C)*** *Low-risk control vs high-risk control vs LBD in mesencephalon: Chi square=0.013, p = 0.994, df=2 (Kruskal-Wallis test, SPSS).* ***D)*** *Low-risk control vs high-risk control vs LBD in ACC: Chi square = 5.078, p = 0.079, df=2 (Kruskal-Wallis test, SPSS).* ***E)*** *Braak group 0-2 vs 3-5 in mesencephalon: W=67, p = 0.426 (Wilcoxon rank sum with continuity correction, RStudio). Neither outlier was excluded as non-parametric tests were performed.*

4.2.2 PS-129 quantification

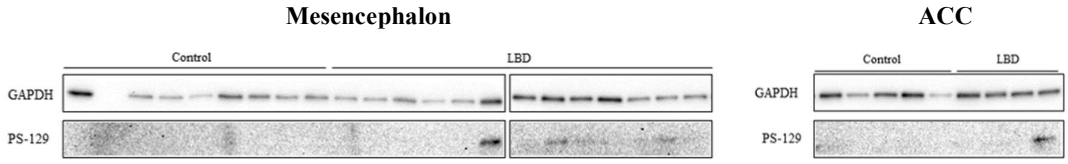

Figure 25. *Western blot membranes of PS-129 and GAPDH with mesencephalon and ACC homogenate.*

Signals of PS-129 and GAPDH were measured using FIJI. The membranes are presented in figure 25. Some values of PS-129 signal were negative during measurement, due to nonspecific signals at the correct molecular weight or slightly below background level. These observations were set to 0. In mesencephalon, all comparisons were significant: control vs LBD (p<0.001, Wilcoxon rank sum with continuity correction, RStudio); low-risk, high-risk vs LBD (p = 0.001); Braak stage 0-2 vs 3-5 (p<0.001, Wilcoxon rank sum with continuity correction, RStudio). The low-risk vs. high-risk groups were not significantly different (p = 1.00, Kruskal-Wallis, SPSS), while low-risk vs LBD and high-risk vs LBD were significant, both p = 0.013.

In ACC, neither comparison was significant: control vs. LBD (p = 0.111, Wilcoxon rank sum with continuity correction, RStudio); low-risk vs high-risk vs LBD (p = 0.1130, Kruskal-Wallis, SPSS). The regression line in figure 26 D does however show an increasing trend of PS-129 in ACC in the LBD group. Comparisons are presented as boxplots below in figure 26.

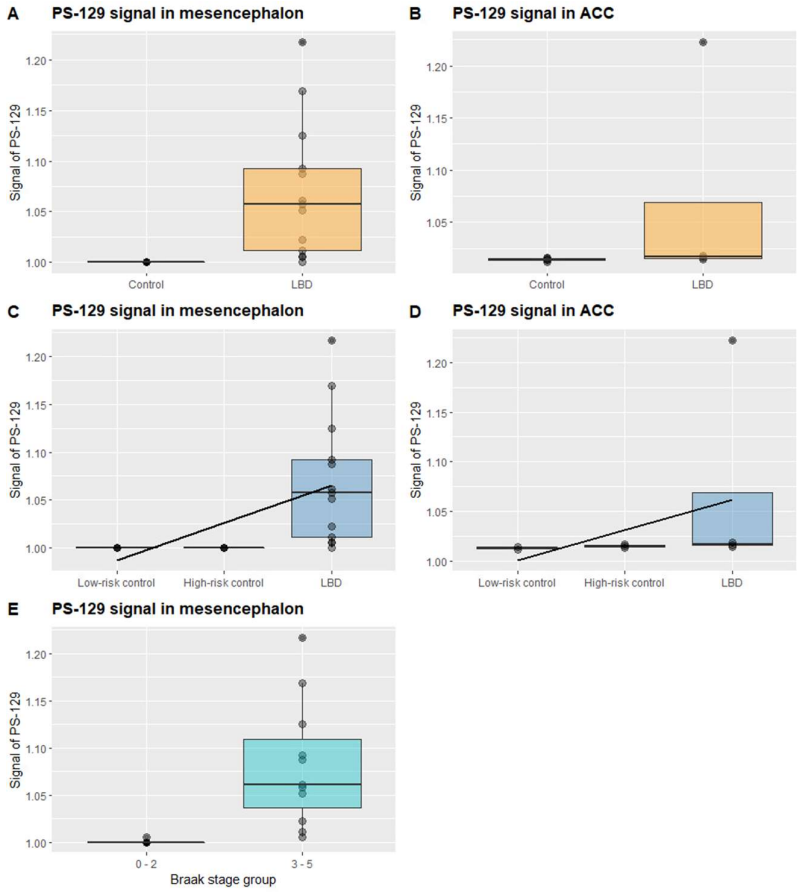

Figure 26 *Difference between PS-129 distributions.* ***A)*** *Control vs LBD in mesencephalon: W=4,* p *= 0.0003 (Wilcoxon Rank sum with continuity correction, RStudio)* ***B)*** *Control vs LBD in ACC: W=3,* p *= 0.1111 (Wilcoxon rank sum with continuity correction, RStudio).* ***C)*** *Low-risk vs high-risk vs LBD in mesencephalon: Chi square=13.105,* p *= 0.001, df=2 (Kruskal-Walli test, SPSS). There was no significant difference between the low-risk and high-risk group (*p *= 0.1130), but a significant difference between both low-risk and LBD (*p *= 0.013, Bonferroni corrected), and high-risk and LBD (*p *= 0.013, Bonferroni corrected).* ***D)*** *Low-risk vs high-risk vs LBD in ACC: Chi square = 4.078,* p *= 0.1130, df=2 (Kruskal-Wallis test, SPSS).* ***E)*** *Braak Group 0-2 vs 3-5 in mesencephalon: W=0,* p *= 6.425e^{-05} (Wilcoxon rank sum with continuity correction, RStudio).*

Moreover, PS-129 signal was plotted against Braak stage in mesencephalon and ACC, see figure 27. The scatter illustrated the significant trend of different PS-129 signal by Braak stage 0-2 (LBs not affecting mesencephalon) vs. 3-5 (LBs affecting mesencephalon) as described above and shows an increasing signal of PS-129 with increasing Braak stage, with as good as no signal from Braak stage 0-2 and increasing signal from Braak stage 3.

In ACC, such a comparison of Braak groups was not performed as there was no fresh frozen ACC tissue from individuals with Braak staging indicating LB affection of ACC in this study. All ACC homogenates had very low PS-129 signals except the homogenate from the subject

with Braak stage 4. The signal of this subject is 15.1 times higher (0.2224/0.0147) than the mean signal of the other subjects with lower Braak stage.

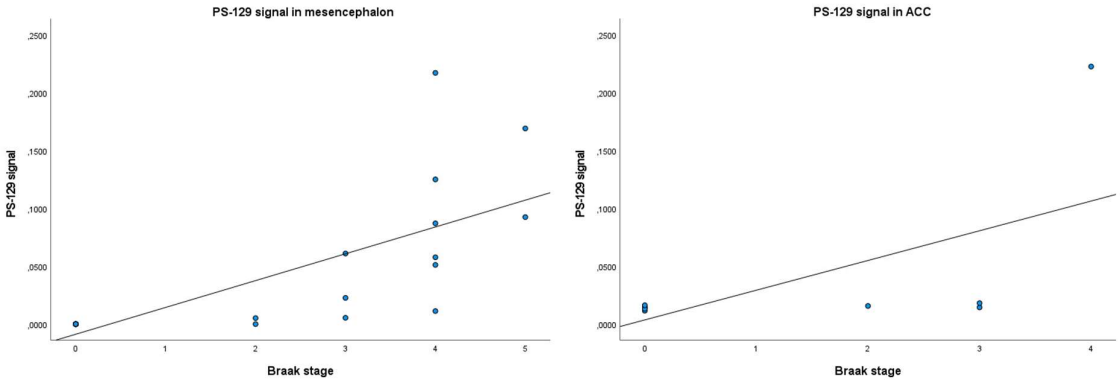

Figure 27. *Scatter plot of PS-129 signal from western blotting by Braak stage. The regression lines are added using the fit line at total function (linear) in SPSS.* ***A)*** *PS-129 signal in mesencephalon.* ***B)*** *PS-129 signal in ACC.*

4.2.3 Ratio of PS-129/α-syn

To evaluate at what time during the LBD severity phosphorylation of α-syn occurs, the ratio of PS-129/α-syn signal was analyzed by performing Wilcoxon rank sum test in RStudio and Kruskal-Wallis test in SPSS.

In mesencephalon, there was a significant difference between the Braak stage groups 0-2 and 3-5 (p = 0.01272, Wilcoxon rank sum with continuity correction, SPSS). The differences in PS-129/α-syn ratio were not significant between control and LBD (p = 0.314, Wilcoxon rank sum with continuity correction), nor low-risk vs high-risk vs LBD (p = 0.143, Kruskal-Wallis, SPSS). In ACC, there were no significant differences in the ratio between neither control and LBD (p = 0.195, Wilcoxon rank sum with continuity correction, SPSS), nor low-risk vs high-risk vs LBD (p = 0.295, Kruskal-Wallis, SPSS).

The ratio of PS-129/α-syn was then plotted against Braak stage, see figure 28. The ratio of PS-129/α-syn in mesencephalon increases at what seems to be a threshold at Braak stage 4, which fits with the difference in mean between Braak stage group 0-2 and 3-5.

The same pattern cannot be observed in ACC, mainly due to the two control subjects with Braak stage 0. These subjects had relatively low signals of α-syn, and relatively normal PS-129 signal measurements compared to the other control subjects. There seems to be a trend of initial phosphorylation at Braak stage 4 (0.15 against 0), however, the scale of the y-axis is

narrow, and no large difference can be observed. If subjects with Braak stage 5 and 6 were to be included, the differences observed in figure 28 B would probably be less prominent.

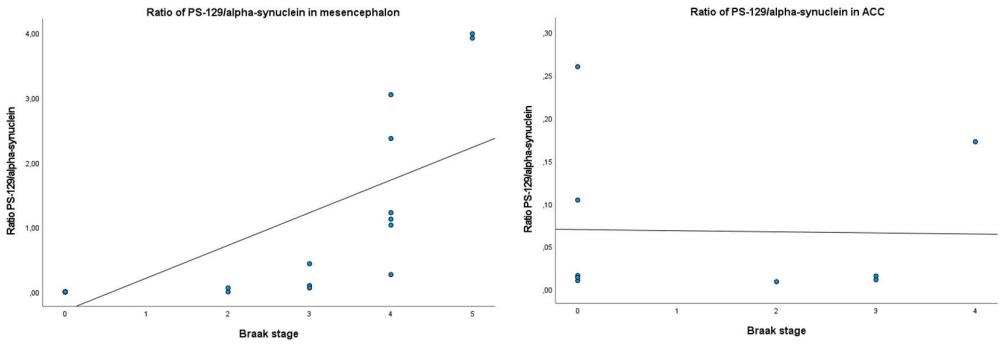

Figure 28. *Scatter plot of ratio of PS-129/α-syn by Braak stage. The regression lines are added using the fit line at total function (linear) in SPSS.* ***A)*** *In mesencephalon, the ratio is low from Braak stage 0-3, and increases at approximately Braak stage 4.* ***B)*** *In ACC, the ratio cannot be said to be different as the scale of the y-axis is narrow.*

4.3 Confocal imaging

Microglia can be in an anti-inflammatory or pro-inflammatory state, in which changes the cell morphology, as previously described. Studies have shown that α-syn can induce pro-inflammatory activation of microglial cells. The cause of aggregation of LB could be less efficient microglial clearance of α-syn. Therefore, the confocal images were analyzed with emphasis on both morphology and presence of α-syn and PS-129 intracellularly.

Analysis of microglia activation was performed on 23 subjects: low-risk controls (n=5); high-risk controls (n=5); iPD (n=5); PD (n=8), see table 15. The LBD group ranged from Braak 3-6, therefore representing the disease after affecting SN. Therefore, no subjects with Braak stage 1-2 are represented in the following analysis.

Several parameters can describe the morphology of cells. As microglial processes contract towards the soma and move towards a more circular shape when pro-inflammatory activated, information about branching, the circumference and circularity are relevant measurements. Number of branches, end-point voxels (endpoints of each branch with less than 2 neighbors) and junctions of skeletonized cells were measured to describe branching.

Table 15. *Characteristics of the subgroup from the confocal analysis.*

	Controls (10)		**LBD (13)**	
	Low-risk (5)	**High-risk (5)**	**iPD (5)**	**PD (8)**
Age Mean (SD)	88.8 (7.4)	80.6 (9.0)	83.6 (5.5)	74.6 (2.4)
Sex Female n (%)	2 (40)	5 (100)	2 (40)	4 (100)
PD PRS Mean (SD)	-0.0215907 (-0.001339)	-0.0118466 (0.001813)	-0.0189828 (-0.001848)	-0.0172504 (-0.004516)
Braak stage Mean (SD)	0 (0)	0 (0)	4 (0.7)	5.3 (0.7)
PMD min Mean	468. (179.2)	422 (48.0)	384 (59.1)	443.8 (166.7)
Microglia in SN n	62	49	43	92
Microglia in ACC n	40 (n=4)	51	54	82

4.3.1 Microglia branching analysis did not show any significant differences or interactions with LBD severity

Differences in the branching measurements (number of branches, end-point voxels and junctions) were compared using one-way ANOVA in SPSS if the assumptions were met. If not, Wilcoxon rank sum in RStudio and Kruskal-Wallis in SPSS were performed.

The low-risk outlier in SN had large microglial cells with many long processes. When merged with high-risk controls, this observation is no longer an outlier. Hence, observations from these images were not considered as outliers.

All measures reflecting microglial branching followed the same pattern, see figure 29. In general, the control groups had a larger variance of branching data than iPD and PD subjects

in SN. In ACC, the iPD group is more similar to the control group than to PD subjects. Figure 30 shows confocal images from two different high-risk control subjects representing this variety.

Both branches, end-point voxels and junctions were at a similar level in both SN and ACC. Neither comparison was significant, see table 16.

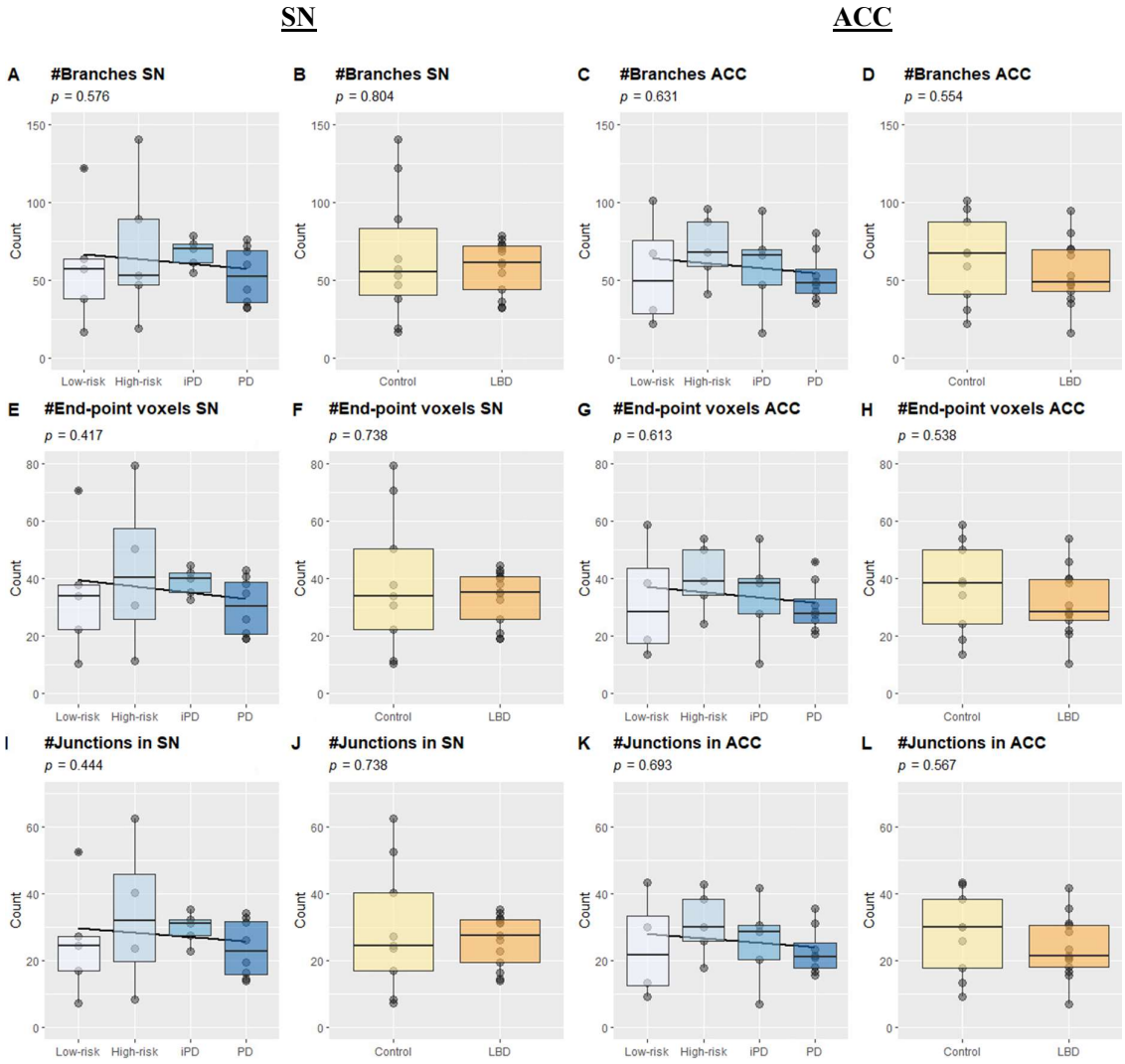

Figure 29 *Box plots illustrating the same pattern for branching measurements by groups in SN and ACC. None of the means were significantly different, see table 16.*

Table 16. *Results of group comparisons of branching measurements.*

	SN (23)		ACC (22)	
	Low-risk vs. high-risk vs. iPD vs. PD	**Control vs. LBD**	**Low-risk vs. high-risk vs. iPD vs. PD**	**Control vs. LBI**
Branches	$\chi^2 = 1.985$ $p = 0.576$ df=3	F(1, 21) = 0.063 $p = 0.804$	$\chi^2 = 1.725$ $p = 0.631$ df = 3	F(1, 20) = 0.363 $p = 0.554$
End point voxels	$\chi^2 = 2.837$ $p = 0.417$ df = 3	W = 71 $p = 0.738$	$\chi^2 = 1.808$ $p = 0.613$ df = 3,	F(1, 20) = 0.393 $p = 0.538$
Junctions	$\chi^2 = 2.678$ $p = 0.444$ df = 3	W = 71 $p = 0.738$	$\chi^2 = 1.452$ $p = 0.693$ df = 3	F(1, 20) = 0.338 $p = 0.567$

Abbreviations: χ^2, chi square statistic; df, degrees of freedom; p, p-value; W, Wilcoxon test; F, F statistic

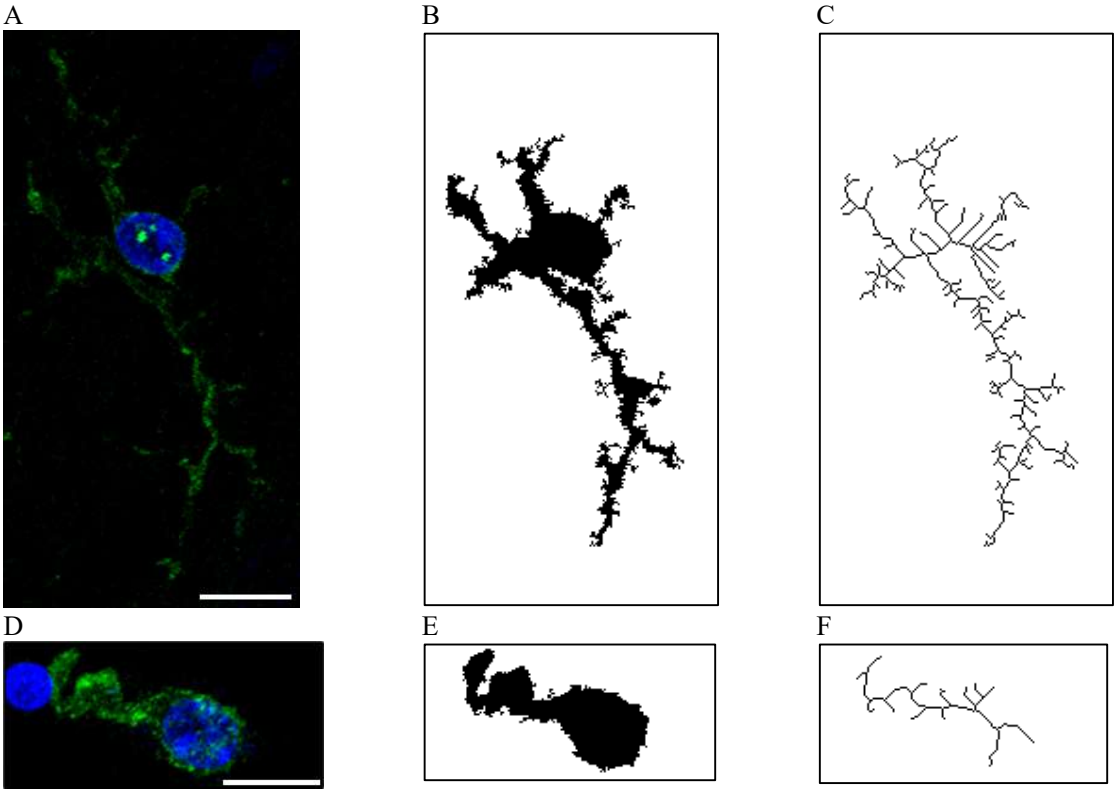

Figure 30. *Microglial branching in section from SN of two different high-risk control subjects illustrating the variety in branching measurements.* ***A*** *and* ***D)*** *Microglia stained with Iba1 (green) with DAPI positive nuclei (blue).* ***B*** *and* ***E)*** *Mask of the corresponding microglial cell.* ***C*** *and* ***F)*** *Skeleton of the corresponding masks used to measure #branches, #end-point voxels and #junctions. The scale bar represents 15 µm.*

Further, branching data was plotted against Braak stage and applied to linear regression models, see figure 31. Neither model significantly correlated with Braak stage: branches in SN (p = 0.544); branches in ACC (p = 0.781); end-point voxels in SN (p = 0.222); end-point voxels in ACC (p = 0.648); junctions in SN (p = 0.262); junctions in ACC (0.802). However, the scatterplots show the same pattern as observed by the boxplots in figure 29, with a wider range of branching in control subjects while LBD subjects seem to have less variation in branching as well as less branching, although not significant.

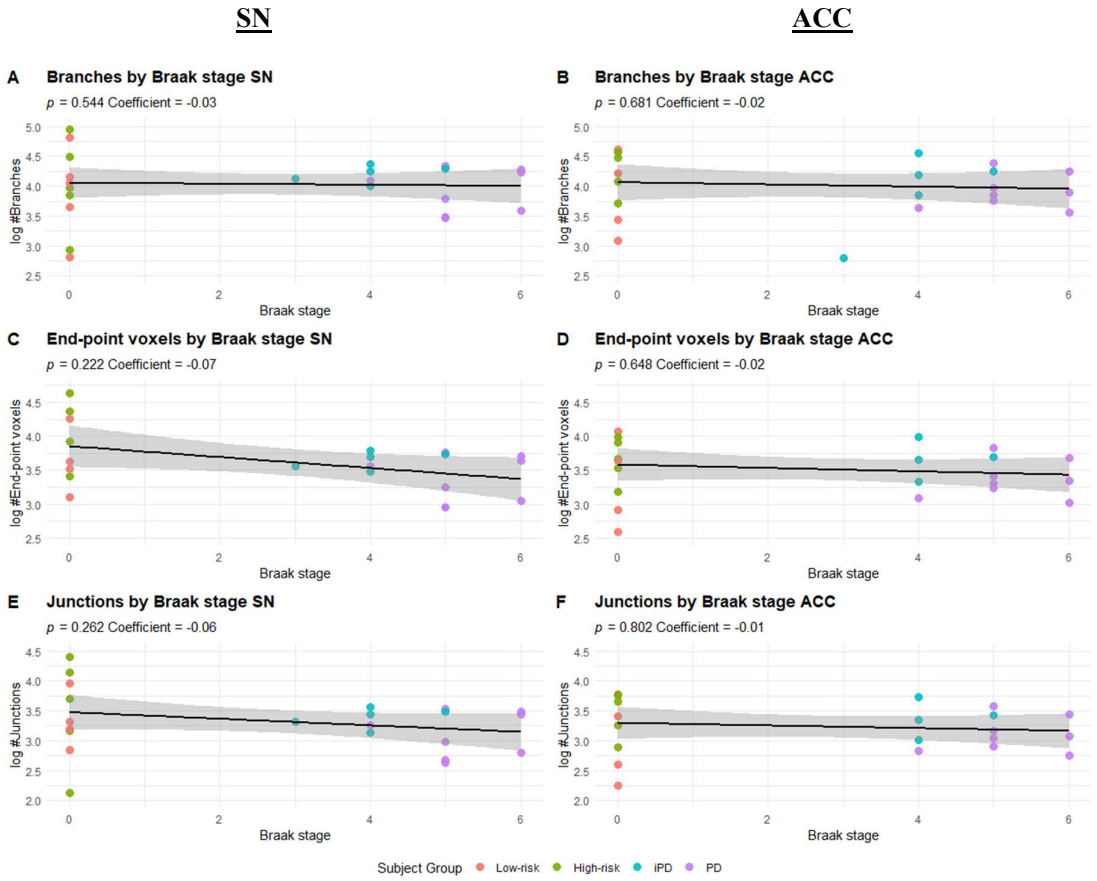

Figure 31. *Linear regression models of branching data by Braak stage. All coefficients were negative. Neither model showed a significant interaction.*

4.3.2 Circularity and perimeter did not significantly differ or show significant interactions with LBD severity

Differences in circularity and perimeter measurements were analyzed using Wilcoxon rank sum in RStudio and Kruskal-Wallis in SPSS. Neither test resulted in significant differences between the groups, see figure 32 and table 17.

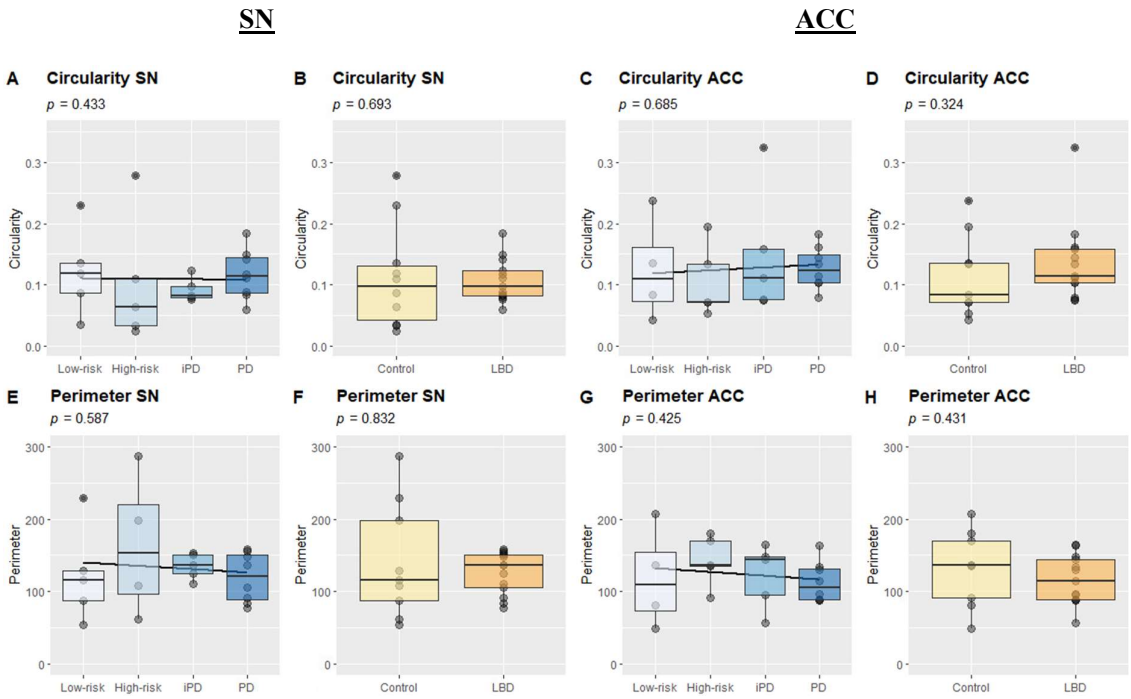

Figure 32. *Boxplots illustrating circularity and perimeter in SN and ACC. None of the means were significantly different, see table 17.*

Table 17. *Results of group comparisons of overall morphology measurements.*

	SN (23)		ACC (22)	
	Low-risk vs. high-risk vs. iPD vs. PD	**Control vs. LBD**	**Low-risk vs. high-risk vs. iPD vs. PD**	**Control vs. LBD**
Circularity	$\chi^2 = 2.685$ $p = 0.433$ df = 3	W = 58 $p = 0.693$	$\chi^2 = 1.488$ $p = 0.685$ df = 3	W = 43 $p = 0.324$
Perimeter	$\chi^2 = 1.933$ $p = 0.587$ df = 3	W = 69 $p = 0.832$	$\chi^2 = 2.790$ $p = 0.425$ df = 3	W = 71 $p = 0.431$

Abbreviations: χ^2, chi square statistic; df, degrees of freedom; p, p-value; W, Wilcoxon test

Data of circularity and perimeter was then applied to linear regression models, see figure 33. The linear regression models of circularity by Braak stage showed no significant association to Braak stage in SN ($p = 0.301$) nor ACC ($p = 0.527$). The interaction between perimeter and Braak stage was not significant either, although the linear regression model of perimeter in

SN (p = 0.135) would be considered as meaningful for the interaction if following the principle used for other independent variables (p<0.2). Braak by perimeter did not show a significant interaction in ACC (p = 0.622). Age was kept as a meaningful variable in SN, with coefficient -0.02 and $p = 0.057$ for circularity, and coefficient $-3.9e^{-03}$ and $p = 0.120$ for perimeter.

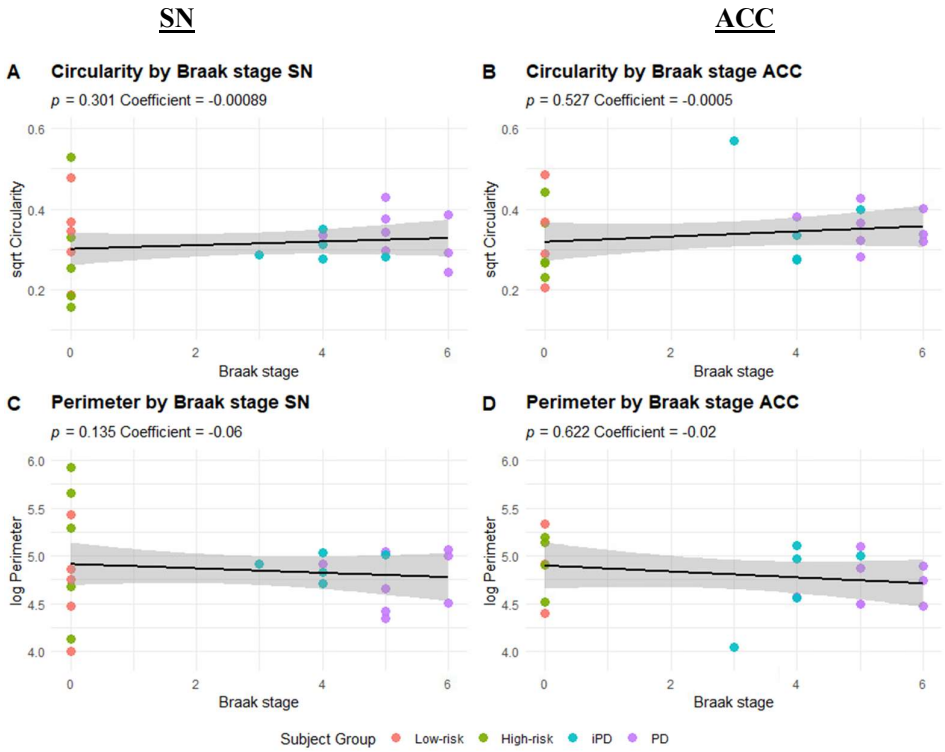

Figure 33. *Coefficient is for Braak stage after excluding insignificant independent variables*

4.3.3 There was no significant difference in intracellular α-syn in microglial cells by LBD severity

The presence of α-syn within the masks of microglia were measured by net mean gray value and net area in percent in FIJI, calculated as described in methods. The measurements were compared using Wilcoxon rank sum in RStudio and Kruskal-Wallis in SPSS. There was no significant difference in the intracellular α-syn by LBD severity, see figure 34 and table 18.

Even though the measurement of net area is flawed, reaching a potential maximum of net area at 7.5 %, the boxplot of SN by subgroups shows that both low-risks, high-risks and iPD all have a range from 0 to 7.5%, while the PD group has less variance than the other subgroups, see figure 34 E.

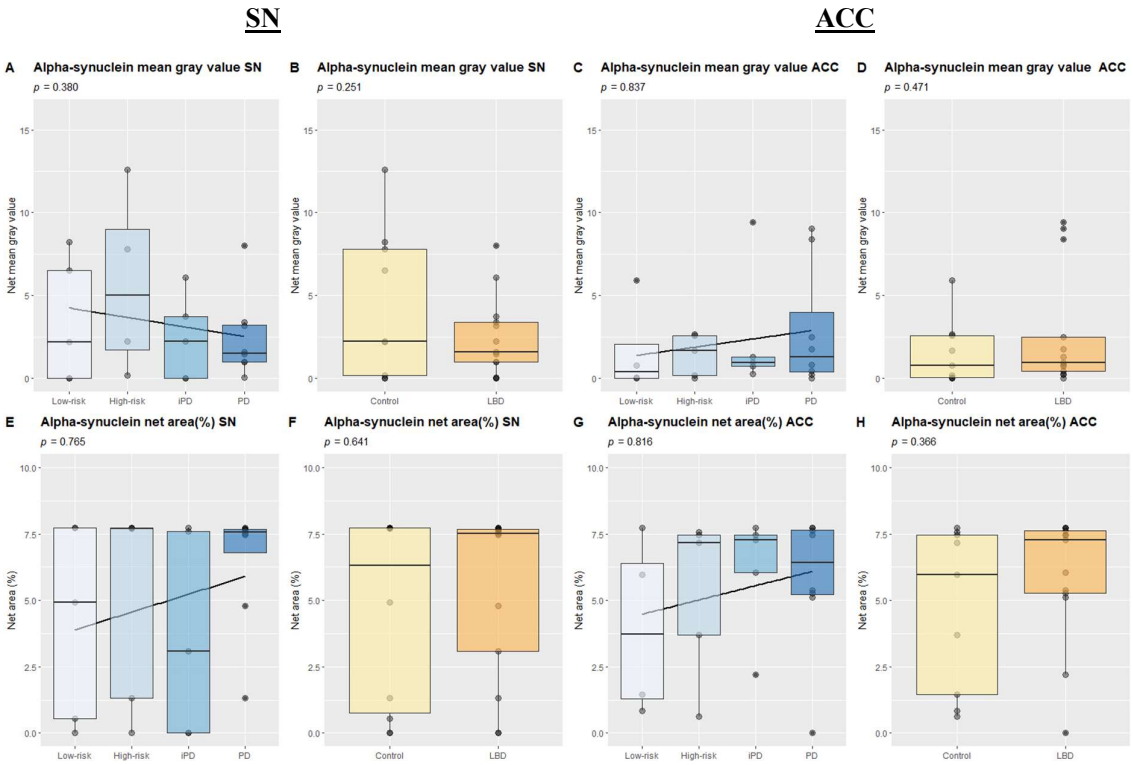

Figure 34. *First row* ***(A-D)*** *includes boxplots of the net mean gray value of intracellular α-syn in microglial masks. Second row* ***(E-H)*** *illustrates the alternative approach to quantify intracellular α-syn by % area α-syn signal detected within a mask. See table 18 for statistics.*

Table 18. *Results of group comparisons of intracellular* α-syn *measurements.*

	SN (23)		ACC (22)	
	Low-risk vs. high-risk vs. iPD vs. PD	**Control vs. LBD**	**Low-risk vs. high-risk vs. iPD vs. PD**	**Control vs. LBD**
Net mean gray value	$\chi^2 = 3.076$ $p = 0.380$ df = 3	W = 84 $p = 0.251$	$\chi^2 = 0.854$ $p = 0.837$ df = 3	W = 47 $p = 0.471$
Net area (%)	$\chi^2 = 1.151$ $p = 0.765$ df = 3	W = 73 $p = 0.641$	$\chi^2 = 938$ $p = 0.816$ df = 3	W = 44.5 $P = 0.366$

Abbreviations: χ^2, chi square statistic; df, degrees of freedom; p, p-value; W, Wilcoxon test

4.3.4 Net intensity of α-syn by LBD severity was significantly correlated in SN

The data of α-syn was then applied to linear regression models for SN and ACC separately. When including age as an independent variable in SN, all linear models gave significant interactions between parameters of LBD severity and α-syn, see table 19. All LBD severity parameters as well as age have a negative coefficient, meaning the less intracellular accumulation of α-syn as PD progresses and age. Sex was not a significant parameter in the SN models of LBD severity, with p-values ranging from 0.6-0.9.

In the linear regression models of net mean gray value of α-syn in ACC, sex was the only significant or nearly significant variable (see table 19), suggesting that sex affects the intracellular accumulation of α-syn in ACC. The sex variable is dichotomous defined as female=1 and male=2, hereby a negative coefficient indicating that male subjects have less accumulation of α-syn in microglia.

Table 19. *Linear regression models of net mean gray value of α-syn in SN and ACC. All models created using raw values, except from the PD PRS model in ACC, in which square root transformed to obtain normally distributed model residuals. All model residuals are normally distributed, confirmed by the Shapiro Wilk test in RStudio.*

	Parameter	Coefficient	SE	95% CI	t (20)	P
Substantia nigra	**(Intercept)**	43.31	9.19	[24.15, 62.47]	4.71	< .001 **
	Group	-2.53	0.72	[-4.02, -1.04]	-3.53	0.002 **
	Age	-0.40	0.10	[-0.61, -0.20]	-4.12	< .001 **
	(Intercept)	38.92	8.26	[21.69, 56.14]	4.71	< .001 **
	MainGroup	-5.36	1.48	[-8.46, -2.26]	-3.61	0.002 **
	Age	-0.33	0.09	[-0.51, -0.15]	-3.79	0.001 **
	(Intercept)	37.80	7.31	[22.55, 53.04]	5.17	< .001 **
	Braak	-1.24	0.29	[-1.85, -0.63]	-4.24	< .001 **
	Age	-0.38	0.08	[-0.56, -0.20]	-4.46	< .001 **
					t (14)	
	(Intercept)	37.91	11.55	[13.13, 62.69]	3.28	0.005 **
	PD PRS	98.71	244.06	[-424.75, 622.17]	0.40	0.692
	Age	-0.38	0.15	[-0.70, -0.06]	-2.58	0.022 .
					t (19)	
Anterior cingulate cortex	**(Intercept)**	3.89	2.22	[-0.75, 8.53]	1.76	0.095
	Group	0.68	0.64	[-0.29, 1.83]	1.25	0.227
	Sex	-2.50	1.26	[-5.13, 0.13]	-1.99	0.061
	(Intercept)	2.96	2.30	[-1.86, 7.78]	1.29	0.213
	MainGroup	2.14	1.27	[-0.51, 4.79]	1.69	0.107
	Sex	-2.92	1.27	[-5.56, -0.27]	-2.30	0.033 .
	(Intercept)	4.84	1.81	[1.05, 8.62]	2.68	0.015 .
	Braak	0.44	0.25	[-0.07, 0.95]	1.79	0.090
	Sex	-2.70	1.22	[-5.26, -0.15]	-2.22	0.039 .
					t (13)	
	(Intercept)	-3.30	2.24	[-8.15, 1.54]	-1.47	0.165
	PD PRS	23.44	46.48	[-76.97, 123.85]	0.50	0.622
	Age	0.06	0.03	[-0.00, 0.12]	2.02	0.065

4.3.5 Intracellular PS-129 in microglia did not significantly interact with LBD severity nor PD PRS

Net mean gray value and net area in percent of PS-129 signal within microglial masks were measured, see figure 35. There were no significant differences in any of the comparisons, see figure 36 and table 20. The two measurements should follow the same pattern, but the net area of PS-129 seems to be higher than the signal intensity (measured by mean gray value). Since the mean gray value was chosen for analysis of intracellular α-syn, the same is to be used for further analysis of PS-129.

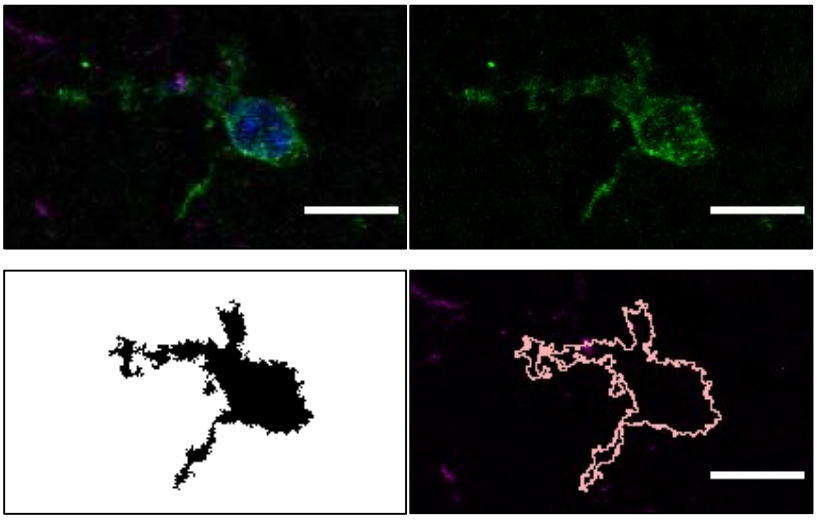

Figure 35. *Measurement of PS-129 intracellularly in microglia* ***A)*** *Merged channels for DAPI (blue), anti-Iba1 (green) and anti-PS-129 (magenta).* ***B)*** *Channel for anti-Iba1.* ***C)*** *Mask of the microglial cell.* ***D)*** *Channel for anti-PS-129 with microglial ROI. The intensity of the signal inside the ROI and fraction of PS-129 signal overlapping within the ROI area. The scale bar represents 10 µm.*

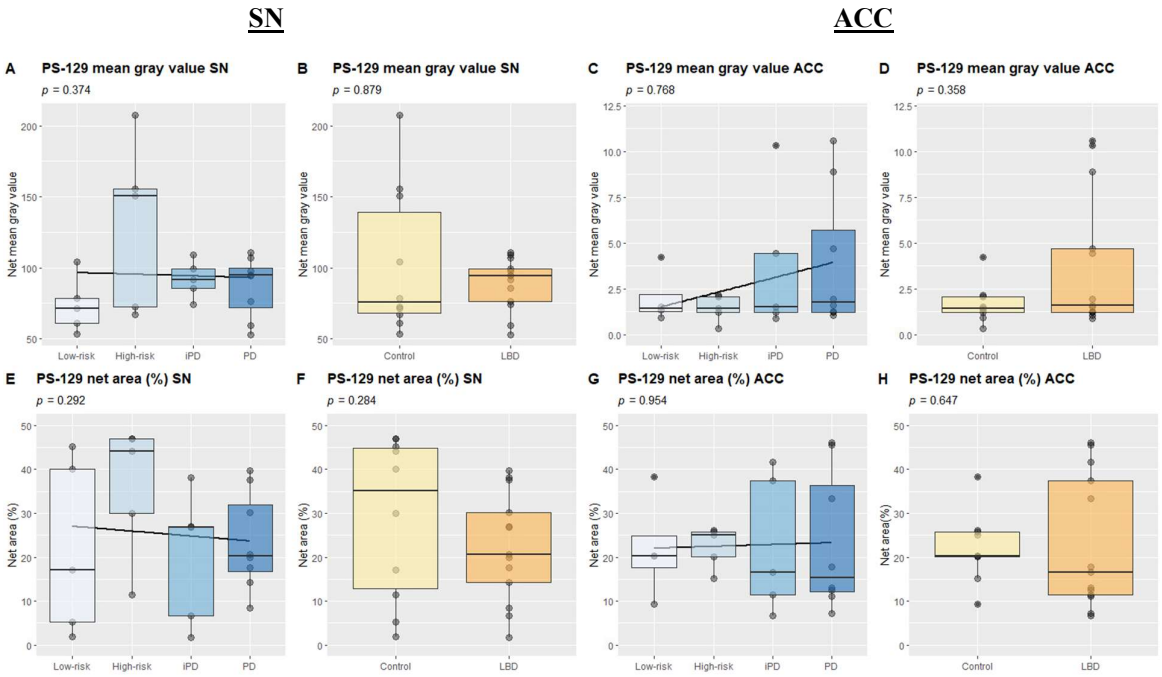

Figure 36. *Comparisons of intracellular PS-129 in microglia.* ***A-D)*** *Comparisons of net mean gray value of PS-129 in microglia. Mean gray value in low-risk vs high-risk vs iPD vs PD in SN (p = 0.374)* ***(A)*** *and ACC (p = 0.768)* ***(D).*** *Mean gray value in control vs LBD (p = 0.879) in SN* ***(B)*** *and ACC (p = 0.358)* ***(C)****.* ***E-H)*** *Comparisons of fraction of PS-129 signal in ROI (net area %) in microglia. Net area (%) in low-risk vs high-risk vs iPD vs PD in SN (p = 0.292)* ***(E)*** *and ACC (p = 0.954)* ***(G)****. Net area (%) in control vs LBD in SN (p = 0.284)* ***(F)*** *and ACC (p = 0.647)* ***(H)****.*

Table 20 *Results of group comparisons of intracellular PS-129 measurements.*

	SN (23)		**ACC (22)**	
	Low-risk vs. high-risk vs. iPD vs. PD	**Control vs. LBD**	**Low-risk vs. high-risk vs. iPD vs. PD**	**Control vs. LBD**
Net mean gray value	$\chi^2 = 3.116$ $p = 0.374$ df =3	W = 62 $p = 0.879$	$\chi^2 = 1.138$ $p = 0.768$ df = d	W = 44 $P = 0.358$
Net area (%)	$\chi^2 = 3.733$ $p = 0.292$ df = 3	W = 83 $p = 0.284$	$\chi^2 = 0.329$ $p = 0.954$ df = 3	W = 66 $p = 0.647$

Abbreviations: χ^2, chi square statistic; df, degrees of freedom; p, p-value; W, Wilcoxon test

The linear mixed regression models of PS-129 by LBD severity were not significant in mesencephalon nor ACC, see table 21 and figure 37. Both age and PMD were meaningful variables in SN. There was a

non-significant trend ($p = 0.084$) towards higher intracellular PS-129 in microglia in SN with increasing PD PRS, but not in ACC ($p = 0.373$).

Table 21. *Linear regression models of net mean gray value of PS-129 in SN and ACC. All models are based on log-transformed PS-129 mean gray values.*

	Parameter	Coefficient	SE	95% CI	t (19)	P
Substantia nigra	**(Intercept)**	5.81	0.93	[3.87, 7.76]	6.27	< .001 **
	Group	-0.06	0.07	[-0.21, 0.09]	-0.88	0.390
	Age	-0.02	$9.70e^{-03}$	[-0.04, 0.00]	-1.90	0.073
	PMD	$7.80e^{-04}$	$5.38e^{-04}$	[0.00, 0.00]	1.45	0.164
	(Intercept)	5.81	0.84	[4.05, 7.57]	6.90	< .001 **
	MainGroup	-0.16	0.15	[-0.47, 0.15]	-1.08	0.292
	Age	-0.02	8.60e-03	[-0.04, 0.00]	-2.00	0.060
	PMD	7.51e-04	5.34e-04	[0.00, 0.00]	1.41	0.176
	(Intercept)	5.84	0.79	[4.19, 7.50]	7.38	< .001 **
	Braak	-0.04	0.03	[-0.11, 0.02]	-1.34	0.197
	Age	-0.02	8.85e-03	[-0.04, 0.00]	-2.17	0.043 .
	PMD	7.17e-04	5.27e-04	[0.00, 0.00]	1.36	0.190
					(14)	
	(Intercept)	7.28	0.74	[5.70, 8.87]	9.84	< .001 **
	PD PRS	29.14	15.64	[-4.41, 62.69]	1.86	0.084
	Age	-0.03	9.53e-03	[-0.05, -0.01]	-2.85	0.013 .
					t (20)	
Anterior cingulate cortex	**(Intercept)**	0.10	0.48	[-0.91, 1.11]	0.20	0.842
	Group	0.21	0.16	[-0.13, 0.55]	1.31	0.205
	(Intercept)	-0.23	0.61	[-1.50, 1.03]	-0.39	0.704
	MainGroup	0.58	0.36	[-0.18, 1.34]	1.59	0.128
	(Intercept)	0.34	0.27	[-0.22, 0.91]	1.26	0.222
	Braak	0.12	0.07	[-0.03, 0.27]	1.67	0.110
					t (14)	
	(Intercept)	-0.12	0.81	[-1.85, 1.61]	-0.15	0.885
	PRS	-42.28	45.96	[-140.85, 56.30]	-0.92	0.373

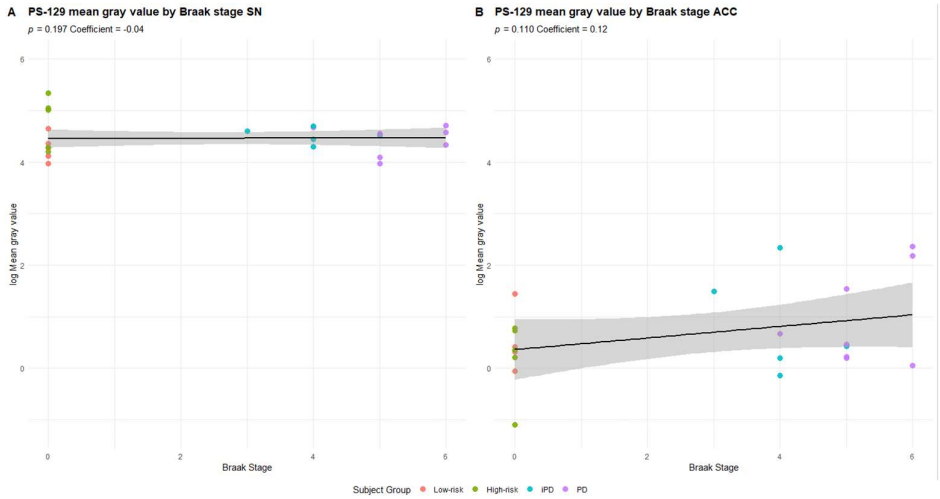

Figure 37. *Linear regression models of intracellular PS-129 by Braak stage were not significant in neither SN* ***(A)*** *nor ACC* ***(B)****.*

4.3.6 Circularity significantly decreased with less intracellular α-syn in mesencephalon

To investigate whether α-syn had an impact on microglial morphology, and hereby activation state, a linear regression model of circularity by net mean gray value of α-syn was tested, see table 22 and figure 38. This resulted in a significant model indicating that the circularity of microglial cells decreases with accumulation of α-syn. This indicates that the amoeboid microglia with high circularity values are less efficient in clearance of α-syn in SN. In ACC, interaction between intracellular α-syn and microglia circularity is not significant, see table 23.

Table 22. *Linear regression models of intracellular α-syn by square root values of circularity.*

	Parameter	Coefficient	SE	95% CI	t (21)	P
SN	**(Intercept)**	0.36	0.02	[0.32, 0.41]	17.18	< .001 **
	α-syn mean gray value	-0.01	$3.67e^{-03}$	[-0.02, 0.00]	-3.09	0.006 **
ACC	**(Intercept)**	0.25	0.07	[0.11, 0.39]	3.76	0.001 **
	α-syn mean gray value	$3.90e^{-03}$	$6.65e^{-03}$	[-0.01, 0.02]	0.59	0.565
	Sex	0.06	0.04	[-0.02, 0.15]	1.55	0.138

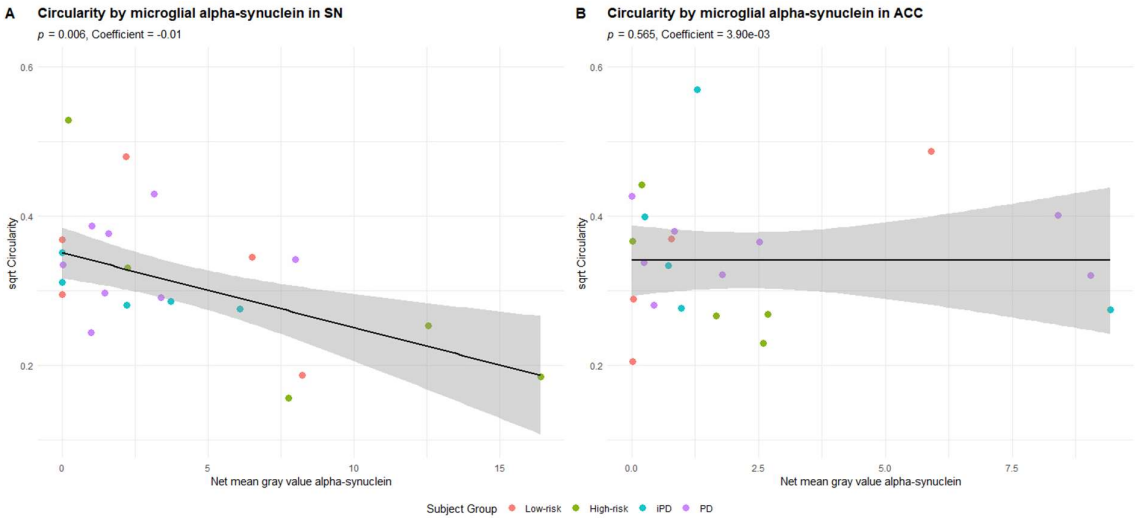

Figure 38. *Linear regression models of intracellular α-syn by square root values of circularity in SN* ***(A)*** *and ACC* ***(B)****.*

4.3.6 Circularity significantly decreased with less intracellular PS-129 in mesencephalon

In SN, higher PS-129 intensity is seen within microglial cells of those with low microglial circularity (p<0.001). The model also includes sex, as this covariate is above the predefined a-level for covariates of 0.2 (p = 0.091). The same interaction between circularity and microglial PS-129 was not significant in ACC, although sex again was the only variable with a p-value low enough not to be excluded (p = 0.092), suggesting sex might be of importance for microglial engulfment of PS-129. The models are presented in table 23.

Table 23. *Linear regression models of intracellular PS-129 intensity by square root-transformed values in SN, and log-transformed values of circularity in ACC.*

	Parameter	Coefficient	SE	95% CI	t (21)	P
SN	**(Intercept)**	0.56	0.05	[0.46, 0.66]	11.62	< .001**
	PS-129 mean gray value	-1.89e^{-03}	3.27e^{-03}	[0.00, 0.00]	-5.79	< .001**
	Sex	-0.04	0.02	[-0.09, 0.01]	-1.78	0.091
ACC	**(Intercept)**	-2.83	0.35	[-3.56, -2.09]	-8.03	< .001**
	PS-129 mean gray value	0.04	0.03	[-0.03, 0.11]	1.12	0.277
	Sex	0.38	0.21	[-0.07, 0.82]	1.77	0.092

4.3.7 Total levels vs intracellular levels of α-syn and PS-129 in mesencephalon did not correlate

Linear regression was only performed for mesencephalon, as the values from ACC did not meet the requirements for parametrical tests for any of the transformation alternatives. No significant correlation was seen for either α-syn (p = 0.123) nor PS-129 (p = 0.138), see table 24 and figure 39.

Table 24. *Linear regression models of total by intracellular α-syn and PS-129 in mesencephalon. Both intracellular and total α-syn variables were log-transformed.*

Parameter	Coefficient	SE	95% CI	t (9)	P
(Intercept)	0.83	0.46	[-0.20, 1.86]	1.82	0.102
α-syn WB	7.89	4.69	[-2.64, 18.59]	1.70	0.123
				t (8)	
(Intercept)	30.36	9.98	[7.35, 53.37]	3.04	0.016 .
PS-129 WB	-36.74	22.31	[-88.19, 14.71]	-2.40	0.138
Age	-0.29	0.12	[-0.57, -0.01]	-2.40	0.043 .

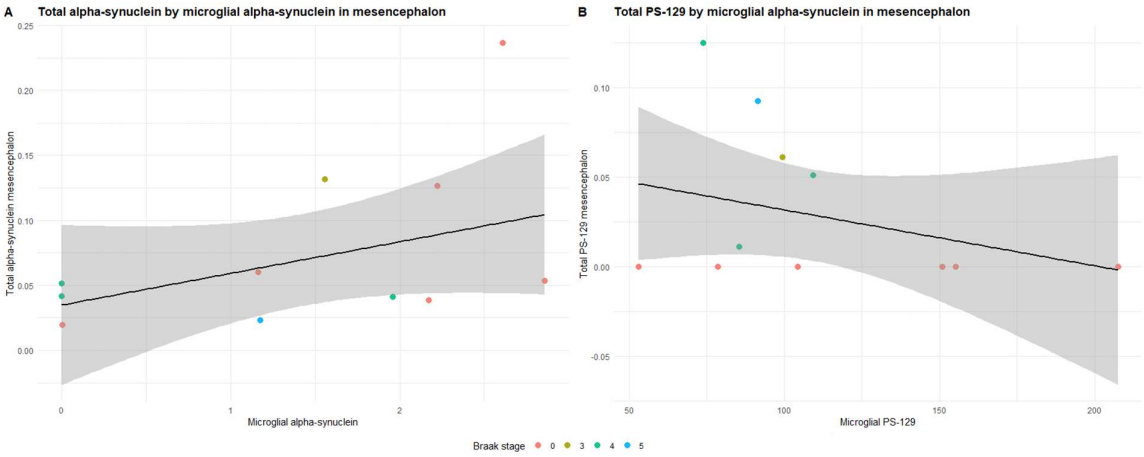

Figure 39. *Scatter plots of measurements from western blot and confocal imaging (mean gray value) **A)** intracellular by microglial α-syn in mesencephalon and **B)** intracellular by microglial PS-129 in mesencephalon.*

4.3.8 DJ-1 concentration and morphological measurements of microglial activation correlated significantly

Both DJ-1 and morphological measurements of microglia are thought to describe microglial activation. The concentration of DJ-1 from Luminex and circularity and end-point voxels from confocal imaging from the same patients were used in linear mixed regression models with patient ID as random intercept. The preferred measurement of processes was branching, but this model did not satisfy the normality assumption of model residuals. As the end-point voxel measurements were previously seen to follow the same pattern as branching, end-point voxels were used as measurements of processes instead. The linear mixed regression models are presented in table 25.

DJ-1 and circularity showed a significant negative correlation ($p = 0.005$). DJ-1 concentrations by end-point voxels also showed a significant declining correlation ($p = 0.009$. Age was a significant independent variable for both interactions ($p = 0.008$ and $p = 0.011$, respectively). The coefficient of end-point voxels (coefficient = $-4.03e^{-03}$) was noticeably smaller than the coefficient of circularity (coefficient = -1.22), see figure 40.

Table 25. *Linear mixed regression model of log DJ-1 log by raw values of circularity and end-point voxels. The models showed a significant declining DJ-1 concentration by both the microglial activation measurements.*

Parameter	Coefficient	SE	95% CI	t (12)	P
(Intercept)	10.14	0.38	[9.33, 10.96]	27.00	< .001 **
Circularity	-1.22	0.36	[-2.00, -0.43]	-3.38	0.005 *
Age	0.01	$4.65e^{-03}$	[0.00, 0.02]	3.19	0.008 *
(Intercept)	9.74	0.46	[8.73, 10.75]	21.07	< .001 **
End-point voxels	$4.03e^{-03}$	$1.30e^{-03}$	[0.00, 0.01]	3.10	0.009 *
Age	0.02	$5.33e^{-03}$	[0.00, 0.03]	3.02	0.011 .

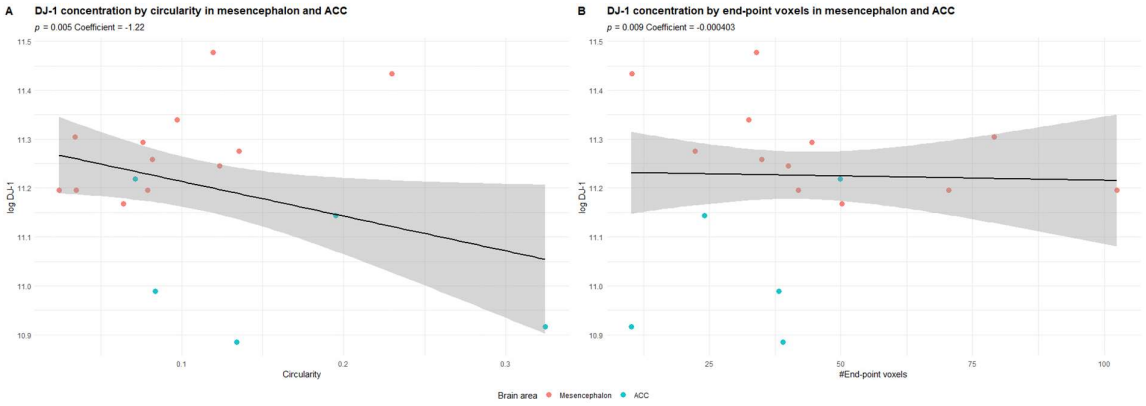

Figure 40. *Linear regression models including measurements from mesencephalon and ACC of* ***A)*** *DJ-1 by circularity significantly correlated (*p *= 0.005) and* ***B)*** *DJ-1 concentration by number of end-point voxels (*p *= 0.009). Colors represents brain area.*

5. Discussion

5.1 Interpretation of results

In ACC, representing a brain area affected by LBs late in the PD trajectory, there was a significantly higher total α-syn among those with early LBD (mean Braak = 3) compared to controls, measured with semi-quantitative western (p = 0.03, Wilcoxon rank sum with continuity correction), and a non-significant tendency of higher intracellular α-syn in microglia quantified from z-stacks achieved by confocal microscopy (coeff. = 0.44, 95% CI -0.07, 0.95, p = 0.090, linear regression) with higher LBD severity measured as Braak stage. In mesencephalon, on the other hand, there was no difference in the total α-syn measured with semi-quantitative western (p=1.0, Wilcoxon rank sum with continuity correction) between controls and LBD patents, but a reduced amount of α-syn intracellularly in microglia (coeff. = -1.24, 95% CI -1.85, -0.63, p < 0.001, linear regression) with increasing LBD severity in SN. In total, microglial cells in ACC tend to engulf more α-syn than microglial cells in SN. When α-syn is not engulfed by microglia in SN, it cannot be cleared by microglial synucleinphagy either, making the clearance of α-syn dependent on other potential clearing mechanisms. Accumulation and aggregation of α-syn itself, leads to neurotoxicity and disturbs the dopamine homeostasis among several other key aspects related to PD. The results hereby suggest that the degenerative susceptibility of dopaminergic neurons in SN may also be contributed by less efficient clearance of α-syn by microglial cells in SN with more severe LBD. As the location of α-syn is widespread in the brain and its roles mainly described related to neurotransmission, orthogonal view would have been a nice contribution to show microglial localization more certainly.

In pre-LB ACC tissue, there was no difference in amount of total α-syn phosphorylated at S-129 (PS-129) between cases and controls (p=0.11, Wilcoxon rank sum with continuity correction), while in mesencephalon there were a significant increase in total phosphorylated α-syn from the Braak stage of which mesencephalon develop LBs ($p=6.43 \times 10^{-5}$, Wilcoxon rank sum with continuity correction), measured with semi-quantitative western blotting. More post-translational phosphorylated α-syn might hence contribute to the non-significant difference of α-syn in SN with increasing LBD severity. These findings all suggest phosphorylation of α-syn causing LB pathology occurs after Braak stage 3 in ACC and prior to Braak stage 3 in mesencephalon, consistent with the Braak hypothesis.

Further, there was no difference in intracellular PS-129 in microglia between LBD and controls in neither ACC (p=0.36), nor substantia nigra (p=0.88) quantified from z-stacks achieved by confocal microscopy. The confocal images did however reveal PS-129 staining inside what can look like cellular processes from other cells than microglia. This need to be investigated further in subsequent work.

There was not detected a general microglial activation in neither ACC, nor mesencephalon in this study. There were no differences between LBD and controls in levels of fractalkine, IL-4, IL-6 or MCP-1 measured with Luminex from brain homogenate. These Luminex measurements had, however, methodological limitations, as several of the samples were unmeasurable in a non-significant pattern between both brain areas of the measurements and subject group. The finding of no significant difference of the pro-inflammatory IL-6 and MCP-1 can however be indicative of non-elevated levels of pro-inflammatory markers in PD.

There were no differences between LBD and controls in number of microglial branches, endpoints, perimeter or circularity measured from confocal images. As microglial cells are dynamic cells, continuously contracting and retracting processes, a clear threshold of morphology parameters of what should be characterized as an anti- or pro-inflammatory microglia is difficult to establish (114). It should however be possible to find significant differences between groups known to have extensive neuroinflammation as opposed to a healthy state. The biological processes happening *post mortem* could affect the morphology of microglia. PMD was however not a significant or meaningful variable in either of the linear regression models of morphology, hence is probably not the reason for insignificant differences in morphology with LBD severity. In the confocal images analyzed in this study, many of the processes were unattached to the soma, making the cells seem less branched and

rounder than their actual biology. This might partly explain the insignificant differences of cell morphology by LBD severity.

In ACC and mesencephalon analyzed together in a linear mixed model, there was, however, lower anti-inflammatory DJ-1 levels with increased LBD severity measured with Braak stage (coeff. = -0.02, 95% CI -0.04, 0.00, p=0.040). This correlation was especially relevant for mecencephalon (p = 0.025, RStudio). As DJ-1 exerts several neuroprotective functions, this finding might be a contributing factor to loss of dopaminergic neurons in SN, indirectly caused by reduced microglial clearance. This study cannot determine whether this effect is through inhibiting misfolded α-syn by chaperone activity or general protective effects from oxidative stress and ROS. Further, DJ-1 concentrations increased significantly with higher age of death, possibly reflecting a general higher level of oxidative stress and ROS with ageing. This could be connected to accumulation of mutations in genes for mitochondria and oxidative stress with age, as described by Reeve et al. (12). DJ-1 concentration decreased significantly with PMD in several of these models, suggesting denaturation of DJ-1 *post mortem*.

The same correlation between DJ-1 and LBD severity was not seen in ACC when analyzed separately (Braak, p = 0.453, RStudio). This could either be due to less oxidative stress and ROS in ACC due to less degeneration or indicate that the reduced DJ-1 occurs as a result of LB pathology as the homogenates from ACC only included LBD subjects with Braak stage 2-4 when ACC is still unaffected from LB pathology. Further studies should include ACC from LBD subjects with a higher level of Braak stage to evaluate DJ-1 association with LBD severity.

In ACC, DJ-1 showed a non-significant trend with increasing DJ-1 in ACC with higher PD PRS (p = 0.056, RStudio). The sample size of the linear regression model was only 8, and it would be interesting to increase the sample size and to evaluate this trend further. This could possibly also be investigated at the mRNA level in larger RNA sequencing datasets. The interaction between DJ-1 and PD PRS was not significant in mesencephalon (p = 0.763), which explains why the linear mixed model did not catch the possible interaction between PD PRS and DJ-1. Mutations in *PARK7* massively increase the risk of developing PD, but DJ-1 mutations are rare and result in less functional DJ-1. Hereby, the increased DJ-1 in ACC by PD PRS suggests that individuals with high PD PRS of developing PD have a compensatory mechanism by increased DJ-1 production early in the disease trajectory as it is not seen in mesencephalon from the same subjects, as ACC in this cohort is not yet affected by LBs. As

WT DJ-1 inhibits α-syn aggregation, this could be a potential cause of why some individuals do not develop PD despite high polygenic risk.

There was no difference in the VMAT2 levels between LBD and controls (p=0.69) or Braak stage group 0-2 vs 3-5 (p = 0.276, one-way ANOVA, SPSS) in brain tissue from mesencephalon. This finding is contrary to previous imaging studies performed in humans, where VMAT2 levels were significantly lower in PD patients beyond what dopaminergic degeneration could explain. The difference in VMAT2 concentration between Braak stage group 0-2 vs 3-5 had a lower p-value than controls vs LBD, pointing in the direction of degenerated dopaminergic neurons in the Braak stage group where SN is affected by neuropathology, although not significant. The statistical comparisons are probably limited by a small sample size. By increasing the sample size, the same trend might be seen provided that Braak stage is correlated with dopaminergic degeneration in the iPD group.

There was no difference in GDNF levels between LBD and controls (coeff. = -0.009, 95% CI -0.21, 0.19, p = 0.93, linear mixed model) when ACC and mesencephalon was analyzed together. There was reduced GDNF levels in the brain homogenate from ACC and mesencephalon analyzed against LBD risk, measured as PD PRS (coeff. = -18.67, 95% CI -52.35, -4.99, p = 0.02, linear mixed model). GDNF has a complex mechanism of action, involving several pathways. Low concentrations of GDNF might be one of the unfavorable changes contributing to the high PD PRS actually having a high PD risk, as genes upstream and downstream often also are affected. This finding could also indicate a higher need of neuroprotection in mesencephalon due to neuronal damage caused by the cumulative polymorphisms in patients with a high PD PRS.

GDNF concentrations had significantly higher measurability in mesencephalon compared to ACC ($p<0.001$, Fisher's Exact test, SPSS). As the non-measurable observations were under the lower limit of detection, this also indirectly indicates higher GDNF concentrations in mesencephalon compared to ACC. It could also be indicative of a lower need for neuroprotection in ACC prior to LB affection. At the same time, ACC is not characterized by neurodegeneration, possible explaining lower levels of GDNF in ACC despite the ACC samples originating from patients without LB affection. A kit with higher sensitivity would be preferred, as the GDNF concentrations in ACC most likely are not zero. Further investigation of GDNF could be to look at PD PRS against mRNA levels of GDNF. This data already exists and has a much bigger sample size.

The low-risk controls (mean = 91.0) were significantly older than the high-risk group (mean = 77.0) ($p<0.01$, ANOVA) and higher than in the LBD group (mean = 84.3). The control group and LBD group were not significantly different in age (ANOVA post-hoc, SPSS). Age was a significant variable in several of the models. Age of death had a significant positive coefficient in the regression models of GDNF against LBD severity (coeff. = 1.21, 95% CI 0.00, 0.02, p = 0.046). Intracellular accumulation of a-syn in SN and ACC decreased with older age. The amount of intracellular PS-129 also decreased with age. Concentrations of DJ-1 increased with increasing age in both mesencephalon and ACC when used in the model comparing LBD severity by control vs LBD (coeff. 6.81×10^{-5}, p = 0.012, linear mixed regression).

Males are known to have a higher risk of developing PD. In ACC, men had significantly less a-syn intracellularly (coeff. -2.70, $p = 0.039$, linear regression) with increasing LBD severity, and borderline significant more amoeboid shaped microglia (coeff. 0.38, $p = 0.092$, linear regression) by intracellular PS-129. This is indicative of men having less efficient clearance of a-syn in ACC, and more pro-inflammatory activated microglia as a result, shown as an interaction by increasing PS-129. This suggest that less effective clearance of a-syn in ACC, lead to more phosphorylation of a-syn, seemingly enhancing proinflammatory activation of microglia. Alternatively, microglia more prone to pro-inflammatory activation and hence lower a-syn clearance efficiency. This finding could contribute to on-going work in the field of why male sex is a risk factor for developing PD.

5.2 Methodical discussion

5.2.1 Study design

The appropriate study design to investigate the individual changes and variation in a disease development, is a longitudinal design where characteristics of the subjects are gathered over a prolonged period of time. In this study, a cross-sectional design was used to investigate aspects of neuroinflammation along the LBD development, imitating a longitudinal design as the disease is believed to progress if a longitudinal design was feasible. By this, the intraindividual variation with time is lost, in which is of great importance in progressive diseases such as PD.

In this study, Braak stage 1 and 2 are assumed to be preliminary stages of Braak stage 3 when LB pathology reaches SN and patients become symptomatic. However, it is uncertain whether

these study subjects with Braak stage 1 and 2 would ever progress to a clinical diagnosis of PD, and hereby if they actually represent an iPD group. This assumption cannot be followed, as the staging is based on thorough neuropathological examinations that could not be archived in living patients.

A longitudinal design is not possible to investigate the aims of this study. Technically, it is not possible to do repeated brain biopsies from the same brain area without affecting subsequent biopsies. Further, all afferent and efferent nerve signals pass through the brainstem. Due to this, SN is an impossible brain area to use for biopsies. In addition, the ethical aspect restricts repeated brain biopsies in humans for this purpose.

Animal models could be a solution to the ethical aspect. As availability of human brain tissue is limited, most studies of PD pathogenesis are studies performed in animal models and *in vitro* models. Although these models have made valuable contributions to the understanding of PD, the models only imitate an isolated part of the pathogenesis of PD. The translational value is limited by the physiologically correctness of i.e., studying human proteins in non-human species in transgenic models, or acute loss of dopaminergic neurons induced by the toxicant 1-Methyl-4-phenyl-1,2,3,6-tetrahydropyridine (MPTP) rather than the gradual loss caused by LB pathology as in human PD (115). As the progression of PD is poorly imitated in animal models, a cross-sectional design for human brain tissue analysis is the best alternative for our purpose. The results of the study must therefore be interpreted within the limitations of assumptions of the study design.

5.2.2 Statistics regarding human brain tissue

Finding associations in human subjects who have been exposed to known and unknown risk factors for disease is challenging. Medical history and lifestyle, including smoking and drinking habits, were available for our patient samples, which could influence the measurements obtained in this study. With few exceptions, however, the sample size is too small for most of these factors to be a significant covariate in our statistical models.

Tissue quality is affected by pre- and postmortem conditions, especially the interval from the time between death and removal of the brain. In order to adjust for tissue quality, PMD was used as a covariate and independent variable in the models. PMD rarely turned out as a significant factor, and alternative measurements to use for correction of tissue quality were discussed, like RNA integrity number (RIN). As RIN values were only available for a subset

of the cohort, PMD was kept as a substitute measurement for tissue quality. *Postmortem* pH from the brain tissue could be an alternative measure for tissue quality, but this information was only available for a subset of the cohort.

5.2.3 Homogenization and sonication

As the pieces of tissue that were homogenized were of different size, they required different amounts of time homogenizing. To compensate for the longer homogenization process, potentially exposing larger autopsy samples to higher temperatures, the samples were taken on and off ice during the process.

To homogenize brain tissue, the use of a plastic pestle and syringe was suitable. However, this method is not appropriate for homogenization of tissues containing more connective tissue, such as heart, liver and kidney. An alternative homogenization technique to using a plastic pestle is cryogenic homogenization, meaning crushing the tissue in liquid nitrogen. This is a time efficient technique that ensures that the tissue remains frozen for the entire time, reducing heat induced protein degradation.

Sonication was performed to extract nuclear proteins. The ultrasonic waves also generate heat and can cause protein degradation. To minimize the risk of protein degradation, a minimum of 15 minutes was spent between each run. The automated sonication cycles make the procedure more reproducible and was found appropriate in this study compared to using a probe sonicator.

5.2.4 Western blotting

In order to quantify protein amount, the protein concentration added to each well should be as equal as possible. Although all samples are protein measured, diluted to the same concentration, and added in the same amount, the protein concentration can vary. Therefore, the use of a loading control is necessary. GAPDH was used as a loading control as the protein has an appropriate size in relation to the proteins for investigation. In addition, GAPDH is an abundant protein and is a well characterized loading control. However, Chinese case-control studies have found that polymorphisms of the GAPDH gene could potentially have a role in the pathogenesis of PD, as one of the rs1136666 polymorphism of GAPDH strongly correlates with sporadic PD and increases the risk of developing PD particularly in older men

(29, 70). A possibility to resolve this potential issue, is to include another loading control i.e., vinculin, and use the mean signal of both GAPDH and vinculin.

A study of dephosphorylation of PS-129 left *post mortem* rat brains in room temperature after decapitation for 30 minutes up to 4 hours (42). Reactivity with PS-129 decreased rapidly at 30 minutes, and was abolished after 1 hour, suggesting that PS-129 is dephosphorylated rapidly *post mortem* (42). In the western blot performed in this study, human tissue samples with PMD up to 7 hours and 30 minutes gave bands. However, it should be kept in mind that samples with long PMD could have given bands if the PMD affects dephosphorylation or denaturation. α-syn was recognizable after 11 hours and 45 minutes, suggesting that α-syn is not as affected by PMD as PS-129. This follows the conclusion by Fujiwara et. al (42).

During antibody validation, GAPDH gave extra bands at approximately 15 kDa and 20 kDa when image acquisition was run for longer than approximately 5 minutes, which would disturb the analysis of α-syn and PS-129 around the same molecular weight. However, this problem was avoided by cutting the membrane horizontally above these extra GAPDH bands and the membranes were incubated with primary antibodies separately.

5.2.5 Luminex and ELISA

Although Luminex and ELISA are reliable methods for protein quantification, the experiments had some limitations. The blank samples used for ELISA were different from the diluent. For Luminex, SDS in the homogenate can potentially affect the measurements. By this, the absolute concentrations from ELISA and Luminex should be interpreted carefully. The results are still relevant to describe relative concentrations between individuals, as done in this study.

5.2.5 Microtome sectioning

There were provided paraffin blocks, ready sectioned paraffin embedded brain tissue, fixed brain tissue embedded at the Department of Pathology at Oslo University Hospital, RadiumHospitalet and also frozen tissue later fixed, and paraffin embedded. There seemed to be a difference in paraffin used from the different sources as they behaved differently when being sectioned. In addition, the sectioning was performed by three different people, in addition to those sectioned before shipment from the Netherlands. Although all sections

should be treated exactly the same, different settings during microtome sectioning are unlikely to cause significant alterations to the fixated tissue. The difference in IF-staining is more likely to follow from the various tissue treatments.

5.2.6 Immunohistochemistry

5.2.6.1 Antibody verification

In antibody-based methods, specificity of the primary antibodies is key. The preferred microglial marker was Iba1 produced in goat or guinea pig, as anti-α-syn was produced in mouse and anti-PS-129 in rabbit. Although 100% of the anti-Iba1 goat positive cells were also anti-Iba1 Rabbit positive in the anti-Iba1 specificity testing, there were some anti-Iba1 rabbit staining that was not overlapping with anti-Iba1 goat. However, this anti-Iba1 rabbit staining was vague outlines of cells with no processes. Since DAPI was not included, these anti-Iba1 rabbit positive cells cannot certainly be identified as microglia, although they did not overlap with channels for anti-GFAP.

5.2.6.2 Antigen retrieval

Proper tissue preparation prior to immunohistochemical staining is critical for successful epitope detection (71). The reproducibility of immunohistochemical staining can vary due to tissue fixation (65). Tissue fixation is performed to prevent autolysis and degradation of the tissue (66), by forming cross-links via methylene bridges between the proteins and the fixative (67). These cross-links cause the tertiary and quaternary structures of many proteins which can decrease the antigenicity, thus making many of the antigens undetectable by antibodies (68). Antigen retrieval methods are performed to retrieve lost antigenicity by returning the modified proteins back to their prefixation confirmation (68, 71).

Antigen retrieval was necessary for the human tissue sections. The epitopes of Iba1, α-syn and PS-129 all preferred different antigen retrieval protocols. Preliminary studies were performed to optimize the antigen retrieval procedure for this tissue with emphasis on antigen retrieval solution, temperature, time and section protection. During preliminary testing, undiluted formic acid was used as an antigen retrieval solution as it was recommended for α-syn. This treatment was too rough for Iba1, resulting in poor staining.

Temperature is most important for successful antigen retrieval. The pH of the antigen retrieval solution is important. Solutions with neutral pH are less likely to affect the tissue morphology compared to acidic or basic conditions, while the two latter are often more effective (116).

An alternative to HIER is protease induced epitope retrieval (PIER). In PIER, the use of enzymes, such as pepsin, trypsin and proteinase K, are used to restore epitope conformation. However, this method is more likely to destroy both tissue morphology and antigens, hence lower rate of successful immunohistochemical staining (116).

5.2.7 Confocal microscopy

Since the sections were fixed for different amounts of time, it was expected to be different signals with the same settings at the confocal microscope. This made it impossible to have the same settings on all sections. Also, sections from SN had in general weaker signals. Settings for α-syn and PS-129 were not adjusted at all, but for analysis of microglia, laser for the Iba1 channel was adjusted to approximately the same for SN and ACC to make at a minimum the soma visible. Therefore, microglial morphology measurements can be underestimated. This underlines the importance of standardized sample preparation and optimization of protocols for comparable results.

Only a subgroup of the patients with paraffin embedded tissue was analyzed due to time limitations. The patient samples that were analyzed were chosen to represent at least 5 patients in each subgroup to meet the assumptions for statistical analysis. Low-controls and patients with high Braak stages, representing the two most extreme scenarios of the PD trajectory, were prioritized to have the best possibility of discovering differences across the groups. Despite blinding the sections, the amount of neuromelanin and degenerated tissue in SN, presence of LBs, as well as the morphology of microglial cells disclosed the patient group during image acquisition. The amount present of α-syn and PS-129 could have disclosed the patient group. To avoid this affecting inclusion of microglial cells, the channels for α-syn and PS-129 were not looked at prior to imaging.

One section did not have any staining, probably due to drying during incubation with primary antibodies, as the section clearly had been incubated with secondary antibodies due to non-specific background.

6. Conclusion and future perspective

This study has aimed to describe the role of microglial cells in neuroinflammation and clearance of α-syn and PS-129. Taken together, there are higher total α-syn in ACC in the pre-LB phase, while there are higher PS-129 levels in mesencephalon in the post-LB phase. Ameboid microglial cells with higher circularity are associated with decreased α-syn levels intracellularly, indicative of reduced α-syn clearance efficiency. Both the anti-inflammatory DJ-1 level and the amount of microglial α-syn intracellularly are lower in mesencephalon with more pronounced neuropathological LBD severity, suggesting microglial deactivation and reduced α-syn autophagy. Together, this might enhance α-syn accumulation through reduced microglial clearance, seen as increased posttranslational phosphorylation of α-syn and LB development.

References

1. Antony PM, Diederich NJ, Krüger R, Balling R. The hallmarks of Parkinson's disease. Febs j. 2013;280(23):5981-93.
2. Balestrino R, Schapira AHV. Parkinson disease. Eur J Neurol. 2020;27(1):27-42.
3. Tysnes OB, Storstein A. Epidemiology of Parkinson's disease. J Neural Transm (Vienna). 2017;124(8):901-5.
4. Poewe W, Seppi K, Tanner CM, Halliday GM, Brundin P, Volkmann J, et al. Parkinson disease. Nature Reviews Disease Primers. 2017;3(1):17013.
5. Macleod AD, Taylor KS, Counsell CE. Mortality in Parkinson's disease: a systematic review and meta-analysis. Mov Disord. 2014;29(13):1615-22.
6. Dorsey ER, Bloem BR. The Parkinson Pandemic—A Call to Action. JAMA Neurology. 2018;75(1):9-10.
7. Simon DK, Tanner CM, Brundin P. Parkinson Disease Epidemiology, Pathology, Genetics, and Pathophysiology. Clinics in Geriatric Medicine. 2020;36(1):1-12.
8. Braak H, Tredici KD, Rüb U, de Vos RAI, Jansen Steur ENH, Braak E. Staging of brain pathology related to sporadic Parkinson's disease. Neurobiology of Aging. 2003;24(2):197-211.
9. Holck P. Substantia nigra2021 [cited 2022 10. april]. Available from: https://sml.snl.no/substantia_nigra.
10. Sand O, Sjaastad ØV, Haug E, Toverud KC. Menneskets fysiologi. 2. utg. ed. Oslo: Gyldendal akademisk; 2014.
11. Puchades M, Sogn CJ, Maehlen J, Bergersen LH, Gundersen V. Unaltered lactate and glucose transporter levels in the MPTP mouse model of Parkinson's disease. J Parkinsons Dis. 2013;3(3):371-85.
12. Reeve A, Simcox E, Turnbull D. Ageing and Parkinson's disease: why is advancing age the biggest risk factor? Ageing Res Rev. 2014;14(100):19-30.
13. Venda LL, Cragg SJ, Buchman VL, Wade-Martins R. α-Synuclein and dopamine at the crossroads of Parkinson's disease. Trends Neurosci. 2010;33(12):559-68.
14. Block ML, Zecca L, Hong JS. Microglia-mediated neurotoxicity: uncovering the molecular mechanisms. Nat Rev Neurosci. 2007;8(1):57-69.

15. Burbulla LF, Song P, Mazzulli JR, Zampese E, Wong YC, Jeon S, et al. Dopamine oxidation mediates mitochondrial and lysosomal dysfunction in Parkinson's disease. Science. 2017;357(6357):1255-61.
16. Perez RG, Waymire JC, Lin E, Liu JJ, Guo F, Zigmond MJ. A role for alpha-synuclein in the regulation of dopamine biosynthesis. J Neurosci. 2002;22(8):3090-9.
17. Lotharius J, Brundin P. Pathogenesis of parkinson's disease: dopamine, vesicles and α-synuclein. Nature Reviews Neuroscience. 2002;3(12):932-42.
18. Mulvihill KG. Presynaptic regulation of dopamine release: Role of the DAT and VMAT2 transporters. Neurochem Int. 2019;122:94-105.
19. Bridi JC, Hirth F. Mechanisms of α-Synuclein Induced Synaptopathy in Parkinson's Disease. Front Neurosci. 2018;12:80.
20. Lee CS, Samii A, Sossi V, Ruth TJ, Schulzer M, Holden JE, et al. In vivo positron emission tomographic evidence for compensatory changes in presynaptic dopaminergic nerve terminals in Parkinson's disease. Ann Neurol. 2000;47(4):493-503.
21. Henderson G, Flower RJ, Ritter JM, Dale MM, Rang HP. Rang and Dale's pharmacology. 8th ed. ed. Edinburgh: Elsevier Churchill Livingstone; 2016.
22. Jagadeesan AJ, Murugesan R, Vimala Devi S, Meera M, Madhumala G, Vishwanathan Padmaja M, et al. Current trends in etiology, prognosis and therapeutic aspects of Parkinson's disease: a review. Acta Biomed. 2017;88(3):249-62.
23. Jankovic J, Tan EK. Parkinson's disease: etiopathogenesis and treatment. J Neurol Neurosurg Psychiatry. 2020;91(8):795-808.
24. Cosgrove J, Alty JE, Jamieson S. Cognitive impairment in Parkinson's disease. Postgrad Med J. 2015;91(1074):212-20.
25. Vogt BA. Chapter 13 - Cingulate cortex in Parkinson's disease. In: Vogt BA, editor. Handbook of Clinical Neurology. 166: Elsevier; 2019. p. 253-66.
26. Polymeropoulos MH, Lavedan C, Leroy E, Ide SE, Dehejia A, Dutra A, et al. Mutation in the alpha-synuclein gene identified in families with Parkinson's disease. Science. 1997;276(5321):2045-7.
27. Burré J, Sharma M, Südhof TC. Cell Biology and Pathophysiology of α-Synuclein. Cold Spring Harb Perspect Med. 2018;8(3).
28. George S, Rey NL, Tyson T, Esquibel C, Meyerdirk L, Schulz E, et al. Microglia affect α-synuclein cell-to-cell transfer in a mouse model of Parkinson's disease. Mol Neurodegener [Internet]. 2019 2019/08//; 14(1):[34 p.]. Available from: http://europepmc.org/abstract/MED/31419995

https://doi.org/10.1186/s13024-019-0335-3

https://europepmc.org/articles/PMC6697982

https://europepmc.org/articles/PMC6697982?pdf=render.

29. Choi I, Zhang Y, Seegobin SP, Pruvost M, Wang Q, Purtell K, et al. Microglia clear neuron-released α-synuclein via selective autophagy and prevent neurodegeneration. Nat Commun. 2020;11(1):1386.

30. Rocha EM, De Miranda B, Sanders LH. Alpha-synuclein: Pathology, mitochondrial dysfunction and neuroinflammation in Parkinson's disease. Neurobiology of Disease. 2018;109:249-57.

31. Ghosh D, Mehra S, Sahay S, Singh PK, Maji SK. α-synuclein aggregation and its modulation. Int J Biol Macromol. 2017;100:37-54.

32. Wang Y, Shi M, Chung KA, Zabetian CP, Leverenz JB, Berg D, et al. Phosphorylated α-synuclein in Parkinson's disease. Sci Transl Med. 2012;4(121):121ra20-ra20.

33. Kahle PJ, Neumann M, Ozmen L, Müller V, Jacobsen H, Schindzielorz A, et al. Subcellular Localization of Wild-Type and Parkinson's Disease-Associated Mutant α-Synuclein in Human and Transgenic Mouse Brain. The Journal of Neuroscience. 2000;20(17):6365-73.

34. Fujiwara H, Hasegawa M, Dohmae N, Kawashima A, Masliah E, Goldberg MS, et al. α-Synuclein is phosphorylated in synucleinopathy lesions. Nature Cell Biology. 2002;4(2):160-4.

35. Chen L, Periquet M, Wang X, Negro A, McLean PJ, Hyman BT, et al. Tyrosine and serine phosphorylation of alpha-synuclein have opposing effects on neurotoxicity and soluble oligomer formation. J Clin Invest. 2009;119(11):3257-65.

36. Braak H, Del Tredici K, Bratzke H, Hamm-Clement J, Sandmann-Keil D, Rüb U. Staging of the intracerebral inclusion body pathology associated with idiopathic Parkinson's disease (preclinical and clinical stages). J Neurol. 2002;249 Suppl 3:Iii/1-5.

37. Fornari S, Schäfer A, Jucker M, Goriely A, Kuhl E. Prion-like spreading of Alzheimer's disease within the brain's connectome. J R Soc Interface. 2019;16(159):20190356.

38. Goedert M, Masuda-Suzukake M, Falcon B. Like prions: The propagation of aggregated tau and α-synuclein in neurodegeneration. Brain. 2017;140(2):266-78.

39. Holck P. Neocortex2022 [cited 2022 28. april]. Available from: https://snl.no/neocortex.

40. Wei L, Hu X, Yuan Y, Liu W, Chen H. Abnormal ventral tegmental area-anterior cingulate cortex connectivity in Parkinson's disease with depression. Behavioural Brain Research. 2018;347:132-9.
41. Imamura K, Hishikawa N, Sawada M, Nagatsu T, Yoshida M, Hashizume Y. Distribution of major histocompatibility complex class II-positive microglia and cytokine profile of Parkinson's disease brains. Acta Neuropathologica. 2003;106(6):518-26.
42. Greenland TBSJC. Parkinson's Disease: Pathogenesis and Clinical Aspects. In: Stoker TB, Greenland JC, editors. Parkinson's Disease: Pathogenesis and Clinical Aspects. Brisbane (AU): Codon Publications

43. Domenighetti C, Sugier P-E, Sreelatha AAK, Schulte C, Grover S, Mohamed O, et al. Mendelian Randomisation Study of Smoking, Alcohol, and Coffee Drinking in Relation to Parkinson's Disease. Journal of Parkinson's Disease. 2022;12:267-82.
44. Pankratz N, Foroud T. Genetics of Parkinson disease. Genetics in Medicine. 2007;9(12):801-11.
45. Ritz B, Lee PC, Lassen CF, Arah OA. Parkinson disease and smoking revisited: ease of quitting is an early sign of the disease. Neurology. 2014;83(16):1396-402.
46. Cacabelos R. Parkinson's Disease: From Pathogenesis to Pharmacogenomics. Int J Mol Sci. 2017;18(3).
47. Cerri S, Mus L, Blandini F. Parkinson's Disease in Women and Men: What's the Difference? J Parkinsons Dis. 2019;9(3):501-15.
48. Blauwendraat C, Nalls MA, Singleton AB. The genetic architecture of Parkinson's disease. Lancet Neurol. 2020;19(2):170-8.
49. Lvovs D, Favorova OO, Favorov AV. A Polygenic Approach to the Study of Polygenic Diseases. Acta Naturae. 2012;4(3):59-71.
50. Reed X, Bandrés-Ciga S, Blauwendraat C, Cookson MR. The role of monogenic genes in idiopathic Parkinson's disease. Neurobiol Dis. 2019;124:230-9.
51. Dehestani M, Liu H, Gasser T. Polygenic Risk Scores Contribute to Personalized Medicine of Parkinson's Disease. J Pers Med. 2021;11(10).
52. Iwai A, Masliah E, Yoshimoto M, Ge N, Flanagan L, de Silva HA, et al. The precursor protein of non-A beta component of Alzheimer's disease amyloid is a presynaptic protein of the central nervous system. Neuron. 1995;14(2):467-75.

53. Chartier-Harlin MC, Kachergus J, Roumier C, Mouroux V, Douay X, Lincoln S, et al. Alpha-synuclein locus duplication as a cause of familial Parkinson's disease. Lancet. 2004;364(9440):1167-9.
54. Ritchie CM, Thomas PJ. Alpha-synuclein truncation and disease. Health. 2012;Vol.04No.11:11.
55. Kara E, Lewis PA, Ling H, Proukakis C, Houlden H, Hardy J. α-Synuclein mutations cluster around a putative protein loop. Neuroscience Letters. 2013;546:67-70.
56. Fauvet B, Butterfield SM, Fuks J, Brik A, Lashuel HA. One-pot total chemical synthesis of human α-synuclein. Chemical Communications. 2013;49(81):9254-6.
57. Ariga H, Takahashi-Niki K, Kato I, Maita H, Niki T, Iguchi-Ariga SMM. Neuroprotective Function of DJ-1 in Parkinson's Disease. Oxid Med Cell Longev. 2013;2013:683920-9.
58. Zhang L, Wang J, Wang J, Yang B, He Q, Weng Q. Role of DJ-1 in Immune and Inflammatory Diseases. Frontiers in Immunology. 2020;11(994).
59. Hijioka M, Inden M, Yanagisawa D, Kitamura Y. DJ-1/PARK7: A New Therapeutic Target for Neurodegenerative Disorders. Biol Pharm Bull. 2017;40(5):548-52.
60. Dolgacheva LP, Berezhnov AV, Fedotova EI, Zinchenko VP, Abramov AY. Role of DJ-1 in the mechanism of pathogenesis of Parkinson's disease. J Bioenerg Biomembr. 2019;51(3):175-88.
61. Repici M, Giorgini F. DJ-1 in Parkinson's Disease: Clinical Insights and Therapeutic Perspectives. J Clin Med. 2019;8(9):1377.
62. Bonifati V, Rizzu P, Baren MJv, Schaap O, Breedveld GJ, Krieger E, et al. Mutations in the DJ-1 Gene Associated with Autosomal Recessive Early-Onset Parkinsonism. Science. 2003;299(5604):256-9.
63. Buneeva OA, Medvedev AE. DJ-1 Protein and Its Role in the Development of Parkinson's Disease: Studies on Experimental Models. Biochemistry (Moscow). 2021;86(6):627-40.
64. Moore DJ, Zhang L, Dawson TM, Dawson VL. A missense mutation (L166P) in DJ-1, linked to familial Parkinson's disease, confers reduced protein stability and impairs homo-oligomerization. J Neurochem. 2003;87(6):1558-67.
65. Canet-Aviles RM, Wilson MA, Miller DW, Ahmad R, McLendon C, Bandyopadhyay S, et al. The Parkinson's Disease Protein DJ-1 Is Neuroprotective Due to Cysteine-Sulfinic Acid-Driven Mitochondrial Localization. Proc Natl Acad Sci U S A. 2004;101(24):9103-8.

66. Olanow CW. The pathogenesis of cell death in Parkinson's disease - 2007. Mov Disord. 2007;22(S17):S335-S42.
67. Wang Y, Liu W, He X, Zhou F. Parkinson's disease-associated DJ-1 mutations increase abnormal phosphorylation of tau protein through Akt/GSK-3β pathways. J Mol Neurosci. 2013;51(3):911-8.
68. Pan L, Meng L, He M, Zhang Z. Tau in the Pathophysiology of Parkinson's Disease. J Mol Neurosci. 2021;71(11):2179-91.
69. Pickrell AM, Youle RJ. The roles of PINK1, parkin, and mitochondrial fidelity in Parkinson's disease. Neuron. 2015;85(2):257-73.
70. Zhang P-L, Chen Y, Zhang C-H, Wang Y-X, Fernandez-Funez P. Genetics of Parkinson's disease and related disorders. Journal of Medical Genetics. 2018;55(2):73.
71. Kim CY, Alcalay RN. Genetic Forms of Parkinson's Disease. Semin Neurol. 2017;37(2):135-46.
72. Matsumine H, Saito M, Shimoda-Matsubayashi S, Tanaka H, Ishikawa A, Nakagawa-Hattori Y, et al. Localization of a gene for an autosomal recessive form of juvenile Parkinsonism to chromosome 6q25.2-27. Am J Hum Genet. 1997;60(3):588-96.
73. Malek N. Deep Brain Stimulation in Parkinson's Disease. Neurol India. 2019;67(4):968-78.
74. Habets JGV, Heijmans M, Kuijf ML, Janssen MLF, Temel Y, Kubben PL. An update on adaptive deep brain stimulation in Parkinson's disease. Mov Disord. 2018;33(12):1834-43.
75. Iadecola C, Anrather J. The immunology of stroke: from mechanisms to translation. Nature Medicine. 2011;17(7):796-808.
76. Gundersen V. Parkinson's Disease: Can Targeting Inflammation Be an Effective Neuroprotective Strategy? Frontiers in Neuroscience. 2021;14.
77. Angelopoulou E, Paudel YN, Shaikh MF, Piperi C. Fractalkine (CX3CL1) signaling and neuroinflammation in Parkinson's disease: Potential clinical and therapeutic implications. Pharmacological Research. 2020;158:104930.
78. Nayak D, Roth TL, McGavern DB. Microglia Development and Function. Annu Rev Immunol. 2014;32(1):367-402.
79. Davalos D, Akassoglou K, Cardona AE. Chapter 41 - Microglia. In: Rubenstein J, Rakic P, Chen B, Kwan KY, editors. Patterning and Cell Type Specification in the Developing CNS and PNS (Second Edition): Academic Press; 2020. p. 995-1020.

80. Ho MS. Microglia in Parkinson's Disease. In: Verkhratsky A, Ho MS, Zorec R, Parpura V, editors. Neuroglia in Neurodegenerative Diseases. Singapore: Springer Singapore; 2019. p. 335-53.
81. Doorn KJ, Moors T, Drukarch B, van de Berg WDJ, Lucassen PJ, van Dam A-M. Microglial phenotypes and toll-like receptor 2 in the substantia nigra and hippocampus of incidental Lewy body disease cases and Parkinson's disease patients. Acta Neuropathologica Communications. 2014;2(1):90.
82. Marogianni C, Sokratous M, Dardiotis E, Hadjigeorgiou GM, Bogdanos D, Xiromerisiou G. Neurodegeneration and Inflammation-An Interesting Interplay in Parkinson's Disease. International journal of molecular sciences. 2020;21(22):8421.
83. Wolf SA, Boddeke HWGM, Kettenmann H. Microglia in Physiology and Disease. Annual Review of Physiology. 2017;79(1):619-43.
84. Le W, Wu J, Tang Y. Protective microglia and their regulation in Parkinson's disease. Front Mol Neurosci. 2016;9(2016):89-.
85. Tang Y, Le W. Differential Roles of M1 and M2 Microglia in Neurodegenerative Diseases. Molecular Neurobiology. 2016;53(2):1181-94.
86. Lu B, Nagappan G, Lu Y. BDNF and synaptic plasticity, cognitive function, and dysfunction. Handb Exp Pharmacol. 2014;220:223-50.
87. Gash DM, Gerhardt GA, Bradley LH, Wagner R, Slevin JT. GDNF clinical trials for Parkinson's disease: a critical human dimension. Cell and Tissue Research. 2020;382(1):65-70.
88. Kearns CM, Gash DM. GDNF protects nigral dopamine neurons against 6-hydroxydopamine in vivo. Brain Research. 1995;672(1):104-11.
89. Tomac A, Lindqvist E, Lin LFH, Ögren SO, Young D, Hoffer BJ, et al. Protection and repair of the nigrostriatal dopaminergic system by GDNF in vivo. Nature. 1995;373(6512):335-9.
90. Barker RA, Björklund A, Gash DM, Whone A, Van Laar A, Kordower JH, et al. GDNF and Parkinson's Disease: Where Next? A Summary from a Recent Workshop. J Parkinsons Dis. 2020;10(3):875-91.
91. Gupta M, Paliwal VK, Babu GN. Serum fractalkine and 3-nitrotyrosine levels correlate with disease severity in Parkinson's disease: a pilot study. Metabolic Brain Disease. 2022;37(1):209-17.

92. Torres-Platas SG, Comeau S, Rachalski A, Bo GD, Cruceanu C, Turecki G, et al. Morphometric characterization of microglial phenotypes in human cerebral cortex. J Neuroinflammation. 2014;11:12.
93. Wang Y, Zhou M, Wang Y, Jiang D, Deng X. Association of polymorphisms in the MCP-1 and CCR2 genes with the risk of Parkinson's disease. J Neural Transm (Vienna). 2019;126(11):1465-70.
94. Singh S, Anshita D, Ravichandiran V. MCP-1: Function, regulation, and involvement in disease. Int Immunopharmacol. 2021;101(Pt B):107598.
95. Grozdanov V, Danzer KM. Release and uptake of pathologic alpha-synuclein. Cell and Tissue Research. 2018;373(1):175-82.
96. NABCA. Dissection 2022 [Available from: http://nabca.eu/data-collection/dissection/.
97. NBB. Information for tissue applicants: Netherlands Brain Bank; 2019 [
98. proteinaltas.org. GDNF: The Human Protein Atlas; [cited 2022 April 10th]. Available from: https://www.proteinatlas.org/ENSG00000168621-GDNF.
99. proteinaltas.org. PARK7: The Human Protein Atlas; [cited 2022 April 19th]. Available from: https://www.proteinatlas.org/ENSG00000116288-PARK7.
100. ThermoFisherScientific. PierceTM BCA Protein Assay Kit: Thermo Fisher Scientific; 2022 [cited 2022 May 15th]. Available from: https://www.thermofisher.com/order/catalog/product/23227.
101. Weickert CS, Rothmond DA, Purves-Tyson TD. Chapter 16 - Considerations for optimal use of postmortem human brains for molecular psychiatry: lessons from schizophrenia. In: Huitinga I, Webster MJ, editors. Handbook of Clinical Neurology. 150: Elsevier; 2018. p. 221-35.
102. Liu J, Haorah J, Xiong H. Western Blotting Technique in Biomedical Research. In: Xiong H, Gendelman HE, editors. Current Laboratory Methods in Neuroscience Research. New York, NY: Springer New York; 2014. p. 187-200.
103. Bordeaux J, Welsh AW, Agarwal S, Killiam E, Baquero MT, Hanna JA, et al. Antibody validation. Biotechniques. 2010;48(3):197-209.
104. Barber RD, Harmer DW, Coleman RA, Clark BJ. GAPDH as a housekeeping gene: analysis of GAPDH mRNA expression in a panel of 72 human tissues. Physiol Genomics. 2005;21(3):389-95.
105. BioTechne. Luminex Assay Principle mdsystems.com: BioTechne R&D Systems; [cited 2022 May 15th]. Available from: https://www.rndsystems.com/resources/technical/luminex-assay-principle.

106. Asai DJ. Immunofluorescence Microscopy. Current Protocols Essential Laboratory Techniques. 2015;10(1):9.2.1-9.2.23.
107. Ramos-Vara JA. Principles and Methods of Immunohistochemistry. In: Gautier J-C, editor. Drug Safety Evaluation: Methods and Protocols. New York, NY: Springer New York; 2017. p. 115-28.
108. K RV, Jones D, Udupa V. A simple and effective heat induced antigen retrieval method. MethodsX. 2016;3:315-9.
109. Elliott AD. Confocal Microscopy: Principles and Modern Practices. Curr Protoc Cytom. 2020;92(1):e68.
110. Fernández-Arjona MdM, Grondona JM, Granados-Durán P, Fernández-Llebrez P, López-Ávalos MD. Microglia Morphological Categorization in a Rat Model of Neuroinflammation by Hierarchical Cluster and Principal Components Analysis. Frontiers in Cellular Neuroscience. 2017;11.
111. Leyh J, Paeschke S, Mages B, Michalski D, Nowicki M, Bechmann I, et al. Classification of Microglial Morphological Phenotypes Using Machine Learning. Front Cell Neurosci. 2021;15:701673.
112. Lee KH, Lee DW, Kang BC. The 'R' principles in laboratory animal experiments. Laboratory Animal Research. 2020;36(1):45.
113. Russell WMS, Burch RL. The principles of humane experimental technique: Methuen; 1959.
114. Stopper L, Bălşeanu TA, Cătălin B, Rogoveanu OC, Mogoantă L, Scheller A. Microglia morphology in the physiological and diseased brain - from fixed tissue to in vivo conditions. Rom J Morphol Embryol. 2018;59(1):7-12.
115. Blandini F, Armentero MT. Animal models of Parkinson's disease. Febs j. 2012;279(7):1156-66.
116. R&DSystems. Antigen Retrieval Methods: BioTechne R&D Systems; [cited 2022 May 15th]. Available from: https://www.rndsystems.com/resources/protocols/antigen-retrieval-methods.